DISS. ETH No. 13749

Ab Initio Study of Neutral and Cationic Double Bond Systems Containing Group 15 Elements

A dissertation submitted to the

SWISS FEDERAL INSITUTE OF TECHNOLOGY ZÜRICH

For the degree of
Doctor of Natural Sciences

presented by
CHRISTOPH WIDAUER
Dipl. Chem. ETH

born December 4, 1967
Zizers, GR

Accepted on the recommendation of:
Prof. Dr. H. Grützmacher, Examiner
Prof. Dr. U. Röthlisberger, Co-Examiner

2000

Contents

Acknowledgments

Seite Leer /
Blank leaf

Abstract

Within the scope of this work, we present a systematic ab initio study at various levels of theory for neutral double bond systems and their protonated derivatives containing group 15 elements. The structures of selected isomers for each system were optimized at the MP2 and QCISD levels of theory with pseudopotentials on all hetero atoms and valence basis sets of double-ζ quality (VDZP[1]). Vibrational frequencies were calculated in order to characterize the stationary points on the hypersurfaces as minima or transition states. Refined energies were obtained in CCSD(T) single-point calculations using splitted valence basis sets of triple-ζ quality with polarization functions up to f (VTZP[1,2]). For the systems with either planar or trans-bent double bonds, the charge distributions together with the corresponding σ and π populations were derived from NBO analyses. Double bond strengths and proton affinities (PA) were assessed by calculations of the reaction enthalpies for the corresponding dissociation and protonation reactions, respectively. The amount to which the π-bond strengths contribute to the total bonding energies were estimated by the rotation barriers around the double bond axes. Thus the corresponding σ-bond strengths refer to the difference between the total bond strength and the π-bond increment.

Topographical bond analyses according to the Atoms in Molecules (AIM) theory and Electron Localization Function (ELF) were performed to give insights into the spatial structure of the electron density of the double bond systems.

We calculated the successive protonation reactions $H_2C=XH \xrightarrow{H^+} [H_2C=XH_2]^+ \xrightarrow{H^+} [H_2C-XH_3]^{2+}$ or $[H_3C-XH_2]^{2+}$. While the structures of the neutral methylene pnictanes $H_2C=XH$ are planar, either planar (X = N, P) or trans-bent (X = As,

Sb) structures are found for the protonated derivatives $[H_2C=XH_2]^+$. However, for $[H_2C=AsH_2]^+$ and $[H_2C=SbH_2]^+$, the energy required to convert the trans-bent into the planar geometry is very small ($\leqslant 1$ kcal mol^{-1}). Considering planar structures for $[H_2C=XH_2]^+$, the corresponding C=X double bond lengths for X = P, As, Sb are shorter by $0.05 - 0.04$ Å compared to the precursors $H_2C=XH$, whereas for X = N, the C=N bond is slightly elongated. Trans-bending in the higher homologues $[H_2C=AsH_2]^+$ and $[H_2C=SbH_2]^+$ results in a bond elongation by 0.012 Å and 0.060 Å, respectively. With the exception of $H_2C=NH$ and $[H_2C=NH_2]^+$, where C is positively and N negatively polarized, in all other higher homologues $H_2C=XH$ and $[H_2C=XH_2]^+$ (X = P, As, Sb), the carbon atom is the negative and the X-atom the positive center of charge. Upon protonation of $H_2C=XH$ (X = P, As, Sb) the additional positive charge is mainly accumulated at the X center, while the negative charge does not change significantly. The dissociation energies for the neutral double bond systems $H_2C=XH$ decrease steadily from 150 kcal mol^{-1} (X = N) to 86 kcal mol^{-1} (X = Sb). The corresponding π-bond strengths follow the same trend from ca. 80 kcal mol^{-1} (X = N) to about 30 kcal mol^{-1} (X = Sb). For the protonated derivatives $[H_2C=XH_2]^+$, the dissociation energies are descending rapidly from 208 kcal mol^{-1} (X = N) to 81 kcal mol^{-1} (X = Sb). Conversely, the corresponding π double bond increments change to a much smaller extent, remaining in the range of $20 - 80$ kcal mol^{-1}.

Further protonation of $[H_2C=XH_2]^+$ is endothermic for X = N, almost thermoneutral for X = P and exothermic for X = As, Sb. On the other hand, formation of the C-site protonated dications $[H_3C-XH_2]^{2+}$ is increasingly exothermic for all X = P, As, Sb and these isomers are calculated to be more stable than the pnictonium substituted carbenium ion $[H_2C-XH_3]^{2+}$. The dication $[H_3C-XH_2]^{2+}$ does not correspond to a minima on the potential energy surface (PES). The expected "coulomb explosion" of the heavier dications, $[H_2C-XH_3]^{2+} \rightarrow CH_2^{\bullet+} + XH_3^{\bullet+}$ and $[H_3C-XH_2]^{2+} \rightarrow CH_3^+ + XH_2^+$, are in fact exotherm, but, at least in parts, kinetically hindered by substantial activation barriers. Thus, for X = P an experimental observation of these "superelectrophiles" should be possible.

Protonation reactions starting from the dipnictenes HX=XH, were also investigated: $HX=XH \xrightarrow{H^+} [H_2X=XH]^+ \xrightarrow{H^+} [H_2X=XH_2]^{2+}$. All neutral molecules

$HX=XH$, as well as the monocations $[H_2X-XH]^+$ have planar structures. The corresponding $X=X$ bond lengths are shortened by $0.03 - 0.04$ Å upon protonation. In the series of the dications $[H_2X=XH_2]^{2+}$, only the nitrogen system $[H_2N=NH_2]^{2+}$ has a planar geometry, while the higher congeners adopt trans-bent structures in the ground states. However, for $X = P$, the energy required to attain a planar geometry only amounts 0.2 kcal mol^{-1}. In contrast, substantial barriers are obtained for the As and Sb homologues (5.1 kcal mol^{-1} and 11.8 kcal mol^{-1}). Considering planar structures for all $[H_2X=XH_2]^{2+}$ ($X = N$ - Sb), the corresponding $X=X$ double bond lengths are slightly shorter than in the monocations $[H_2X=XH]^+$, except for $X = N$. However, the transition into the trans-bent ground states significantly lengthens the $X=X$ double bond by $0.02 - 0.13$ Å.

The dissociation energies within each series of homologous double bond systems decrease in the order $N > P > As > Sb$. However, upon protonation of the neutral precursors $H_2C=XH$ and $HX=XH$, these energies increase. Further protonation is leading to a dramatic drop in the dissociation energies, which is endothermic only for $X = N$ (11 kcal mol^{-1}), but strongly exothermic for all other $X = P$, As, Sb ($-40 - -70$ kcal mol^{-1}). Notwithstanding, the homolytical decay of the dications $[H_2X=XH_2]^{2+}$ into $2XH_2^+$ is hindered by relatively high barriers (N: 151 kcal mol^{-1}; P: 42 kcal mol^{-1}; As: 21 kcal mol^{-1}; Sb: 8 kcal mol^{-1}), which should make an experimental observation of these "superelectrophiles" possible. Remarkably, the estimated π-bond strengths for all systems $HX=XH$, $[H_2X=XH]^+$ and $[H_2X=XH_2]^{2+}$ are similar in magnitude so that the differences in the total bond strengths can be essentially attributed to the σ-bond strengths.

A comparison of the neutral molecules $H_2C=XH$ and $HX=XH$ with the monocations $[H_2C=XH_2]^+$ and $[H_2X=XH]^+$, as well as $[H_2X=XH_2]^{2+}$, by means of topographical analyses of the electron densities shows unequivocally that the $X=X$ bonds can be described as double bonds even if the structures deviate from planarity.

With $[H_2C=SbH_2]^+$ as the only exception, the double bonds in all systems investigated become stronger upon protonation for $X = N$, P, As, Sb. In principle, this can be attributed to the increase of the σ double bond increment. This effect is provoked by the rehybridization at the X center due to the protonation of the

lone pair. This results in a increase of the s character of the C–X and X–X valence bonding orbital and thus of the σ-bond strength (isovalent hybridization). The second protonation step ("superelectrophilic activation") reduces the the σ-bond strength. This effect is also based on the increasing accumulation of positive charge at the adjacent centers connected by the C–X and X–X bond paths. The dramatic decrease of the X=X double bond energies of the cationic systems for X = P, As, Sb, in comparison to the nitrogen containing systems, can be understood by the different spin states of the XH_2^+ fragments. Since this state only refers to a triplet ground state for NH_2^+, but to a singlet ground state for all the other XH_2^+ (X = P - Sb) fragments, the promotion energy $\Delta E_{S \rightarrow T}$ is gained as relaxation energy upon homolytical bond fission.

Zusammenfassung

Im Rahmen dieser Arbeit wird eine systematische Untersuchung neutraler Mehrfach-bindungssysteme und ihrer protonierten Derivate, die ein Element der 15. Gruppe enthalten, mit Hilfe von verschiedenen quantenchemischen Verfahren durchgeführt. Die Strukturen verschiedener Isomere der jeweiligen Systeme wurden auf MP2 und QCISD Niveau mit Pseudopotentialen an allen Heteroatomen und Valenzbasissätzen mit double-ζ Qualität optimiert (VDZP[1]). Frequenzanalysen wurden herangezogen, um die stationären Punkte auf den jeweiligen Hyperflächen als Minima oder Über-gangszustände zu charakterisieren. Die Energien dieser Punkte wurden mit Einzel-punktrechnungen auf CCSD(T) mit gesplitteten Basissätzen von triple-ζ Qualität und Polarisationsfunktionen bis zu f verfeinert (VTZP[1,2]). Für die Systeme, die entweder planare oder trans-gewinkelte Doppelbindungen enthalten, wurden die La-dungsverteilungen sowie die σ- und π-Populationen aus NBO-Analysen abgeschätzt. Doppelbindungsenergien und Protonenaffinitäten wurden durch Berechnungen der Reaktionsenthalpien der entsprechenden Dissoziationsenergien bzw. Protonierungs-reaktionen abgeschätzt. Die auf CCSD(T) Niveau erhaltenen Dissoziationsenergien für alle Doppelbindungssysteme mit N, P und As als Schweratome wurden zusätz-lich mit Berechnungen nach der G2 Methode überprüft. Die π-Bindungsbeiträge zur gesamten Doppelbindungsenergie wurden durch Bestimmung der Rotationsbar-rieren um die Doppelbindungs-Achsen ermittelt und durch Differenzbildung die σ-Bindungsinkremente erhalten.

Topographische Bindungsanalysen wurden mit Hilfe der Atoms-in-Molecules (AIM) Theorie und der Elektronenlokalisierungsfunktion (ELF) durchgeführt, um Einblick in die räumliche Struktur der Elektronendichte zu gewinnen.

Die aufeinanderfolgenden Protonierungsreaktionen $H_2C=XH \xrightarrow{H^+} [H_2C=XH_2]^+$ $\xrightarrow{H^+} [H_2C-XH_3]^{2+}$ oder $[H_3C-XH_2]^{2+}$ wurden für X = N, P, As und Sb berechnet. Während die Strukuren aller neutralen Methylenpniktane $H_2C=XH$ planar sind, ergeben sich für die protonierten Derivate $[H_2C=XH_2]^+$ entweder planare (X = N, P) oder trans-gewinkelte Strukturen (X = As, Sb). Allerdings sind die Energien, die für die Einebnung des Molekülgerüstes benötigt werden ($\leqslant 1\,kcal\,mol^{-1}$) sehr klein. Werden planare Strukturen für alle $[H_2C=XH_2]^+$ angenommen, so werden die C=X-Bindungen für X = P, As und Sb um $0.05-0.04$ Å kürzer als in den neutralen Vorläufern $H_2C=XH$, während für X = N die C=N-Bindung etwas verlängert wird. Durch trans-Winkelung der Strukturen von $[H_2C=AsH_2]^+$ und $[H_2C=SbH_2]^+$ wird die C=X-Bindung um 0.012 Å bzw. 0.060 Å verlängert. Mit Ausnahme von $H_2C=NH$ und $[H_2C=NH_2]^+$, in denen C positiv und N negativ polarisiert sind, ist in den Monokationen der höheren Homologen $H_2C=XH$ und $[H_2C=XH_2]^+$ (X = P, As, Sb) das Kohlenstoffatom das negative und das X-Atom das positive Ladungszentrum. Bei Protonierung von $H_2C=XH$ (X = P, As, Sb) wird die positive Ladung im wesentlichen vom X-Zentrum übernommen, während sich die Ladung am C-Atom nicht signifikant ändert. Die Dissoziationsenergien der neutralen Doppelbindungssysteme nehmen von $150\,kcal\,mol^{-1}$ für X = N monoton fallend bis $86\,kcal\,mol^{-1}$ für X = Sb ab. Die berechneten π-Bindungsenergien nehmen ebenfalls mit zunehmender Hauptquantenzahl des X-Zentrums von ca. $80\,kcal\,mol^{-1}$ (X = N) bis zu etwa $30\,kcal\,mol^{-1}$ (X = Sb) ab. In den protonierten Derivaten $[H_2C=XH_2]^+$ fällt die Dissoziationsenergie steiler von $208\,kcal\,mol^{-1}$ (X = N) bis zu $81\,kcal\,mol^{-1}$ (X = Sb) ab. Die π-Bindungsinkremente hingegen ändern sich weniger und bleiben in dem Bereich von $20-80\,kcal\,mol^{-1}$.

Die weitere Protonierung von $[H_2C=XH_2]^+$ zu $[H_2C-XH_3]^{2+}$ ist endotherm für X = N, thermoneutral für X = P und exotherm für X = As, Sb. Dagegen ist die Protonierung am Kohlenstoffzentrum, die zu $[H_3C-XH_2]^{2+}$ führt, für X = P, As, Sb zunehmend exotherm und diese Isomere sind stabiler als die Pnictonium-substituierten Carbeniumionen $[H_2C-XH_3]^{2+}$. Das Dikation $[H_3C-NH_2]^{2+}$ entspricht keinem Minimum auf der Potentialhyperfläche (PES). Die zu erwartenden "Coulomb-Explosionen" der höheren Dikationen $[H_2C-XH_3]^{2+} \rightarrow CH_2^{\bullet+} + XH_3^{\bullet+}$ und $[H_3C-XH_2]^{2+} \rightarrow CH_3^+ + XH_2^+$ sind in der Tat exotherm, jedoch zum Teil durch

ausreichend hohe Aktivierungsbarrieren kinetisch gehemmt, so dass für X = P ein experimenteller Nachweis dieser "Superelektrophile" möglich scheint.

Folgende Protonierungsreaktionen, ausgehend von den Dipnictogenen HX=XH wurden ebenfalls untersucht: $HX=XH \xrightarrow{H^+} [H_2X=XH]^+ \xrightarrow{H^+} [H_2X=XH_2]^{2+}$. Alle neutralen Moleküle HX=XH sowie die Monokationen $[H_2X=XH]^+$ besitzen planare Strukturen. Die X=X-Bindung wird in allen Fällen durch Protonierung um $0.03 - 0.04$ Å verkürzt. In der Serie der Dikationen $[H_2X=XH_2]^{2+}$ hat nur das $[H_2N=NH_2]^{2+}$-Ion eine planare Struktur, die höheren Homologen hingegen weisen trans-gewinkelte Molekülstrukturen im Grundzustand auf. Allerdings ist für X=P nur wenig Energie (0.2 kcal mol^{-1}) nötig, um eine planare Struktur zu erreichen. Dagegen sind die Barrieren für die As- und Sb-Homologen substantiell (5.1 kcal mol^{-1} und 11.8 kcal mol^{-1}). Werden planare Strukturen für alle $[H_2X=XH_2]^{2+}$ (X = N - Sb) angenommen, so sind die X=X-Bindungen mit Ausnahme von X = N etwas kürzer als in den Monokationen $[H_2X=XH]^+$. Der Übergang in den Grundzustand mit gewinkelter Struktur verlängert dagegen die X=X-Bindungen deutlich ($0.02 - 0.13$ Å). Die Dissoziationsenergien nehmen innerhalb einer jeden Serie von homologen Doppelbindungssystemen in der Reihe N > P > As > Sb ab. Jedoch steigt bei Protonierung der neutralen Vorläufer HX=XH zu $[H_2X=XH]^+$ diese Energie für alle X an. Die weitere Protonierung führt dann zu einem dramatischen Abfall der Dissoziationsenergie, die nur noch für X = N schwach endotherm (11 kcal mol^{-1}), für alle anderen X = P - Sb stark exotherm ist ($-40 - -70$ kcal mol^{-1}). Dennoch ist der homolytische Zerfall der Dikationen in $2XH_2^+$ durch relativ hohe Barrieren geschützt (N: 151 kcal mol^{-1}; P: 42 kcal mol^{-1}; As: 21 kcal mol^{-1}; Sb: 8 kcal mol^{-1}), die den experimentellen Nachweis dieser "Superelektrophile" ermöglichen sollten. Bemerkenswerterweise ist die durch Berechnung der X=X-Rotationsbarrieren abgeschätzte π-Bindungsenergie in allen Systemen HX=XH, $[H_2X=XH]^+$ und $[H_2X=XH_2]^{2+}$ in etwa gleich, so dass sich die Bindungsenergieunterschiede im wesentlichen auf die σ-Bindungsinkremente zurückführen lassen.

Ein Vergleich der neutralen Moleküle $H_2C=XH$ und HX=XH mit den Monokationen $[H_2C=XH_2]^+$ und $[H_2X=XH]^+$ sowie den Dikationen $[H_2X=XH_2]^{2+}$ an Hand von topographischen Analysen der Elektronendichte zeigt eindeutig, dass sich die

C=X bzw. X=X-Bindung in allen Spezies als Doppelbindung beschreiben lässt, selbst wenn die Struktur von der Planarität abweicht.

Mit Ausnahme von $H_2C=SbH$ wird die Doppelbindung für alle X in den untersuchten Systemen bei Protonierung verstärkt. Im wesentlichen ist dies auf die Zunahme des σ-Bindungsinkrementes zurückzuführen. Dieser Effekt wird durch eine Umhybridisierung am X-Zentrum bei Anlagerung eines Protons an das freie Elektronenpaar verursacht, wodurch der σ-Anteil am C-X bzw. X-X Bindungsvalenzorbital und damit die σ-Bindungsenergie ansteigt (isovalente Hybridisierung). Der zweite Protonierungsschritt ("superelektrophile Aktivierung") erniedrigt dann wieder die σ-Bindungsstärke. Dieser Effekt beruht auch auf die zunehmende Akkumulation von positiver Ladung auf den über die zentrale C=X- bzw. X=X-Bindung verknüpften Fragmenten. Die zum Teil drastische Abnahme der X=X-Bindungsenergie in den kationischen Systemen beim Übergang von $X = N$ zu $X = P$ - Sb ist zum einen auf die unterschiedlichen Spinzustände der Fragmente XH_2^+ zurückzuführen. Da dieser nur für NH_2^+ dem Triplettzustand als Grundzustand bei homolytischem Bindungsbruch entspricht, aber alle anderen XH_2^+-Fragmente ($X = P$ - Sb) einen Singulettgrundzustand besitzen, wird die Anregungsenergie $\Delta E_{S \to T}$ als Relaxationsenergie bei der Dissoziation gewonnen.

Symbols

Abbreviations and Acronyms

AIL	Atomic interaction line
AIM	Atoms in molecules
AO	Atomic orbital
BCP	Bond critical point
BP	Bond path
BS	Basis set
calc	Calculation
CASSCF	Complete Active Space SCF
CCSD	Coupled Cluster with Singles and Doubles
CGMT	Carter-Goddard-Malrieu-Trinquier
CI	Configuration Interaction
CP	Critical point
ECP	Effective core potential
ELF	Electron Localization Function
EN	Electronegativity
exp	Experiment
HOMO	Highest occupied molecular orbital
IAS	Interatomic surface
LUMO	Lowest unoccupied molecular orbital
MCSCF	Multi Configuration SCF
MEFIT	Multi electron fit

MO   Molecular orbital

MP2   Møller–Plesset Perturbation Theory of Second Order

MRCI   Multi Reference CI

MRCISD   Multi Reference CI with Singles and Doubles

MSE   Methyl stabilization energy

NOH   Non-orbital hybridization

PA   Proton affinity

PES   Potential energy surface

QCISD   Quadratic Configuration Interaction with Singles and Doubles

SCF   Self Consistent Field

SECP   *Stuttgarter* ECP

SOCI   Second-Order CI

SOMO   Singly occupied molecular orbital

TS   Transition state

ZPE   Zero point energy

^{t}Bu   *Tert*-butyl

Me   Methyl

Mes   Mesityl (2,4,6-trimethylphenyl)

Mes*   Supermesityl (2,4,6-tri-*tert*-butylphenyl)

Ph   Phenyl

Tbt   2,4,6-(bistrimethylsilylmethyl)phenyl

Trip   2,4,6-triisopropylphenyl

Mathematical and Physical Symbols

R_e Geometric equilibrium bond length

q Charge given in $e = 1.60219 \cdot 10^{-19}$C

$\mathcal{X}_x$ Electronegativity of atom X

f_{pol}^i Exponent of the ith polarization function

ϕ_X	Flap angle at atom X
ν^{calc}	Calculated frequency
ν^{exp}	Experimental frequency
p_σ	σ population (in electrons)
p_π	π population (in electrons)
R	Universal gas constant, 8.314 J/K
T	Temperature in Kelvin

E_{INT}	Intrinsic interaction energy of two triplet fragments
$\Delta E_{S \to T}$	Singlet-triplet splitting energy
$E_{\sigma+\pi}$	Bond energy of a classical planar double bond system
E_σ	σ increment of $E_{\sigma+\pi}$
E_π	π increment of $E_{\sigma+\pi}$
ΔE_{TBE}	Total bond energy at 0 K
ΔE_{TBE}^0	ZPE corrected total bond energy
ΔE_{snap}	Snapping energy
ΔE_{prep}	Preparation energy
ΔE^0	Steric repulsion
ΔE_{elstat}	Electrostatic interaction energy
ΔE_{Pauli}	Pauli repulsion
D_e	Dissociation energy at 0 K
E_{int}	Orbital interaction energy
D_0	ZPE corrected dissociation energy
D_π	Rotational barrier

ΔH_{298}	Reaction enthalpy at 298 K
ΔE^{elec}	Electronic energy change
ΔE_{298}^{vib}	Vibrational energy change at 298 K
ΔE_{298}^{rot}	Rotational energy change at 298 K

$\Delta E_{298}^{\text{trans}}$ Translational energy change at 298 K

$\Delta(pV)_{298}$ Pressure-volume work at 298 K

$\mathbf{X}_\alpha$ Position vector of nucleus α

$\mathbf{r}_b$ Position vector of bond critical point in electronic charge density

r_b Position of $\mathbf{r}_b$ relative to the position of $\mathbf{X}_\alpha$, given as ratio $\mathbf{X}_\alpha$–r_b/R_e

R_b Bond path length

$S(\mathbf{r}_s)$ Interatomic surface

S_{AB} Interatomic surface between atoms A and B

$\rho(\mathbf{r}), \rho$ Electronic charge density

ρ_b Value of $\rho(\mathbf{r})$ at a bond critical point

$\nabla\rho(\mathbf{r})$ Gradient vector of ρ

$\nabla^2\rho(\mathbf{r})$ Laplacian of ρ

$\nabla^2\rho_b$ Value of $\nabla^2\rho(\mathbf{r})$ at a bond critical point

λ_i Eigenvalue of the Hessian matrix of ρ at a critical point

σ_c Signature of critical point in ρ

ω_c Rank of critical point in ρ

$H(\mathbf{r})$ Local energy density

H_b Value of $H(\mathbf{r})$ at a bond critical point

$G(\mathbf{r})$ Local kinetic energy

$V(\mathbf{r})$ Local potential energy

ϵ Bond ellipticity

ϵ_b Value of ϵ at a bond critical point

D_σ Measure of electron localization

$\mathcal{X}_\sigma$ Dimensionless localization index

$M^{1,2}$ Pair of ELF maxima, double bond attractor pattern

1. Theory

Seite Leer /
Blank leaf

1.1 Models for double bonding

In the description of a classical double bond system such as ethylene, the two major bonding theories for molecular compounds, i.e. Valence Bond (VB) and Molecular Orbital (MO) theory, are essentially equivalent. In VB theory the carbon-carbon double bond is formed by two sp^2 hybridized triplet carbenes, whereas in MO theory, the set of four valence electrons of the double bond is described by a symmetry separated set of one σ and one π molecular orbitals. Strictly by definition, the terms σ and π bond are restricted by symmetry to linear molecules but are commonly used for bond descriptions in planar molecules as well. Alternatively, multiple bonds are described by bent bonds or banana bonds [Schultz and Messmer 1991, 1993a,b,c]. Both approaches are equally legitimate and as approximate descriptions neither of these can be proven to be right or wrong, as demonstrated in [Ogliaro et al. 1999] for example .

$$\pi \qquad \sigma_{pp}^{*} \qquad n_{+}$$
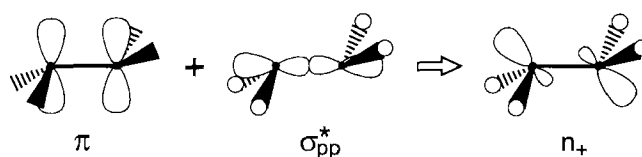
Scheme 1.1

From the viewpoint of MO theory, trans-bending distortion from planarity in a double bond system can be explained by a second-order Jahn-Teller distortion. This allows the σ_{pp}^{*} orbital to mix into the π HOMO, which is transformed into the stabilized n_{+} lone pair combination, as shown in Scheme 1.1. As discussed later in Sec. (1.1.2), double bond systems of the higher row elements have much longer X=X bond lengths due to the *interatomic Pauli repulsion*. As a consequence (among others), the π_{pp} overlap is reduced, resulting in strongly decreased HOMO-LUMO gaps. For instance, the HOMO-LUMO gap is 5.7 eV in ethylene, whereas it is only 1.2?? eV in disilene. Furthermore, also the energy difference between the π HOMO

and the σ_{pp}^* is reduced so that the stabilization which stems from the mixing of these two orbitals is further enhanced. As a result, heavy element double bonds $R_2X=XR_2$ are increasingly unstable towards a second-order Jahn-Teller distortion with increasing atomic number of X.

1.1.1 The Carter-Goddard-Malrieu-Trinquier (CGMT) model

In a hypothetical experiment a double bond system $R_2X=XR_2'$ is homolytically dissociated into its carbenoid triplet fragments XR_2 and XR_2' as depicted in Fig. (1.1). In principle these fragments can either have a triplet or a singlet ground state. By using differently substituted ethylenes Carter and Goddard III [1986] showed that
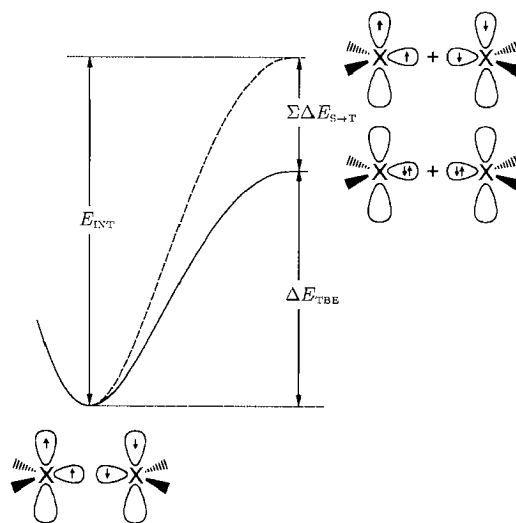
Figure 1.1: Schematic representation of the dissociation of a planar double bond system into its constituting triplet fragments. E_{INT} denotes the *intrinsic* double bond energy and $\Sigma\Delta E_{S\to T}$ denotes the sum of the singlet-triplet splitting energies $\Delta E_{S\to T}$, which in this case are positive (the fragments have a singlet ground state).
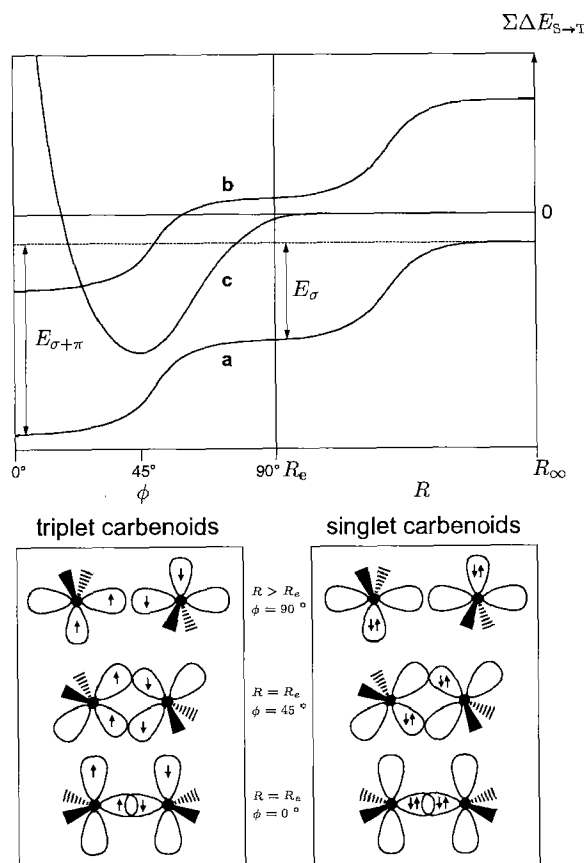
Figure 1.2: Schematic interaction diagram of two carbenes or carbene analogues XR$_2$ as a function of the positional parameter R (distance) and ϕ (flap angle). The origin of the energy scale is arbitrary set to $2\Delta E_{\mathrm{S\rightarrow T}}$ (singlet) $= 0$. Thus, the parralel curves a and b correspond to the interaction of two fragments with triplet ground states ($2\Delta E_{\mathrm{S\rightarrow T}} < 0$) or with excited triplet states ($2\Delta E_{\mathrm{S\rightarrow T}} > 0$), respectively. Curve c describes the interaction of two carbene fragments with singlet ground states.

the total double bond energy ΔE_{TBE} is derived from the *intrinsic* C=C double bond energy, E_{INT}, minus the sum of singlet-triplet splitting energies $\Delta E_{\mathrm{S\rightarrow T}}$ (Eq. (1.1)).

$$\Delta E^0_{\mathrm{TBE}} = E_{\mathrm{INT}} - \Sigma \Delta E_{\mathrm{S\rightarrow T}} \tag{1.1}$$

Trinquier and Malrieu [1987] extended this model so that the prediction of
the preferred geometry of a doubly bonded system depending on $\Delta E_{S \to T}$ of the
constituting fragments is possible. Here the combination of two carbenoid fragments
was considered as a function of their spin state as well as the geometric parameters
R and ϕ. The latter refer to the X–X distance (R) and the angle (ϕ) of the two
orthogonally placed fragments.
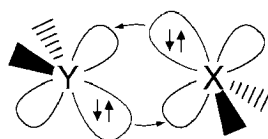
Scheme 1.2

In Fig. (1.2) the procedure is shown graphically. Arbitrary, the zero point on the
energy scale is chosen such it corresponds to two carbene fragments in a singlet state.
All other energies are given in relation to this point, i.e. a system where the triplet
states of the carbene fragments are more stable will start at negative energies, a
system less stable will start at positive values. Curve **a** represents the combination
of two carbene fragments with triplet ground states ($\Sigma \Delta E_{S \to T} < 0$). Firstly, the
distance between the two interacting fragments is reduced to the equilibrium bond
distance R_e. The systems gains the σ bond energy E_σ as a result of the σ_{pp} overlap
of the two singly occupied p orbitals. Then, the orthogonal fragments rotate from
$\phi = 90$ ° to 0 ° where the system gains its maximum stabilization $E_{\sigma + \pi}$. In Curve
c the energy for two carbene fragments is given which combine in their singlet
states. While approaching R_e, almost no energy is gained. However, rotation of the
fragments results in a energy gain with its maximum at $\phi = 45$ °. The interaction
can be described as a mutual dative π-bond where the lone pair of one fragment is
delocalized into the empty p(π) acceptor-orbital of the other, as shown graphically

X	energy of isomers					
C	I					
Si, Ge	II	<	IV	<	V, VI	
Sn, Pb	V, VI	<	III	<	IV	< II
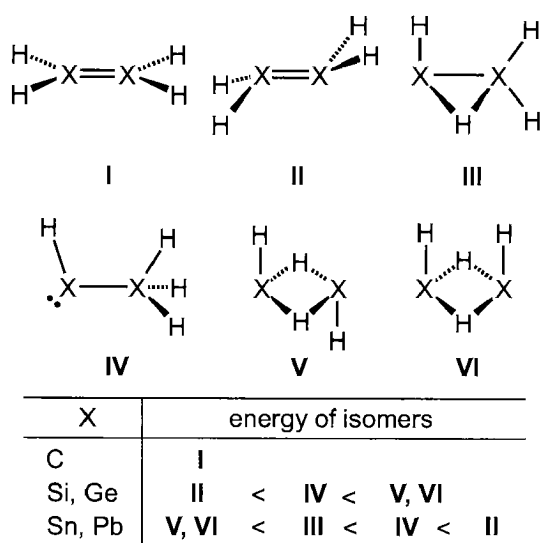
Scheme 1.3

in Scheme 1.2. This description of a slipped double bond as a double donor-acceptor bond was already proposed by Lappert in [Davidson et al. 1976]. The depth of the potential well in curve **c** was estimated to be approximately $1/2E_{\sigma+\pi}$ [Trinquier and Malrieu 1987 , Appendix II]. A "classical" planar geometry therefore occurs if

$$\Sigma\Delta E_{\text{S} \to \text{T}} < 1/2E_{\sigma+\pi} \tag{1.2}$$

whereas a "non-classical" trans-bent geometry is expected if

$$\Sigma\Delta E_{\text{S} \to \text{T}} > 1/2E_{\sigma+\pi} \tag{1.3}$$

Finally, it has to be asked whether a double bond system – be it classical or non-classical – is the only possible stable structure one can imagine (guided by the valence theory). Within the GCMT-model, the requirement for the existence of a planar or trans bent ground state double bond system is given by

$$\Sigma\Delta E_{\text{S} \to \text{T}} < E_{\sigma+\pi} \tag{1.4}$$

This was shown for group 14 X_2H_4 potential surfaces in [Trinquier 1990, 1991]. Accordingly, doubly H-bridged structures **V** and **VI** (Scheme 1.3) represent the

global minima on the electronic hypersurfaces of Sn_2H_4 and Pb_2H_4, because SnH_2 and PbH_2 have very stable singlet states and $E_{\sigma+\pi}$ becomes even smaller than $\Sigma\Delta E_{S\rightarrow T}$. The trans bent double bond forms **II** are the least stable isomers!

1.1.2   The nature of the intrinsic double bond energy E_{INT}

Another important approach to explain the occurrence of trans-bending in the higher homologues of ethylene stems from Jacobsen and Ziegler [1994] who analyzed the bonding of the group 14 $H_2X=XH_2$ systems according to the formation process, shown in Scheme 1.4.

$$2XH_2\ (^1A_1)\ \overset{\Delta E^e_{prep}}{\longrightarrow}\ 2XH_2\ (^3B_1)\ \overset{\Delta E^g_{prep}}{\longrightarrow}\ 2XH_2^{frag}\ (^3B_1)\ \overset{\Delta E_{snap}}{\longrightarrow}\ X_2H_4$$
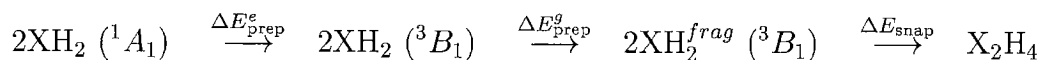
Scheme 1.4

The singlet carbenoids XH_2 are firstly prepared electronically (ΔE^e_{prep}) and structurally (ΔE^g_{prep}) into appropriate triplet $^3B_1$ states. Further, combination of the two triplet fragments results in the so-called snapping energy ΔE_{snap}. The electronic preparation energy ΔE^e_{prep} can be identified with the sum of the *positive* singlet-triplet splitting energies $\Delta E_{S\rightarrow T}$ of the carbenoid fragments. The structural preparation energy ΔE^g_{prep} obtained from the distortion of the unperturbed ligand framework to the geometry in the final molecule was not considered in the CGMT-Model. However, according to the results of Jacobsen and Ziegler [1994], the contribution from ΔE^g_{prep} to the total preparation energy ΔE_{prep} of a singlet CH_2 fragments is negligible. The snapping energy is equivalent with the intrinsic double bond energy E_{INT} described in [Carter and Goddard III 1986]. From Scheme 1.4 it follows

$$\Delta E_{TBE} = \Delta E_{snap} + \Delta E^e_{prep} + \Delta E^g_{prep} \qquad (1.5)$$

which, apart from ΔE^g_{prep} corresponds with Eq. (1.1). The interaction energy ΔE_{snap} was further de-convoluted as

$$\Delta E_{\text{snap}} = \Delta E^0 + \Delta E_{\text{int}} = \Delta E_{\text{elstat}} + \Delta E_{\text{Pauli}} + \Sigma \Delta E^{\Gamma}_{\text{int}} \qquad (1.6)$$

The steric repulsion ΔE^0 consist of two components. The first component ΔE_{elstat} refers to the *attractive* electrostatic interaction of the two triplet fragments which is the mutual interaction between the nuclear charge of one fragment and the electron density of the other fragment. The second component, the so-called interatomic Pauli repulsion ΔE_{Pauli}, counterbalances ΔE_{elstat} and represents repulsive two-center-three-electron (2c-3e) and two-center-four-electron (2c-4e) interactions between occupied orbitals on both fragments. This unfavorable interaction rises with increasing orbital overlap, i.e. upon shortening of any bond. Thus, at the equilibrium geometry ΔE^0 is usually repulsive since contributions from ΔE_{Pauli} dominate. In addition, there are the attractive orbital interactions E_{int} opponent to ΔE^0, which can be further resolved in single orbital interactions $\Delta E^{\Gamma}_{\text{int}}$ within the irreducible representations Γ of the molecular symmetry.

Especially, for heavier main group elements, ΔE_{Pauli} becomes predominant for ΔE^0, already at quite long X–X distances, because the valence np-orbitals of one fragment, which are rather extended in space, underlie a repulsive 2c-3e-interaction with (n-1)p core orbitals on the other fragment. In contrast, elements of the second period have only core electrons in the 1s level. It is the increased Pauli repulsion which is responsible for the well-known fact that X–X bonds of higher row elements are significantly longer than the corresponding bonds for the second row elements. This emphasizes that bonding is not only defined by the maximum valence AO overlap but also has to be reasoned in terms of steric interaction.

1.2   Topographical Analysis of the electron density

The orbital model provides a way for describing the *electronic* structure of many-electron systems. On the other hand, any attempt to describe the *spatial* structure of the electronic charge by means of canonical or localized molecular orbitals remains an approximation and ambiguous. This is so because the summation of the orbital densities over *any* set of molecular orbitals, which are related by a unitary transformation, gives the same total electronic density. However, there are methods invariant upon unitary transformations based on the total electronic density ρ itself which provide insight into the *spatial* distribution of bonded and non-bonded electron pairs: the analysis of the electron density through its Laplacian $\nabla^2\rho(\mathbf{r})$ according to the *Atoms in Molecules* (AIM) theory by Bader [1990] and the *Electron Localization Function* ELF first introduced by Becke and Edgecombe [1990].

1.2.1   Bader Analysis: Atoms in Molecules (AIM) theory

The topography of the *total* electronic charge density ρ of a molecular system is simple in nature with local maxima only at the positions of the nuclei and does not suggest localized electronic groups. It was the pioneering work of Bader and co-workers who emphasized the role of $\rho(\mathbf{r})$ for the chemical bonding through its Laplacian $\nabla^2\rho(\mathbf{r})$ [Bader and Essen 1984, Bader et al. 1984]. As such $\nabla^2\rho(\mathbf{r})$ is a orbital independent electron localization function and reveals charge concentration and depletion within the charge density of a given molecular system.

The gradient of the electron density $\nabla\rho(\mathbf{r})$ is a vector. Thus, the graphical representation of the gradient field shows trajectories, i.e. the field lines of the vector field. In a molecular system the nuclei are three-dimensional attractors where the electron density exhibit local maxima. Since field lines do not cross, the space is separated into atomic regions: an atom in a molecule is defined as one attractor

and its basin. The basin is the space which contain all the trajectories associated with the attractor. The *Atoms in Molecules* (AIM) theory presented in [Bader 1990] demonstrated that such a definition of an atom is appropriate to divide observable quantities of the total system into a sum of atomic contributions. The division of the total electron density $\rho(\mathbf{r})$ (**A**) into separated atomic basins (**B**) is shown in Fig. (1.3) for ethylene.

A   **B**   **C**
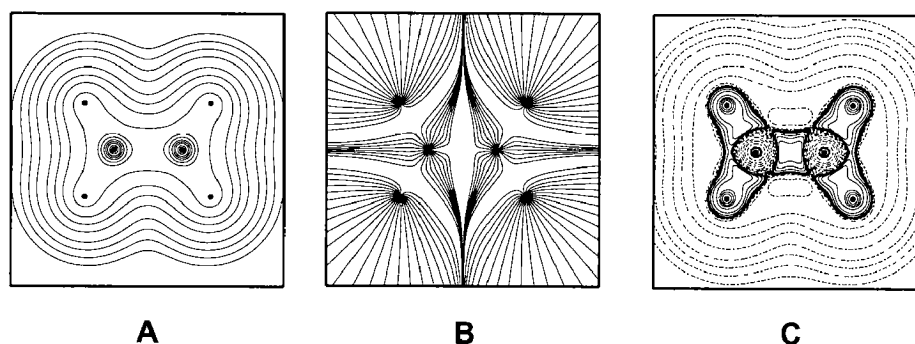
Figure 1.3: Two-dimensional contour plots of the electron density $\rho(\mathbf{r})$ (**A**), its gradient field $\nabla\rho(\mathbf{r})$ (**B**) and the corresponding negative Laplacian $-\nabla^2\rho(\mathbf{r})$ (**C**) for ethylene within the molecular plane.

Critical points (CP) of the electron density occur where the gradient of the vector field vanishes, $\nabla\rho(\mathbf{r}) = 0$. They are characterized by the Hessian matrix, the second derivative of the electron density with respect to the coordinate axes. The Hessian of ρ is a real, symmetric 3×3 matrix which yields, upon diagonalization, three eigenvalues, the *curvatures* λ_1, λ_2 and λ_3. The sign of the curvatures determine whether ρ is a minimum ($\lambda_i > 0$) or a maximum ($\lambda_i < 0$) at an extremum along the corresponding eigenvectors. CPs are classified by a tuple (ω_c, σ_c). The ω_c gives the number of eigenvalues $\neq 0$, i.e $\omega_c = 3$ for the three-dimensional case. The signature σ_c gives the sum of curvatures. Thus, a (3,+3) CP is a maximum in the electron density. Although the electron density is not defined at the nuclei position, they behave like real (3,-3) CPs and are classified as such.

A (3,-1) CP is called a bond critical point (BCP) positioned between two interacting atoms. Associated to the positive eigenvalue λ_3 there are two trajectories which start at the BCP and end at the nuclei positions. They define the bond path where the electron density ρ attains a minimum at the BCP. The mutual interatomic surface S_{AB} is spanned by the two negatively curved eigenvectors which form a plane perpendicular to the bond path (BP). The charge density in S_{AB} attains a maximum in $\mathbf{r}_b$ according to the negative values of the curvatures λ_1 and λ_2. The relative position of the BCP $\mathbf{r}_b$ given as ratio $\mathbf{X}_\alpha\text{-}\mathbf{r}_b/R_b$, together with associated properties ρ_b, $\nabla^2\rho_b$, H_b and ϵ_b allow to classify the bond as shared or closed-shell interaction. The former includes covalent, dative and metallic bonds whereas ionic, hydrogen and van der Waals bonds belong to the latter class.

The Laplacian of the electron density $\nabla^2\rho(\mathbf{r})$ is a scalar quantity. The value of $\nabla^2\rho(\mathbf{r})$ at a given point $\mathbf{r}$ is the trace $\sum_i \lambda_i$ of the Hessian of $\rho(\mathbf{r})$. In a graphical representation of the Laplacian the function plotted is usually $-\nabla^2\rho(\mathbf{r})$ on order to emphasize that the charge is concentrated where the function plotted is positive (see Fig. (1.3) (**C**)). The values of the electron density and its Laplacian at $\mathbf{r}_b$ allow to distinguish between shared and close-shell interactions. When $\nabla^2\rho_b < 0$ and large in magnitude, ρ_b is also large, concentrated along the bond path. This indicates a covalent bond. On the other hand, for ionic bonds $\nabla^2\rho_b$ is positive with relatively low ρ_b.

Cremer and Kraka [1984] introduced the local energy density $H(\mathbf{r})$, which is defined as the local kinetic energy density $G(\mathbf{r})$ (always > 0) plus the local potential energy $V(\mathbf{r})$ (always < 0). The resulting energy density at the BCP H_b is a good measurement for the covalent character of the bond. Pure covalent bonds have strongly negative H_b values whereas closed shell interactions have H_b values close to zero or even positive. Polar shared interaction can be identified with $\nabla^2\rho_b > 0$ and $H_b < 0$.

A measure of the π character of a bond is the ellipticity ϵ, defined as

$$\epsilon = \frac{\lambda_1}{\lambda_2} - 1 \quad \text{with} \quad |\lambda_1| > |\lambda_2| \tag{1.7}$$

Note that here, the indices of λ do not have to coincide with the ordering of λ_1 and λ_2 in the Hessian matrix! Rather, λ_2 is the value of curvature with the smaller magnitude. Its axis, the major axis, defines the "direction" of the ellipticity relative to the molecular frame. For a single bond the distribution of ρ around the BP is cylindrical with $\lambda_1 = \lambda_2$ and hence $\epsilon_b = 0$. For a bond with π symmetry ϵ_b is positive with a typical range $0 < \epsilon_b < 1$. The topography of λ_1 and λ_2 is illustrated graphically in Fig. (1.4) for ethylene. Since for a double bond system electron density is accumulated in the space above and below the bond path the major axis $\mathbf{a}$ is oriented perpendicular to the molecular plane, referring to the "π" domain, whereas the minor axis $\mathbf{b}$ lies in the molecular plane, referring to the "σ" domain. Note that a change in ϵ_b corresponds to the concomitant change of both curvatures λ_2 *and* λ_1, given as relative proportioning of charge concentration by the ratio λ_1/λ_2.
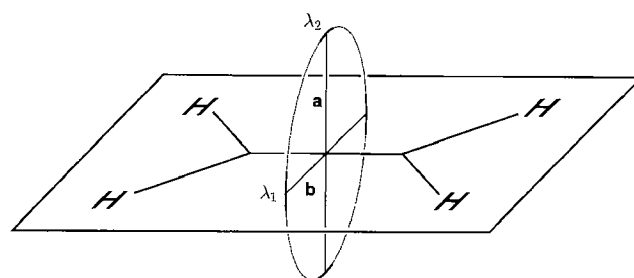
Figure 1.4: Orientation of the major ($\mathbf{a}$) and minor ($\mathbf{b}$) axes associated with the curvatures λ_2 and λ_1 relative to the molecular plane of ethylene.

1.2.2   The electron localization function ELF

Becke and Edgecombe [1990] introduced the Electron Localization Function (ELF) which is, in a simplified way, related to the probability of finding two electrons of the same spin in a given space (Pauli exclusion principle). Its definition is given in Eq. (1.8).

$$\text{ELF} = (1 + \mathcal{X}_\sigma^2)^{-1} \quad \text{with} \quad \mathcal{X}_\sigma = D_\sigma / D_\sigma^0 \tag{1.8}$$

D_σ is derived from the Hartree-Fock conditional pair probability and a measure of the electron localization, whereas D_σ^0 is the uniform-density electron gas as reference. Their ratio $\mathcal{X}_\sigma$ is therefore a calibrated dimensionless localization index so that $0 \leqslant ELF \leqslant 1$, where ELF $= 1$ corresponds to perfect localization.

Like in AIM theory, ELF is a projection of properties of the electron density which reveals the shell structure of atoms, as well as bonded and non-bonded electron pairs. Since ELF is based on the Hartree-Fock electron pair probability, it is closely related to valence shell electron pair repulsion (VSEPR) theory presented by Gillespie [1972].

According to Silvi and Savin [1994] chemical bonds can be classified in terms of Maxima of ELF localized in the bonding domain of a shared-electron interaction. The number of the so-called bond attractors is related to the bond multiplicity. As a generic topographical property of ethylene one finds two bond attractors above and below the molecular plane. This can be understood as follows: in a double bond domain, two α and two β electrons have to be hosted. The Pauli-repulsion will force the electrons with the same spin to localize in separate regions. Or in other words: although the electron density is higher on the C–C connecting line (cf. Sec. (1.2.1)), the electrons formally assigned to the double bond do not localize here due to the Pauli-repulsion. The relation of the observed distribution of bonding
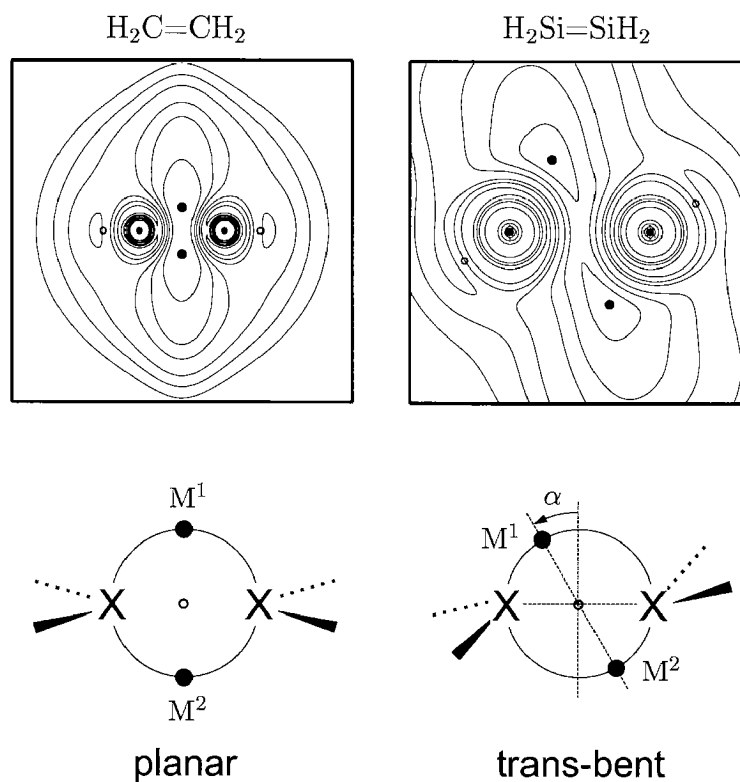
Figure 1.5: Placement of local ELF maxima M^1 and M^2 in planar (unslipped) and trans-bent (slipped) double bonds.

domains - projected from the electron density by the ELF - to the VSEPR model is evident: electron pairs try to keep a maximum distance to each other. The attractor pattern found in ethylene is retained even under trans-bent distortion as shown in [Grützmacher and Fässler 2000] for the heavier group 14 homopolar double bond systems. The bond attractors M^1 and M^2 are tilt with increasing deviation from planarity in the $H_2X=XH_2$ systems. The authors proposed two weakly separated maxima M^1 and M^2 and a local minimum on the X–X vector as a criterion for unslipped (planar) and slipped (trans-bent) double bonds, as shown graphically in Fig. (1.5)

1.3   Computational Methods

All *ab initio* calculations were performed with the program package GAUSSIAN 94 [Frisch et al. 1995]. The heteronuclear systems of the general formulas $[CXH_{3+n}]^{n+}$ with X = N, P, As, Sb and n = 0, 1, 2, discussed in Ch. (2) on page 23 were optimized at the QCISD level [Pople et al. 1987]. The similar homonuclear systems $[X_2H_{2+n}]^{n+}$, presented in Ch. (3) on page 73 were optimized at the MP2 level [Møller and Plesset 1934]. The spin-unrestricted formalism of the respective method was used for open shell species. The nature of the stationary points was investigated by means of frequency analyses, i.e. calculations of the second derivatives of the energies with respect to the nuclear coordinates. Refined energies were obtained at the CCSD(T) level [Bartlett et al. 1990].[1] For the evaluation of dissociation energies we additionally performed G2 calculations [Curtiss et al. 1991] for systems containing elements up to As.

At the level of optimization the 6-31G(d,p) basis set [Francl et al. 1983] was used for carbon and hydrogen. For the Group 15 elements X = N, P, As, Sb MEFIT type effective core potentials (ECPs) were used in conjunction with double-ζ type valence electron basis sets as presented in [Bergner et al. 1993]. These valence basis sets were augmented by one set of six Cartesian d-type polarization functions with exponents recommended in [Huzinaga 1984 , p. 23]. We refer to these basis sets as SECP-VDZP[1]. Since we did not use any other kind of basis sets we simply refer to the combined basis sets 6-31G(d,p) (C,H) + SECP-VDZP (X) as VDZP[1].

For the refined energies obtained at the CCSD(T) level the SECP-VDZP basis sets were splitted into triple-ζ type like basis sets, denoted as SECP-VTZP[1] and combined with corresponding 6-311G(d,p) basis sets for hydrogen and carbon [Krishnan et al. 1980]. This combination of all-electron and ECP basis sets is referred

---

[1]In this method the triplet excitation is approached pertubationally, indicated by (T).

Table 1.1: Computational methods. Exponents of polarization functions used in SECP-VD(T)ZP[1,2] valence electron basis sets.[a]

type			X		
		N	P	As	Sb
P[1]	d	0.864	0.340	0.293	0.211
P[2]	d[b]	0.412	0.153	0.129	0.088
		1.986	0.537	0.434	0.277
		9.573	1.885	1.460	0.872
	f[c]	1.000	0.450	0.420	0.400

[a] All d-type exponents are taken from [Huzinaga 1984]. The f-type exponents for X = N, P, As are taken from from [Frisch et al. 1984].

[b] The third exponents are derived from $(f_{pol}^2)^2/f_{pol}^1$.

[c] The exponent of the f-type polarization function for X = Sb was set close to the value of As.

to VTZP[1]. Furthermore, the SECP-VTZP basis sets were augmented with three d-type (6) and one f-type (7) polarization functions and combined with the corresponding all-electron basis sets 6-311G(3df,2p). This combination refers to VTZP[2]. The exponents used for the polarization functions in the various SECP-VD(T)ZP[1,2] valence basis sets are collected in Tab. (1.1). In the SECP-VTZP[2] basis sets the third d-type exponents were derived from Huzinaga's two-membered polarization sets according to $(f_{pol}^2)^2/f_{pol}^1$. For nitrogen, phosphorus and arsenic the f-type functions were taken from [Frisch et al. 1984].

Calculations with all-electron basis sets [6-31G(d,p),6-311G(d,p)] have been carried out systematically for the compounds with second and third row elements in order to validate the quality of the combined basis sets VD(T)ZP[1,2].[2] In general,

---

[2]In some cases for systems with X = As, all-electron calculations were performed using the 6-311G(d,p) basis set derived for fourth row elements [Curtiss et al. 1995].

the results from these all-electron calcualtions are consice with the findings obtained
by the combined basis sets. All-electron calculations were considered wherever it
was necessary to verify the findings obtained by VD(T)ZP[1,2].

For the various systems considered, atomic charges as well as orbital occupan-
cies were calculated at the levels of optimization according to the NBO analysis
developed by Reed et al. [1988] and implemented in GAUSSIAN 94.

The topographical analyses of the electron density distribution has been carried
out at the level of optimization using the geometries obtained with the combined
basis set VDZP[1]. The Bader analyses as well as the ELF calculations have been
performed with the program package MORPHY98 [Popelier 1998]. Because the
ECP approach may lead to incorrect electron densities [Sierraalta and Ruete 1994,
Vyboishchikov et al. 1996], all electron basis sets were employed in order to calcu-
late the required input wave function files in GAUSSIAN94. For elements of the
first three rows the 6-31G(d,p) basis sets were used. For arsenic and antimony the
(4333/433/4) and (43333/4333/43) basis sets from [Huzinaga 1984] were taken, and
splitted into (43321/4321/311) and (433321/43321/4311) basis sets, respectively, in-
cluding one additional set of Huzinagas d-type polarization function (for exponents
see entries for P[1] in Tab. (1.1)).

1.3.1   Determination of proton affinities

The gas phase proton affinity PA of a molecule B is defined as the negative reaction
enthalpy of the protonation reaction (Rxn. 1.1) and can be calculated according to
Eq. (1.9) [DeFrees and McLean 1986].

$$\text{B} \ + \ \text{H}^+ \ \longrightarrow \ \text{BH}^+, \quad \text{PA} \equiv -\Delta H_{298} \qquad\qquad \text{(Rxn. 1.1)}$$
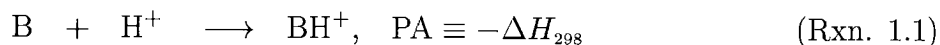
$$\Delta H_{298} = \Delta E^{\text{elec}} + \Delta E^{\text{vib}}_{298} + \Delta E^{\text{rot}}_{298} + \Delta E^{\text{trans}}_{298} + \Delta (pV)_{298} \qquad\qquad (1.9)$$

The electronic energy change ΔE^{elec} for the proton transfer reaction (Rxn. 1.1) were computed using ab initio methods as described above. The vibrational energy differences, $\Delta E_{298}^{\text{vib}}$, were derived using standard statistical mechanical formulas and unscaled vibrational frequencies at the respective levels of theory. The rotational and translational energies, $\Delta E_{298}^{\text{rot}}$ and $\Delta E_{298}^{\text{trans}}$, as well as the pressure-volume work term $\Delta(pV)_{298}$, were calculated classically to be $5RT/2$ (1.5 kcal mol^{-1} at 298 K) for reaction (Rxn. 1.1). Thus, the PA may be written as

$$\text{PA} = -\Delta E^{\text{elec}} - \Delta E_{298}^{\text{vib}} + 5RT/2 \qquad (1.10)$$

1.3.2   Determination of bond energies

The dissociation energy D_{e} of a double bond system $\text{F}^1{=}\text{F}^2$ (planar or trans-bent) is the reaction enthalpy of the dissociation reaction (Rxn. 1.2).

$$\text{F}^1{=}\text{F}^2 \quad \longrightarrow \quad \text{F}^1 \quad + \quad \text{F}^2 \qquad (\text{Rxn. 1.2})$$
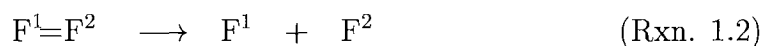
In this process the double bond $\text{F}^1{=}\text{F}^2$ is cleaved homolytically into the ground states of each fragment F^1 and F^2. Thus, D_{e} is equal to the energy difference between the sum over the total energies of F^1 and F^2, minus the total energy of the double bond system $\text{F}^1{=}\text{F}^2$, according to Eq. (1.11). Correction of D_{e} with respect to the difference in zero-point energies, yields the dissociation energy at 0 K, D_0 (Eq. (1.12)).

$$D_e = E(\text{F}^1 + \text{F}^2) - E(\text{F}^1{=}\text{F}^2) \qquad (1.11)$$

$$D_0 = D_e + \Delta\text{ZPE}$$

$$= D_e + \{\text{ZPE}(\text{F}^1 + \text{F}^2) - \text{ZPE}(\text{F}^1{=}\text{F}^2)\} \qquad (1.12)$$

In general, the ZPE of the molecule is higher than the sum of the fragment ZPEs, i.e. ΔZPE $<$ 0 and therefore $D_0 < D_e$. For a graphical explanation of D_e and D_0 see Fig. (1.6).
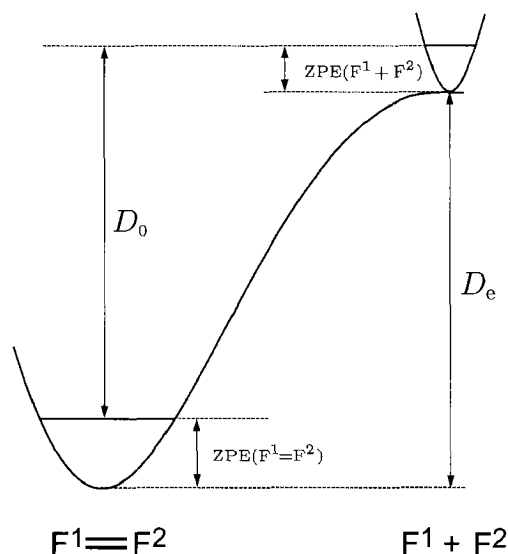
Figure 1.6: Schematic representation of the dissociation of a double bond system $F^1=F^2$ into its ground state fragments F^1 and F^2, together with the corresponding energetic terms D_e and D_0.

The determination of D_e values for doubly bonded systems requires high levels of theory since (Rxn. 1.2) is not isodesmic and involves cleavage of an electron dense 2c-4e bond. Langhoff and W. Bauschlicher [1991] showed that for doubly bonded systems (e.g. N_2H_2) very large basis sets with polarization functions up to h are needed in order to achieve chemical accuracy (± 1.0 kcal mol^{-1}) for D_e. The workload of such calculations is very large and only applicable for small systems containing elements of the first two rows. Alternatively, an extrapolation procedure can be employed, such as the G2 method [Curtiss et al. 1991], which accounts for the remaining basis set incompleteness. It is well known that within the G2 approach

excellent results are obtained with relatively low computational costs.[3] We made use of this method in order to have reliable dissociation energies for systems containing elements up to As, as a reference for the corresponding values calculated at the CCSD(T) level, using the combined basis sets VTP[1,2].

The total bonding energies ΔE_{TBE} and ΔE^0_{TBE} refer to the dissociation energies D_e and D_0, respectively. However, one should be aware that dissociation enthalpies reflect both the strength of a bond *and* the stability of the fragments formed. Furthermore, considerable care must be taken when choosing a value for $E_{\sigma+\pi}$. According to Trinquier and Malrieu [1987] the energy term $E_{\sigma+\pi}$ was introduced as the intrinsic bond strength of a classical *planar* double bond (see Fig. (1.2)). Thus, we define the $E_{\sigma+\pi}$ values as the (ZPE uncorrected) energy difference between the fragments F^1 and F^2 in their triplet state and the double bond system $F^1=F^2$ in its planar form.
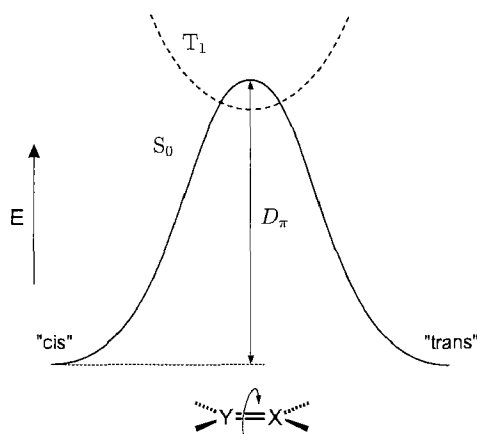
Scheme 1.5

The π-bond strength of a double bond system is of central importance, showing how much the π_{pp} interaction contributes to the total bond energy ΔE_{TBE}. As depicted in Scheme 1.5, Schmidt et al. [1987] first derived π-bond energies from

---

[3]in GAUSSIAN 94 the G2 method is implemented for molecules containing elements up to Kr.

rotational barriers D_π of the cis $\rightarrow$ trans isomerization of the double bond systems $H_2Y{=}XH_2$. In this process, one fragment is rotated around the Y–X axis, while the π-bond breaks homolytically. On the ground state singlet surface S_0 the transition state of this reaction is a closed-shell biradical. On the corresponding triplet surface T_1, rotation is leading to a local minima which is identical to the twisted singlet, apart from the spin coupling of the unpaired electrons. Thus, according to Hund's rule, the triplet minima is expected to lie below the rotated singlet.[4] Accordingly, we approximated D_π of a double bond system from the energy differences between the singlet and twisted triplet minima of its S_0 and T_1 hypersurfaces.

However, there are some problems to consider when using D_π as the definition of a π-bond strength. Firstly, residual π interactions in the twisted conformation of a double bond $H_2Y{=}XH_2$ may still be present in the rotated triplet minima. Moreover, the rotation process itself may lead to new π interactions. Secondly, the Y–X bond length changes during the isomerization process. Possible pyramidalization at the Y or X centers causes a rehybridization of the σ-bond. Nevertheless, these troublesome interactions are always stabilizing the rotation transition state and hence its corresponding triplet form as well. Thus, the D_π values evaluated by this method can be regarded as *lower-limits* of the real π-bond strengths.

---

[4]This rule can be violated in terms of "dynamical spin polarization" [Kollmar and Staemmler 1978] or "antiferromagnetic coupling" [Voter et al. 1985] with ethylene as the most prominent example.

2. Heteronuclear Double Bonding Between Carbon and Group 15 Elements: Methylene pnictanes and pnicto carbenium ions

The first isolable *acyclic* methylene phosphane was the result of an unexpected silyl migration from P to O when Becker [1976] was working on the synthesis of P-silylated acyl-phosphanes. This was the starting point for a rapid exploration which has been furnished many other compounds containing the C=P functional group with bond lengths of $1.62 - 1.71$ Å (for acyclic systems). Two books offer an excellent overview of methylene phosphanes and related multiply bonded systems [Appel 1990, Dillon et al. 1998]. The first synthesis of an methylene arsanes was reported by Becker and Gutekunst [1977]. Today more than 20 compounds, featuring arsenic-carbon multiple bonds, have been isolated and recently reviewed by Weber [1996]. Among these, eight species with acyclic doubly bonded arsenic have been structurally characterized (see for instance in [Power 1999 , p. 3482]). They display a wide range of C=As bond distances from 1.794 Å to 1.876 Å. In most cases, the bond elongation can be rationalized by the interaction of the C=As double bond and a heteroatom lone-pair in α position to the carbon atom, e.g. $-\ddot{N}-C=As$. In contrast, only three compounds featuring carbon-antimony double bonds have been structurally characterized at present, two dimers $[Sb=C(OSiMe_3)R]_2$ (R = Mes, Mes*) [Hitchcock et al. 1995] and one Mes*(O)C–Sb=C(OH)Mes* [Jones et al. 1999]. At present there are no stable examples of bisma alkenes.

Monocationic systems of type $[R_2C=XR_2]^+$ have been studied in the context of α-heteroatom stabilized carbocations. Of course, the corresponding imminium ions $R_2NCR_2^{\oplus}$ are long known structural motifs in synthetic chemistry (for instance, see in [Ohla and Schleyer 1976, Volkmann 1991]). In contrast, for the higher congeners, only methylenephosphonium salts have been synthesized by Grützmacher and co-workers, from P-chloro-phosphorus ylides by chloride abstraction with $AlCl_3$ [Heim et al. 1993, Grützmacher and Pritzkow 1992, 1991, Igau et al. 1989].

2.1 Selected molecular structures of CXH_3 and their protonated forms $[CXH_4]^+$.

The various structures investigated are presented in Fig. (2.1), corresponding structural data is given in Tab. (2.2) (**A**) and Tab. (2.3) (**B**). The folding or flap angle ϕ_X are used throughout the text as a measure of the deviation from planarity of a pyramidalized atomic center X within a molecule. In Scheme 2.1 the flap angles $\phi_{C,X}$ are shown graphically for a trans-bend double bond C=X. Calculated total and relative energies for all species are presented in Tab. (2.1).
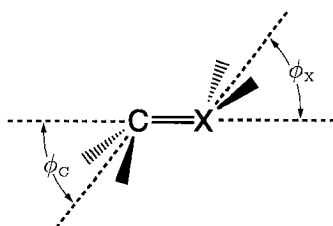
Scheme 2.1

The imine $H_2C=NH$ (**X-1a**) and all heavier congeners have planar C_s symmetric geometries. The shortening of the C=X bond with respect to the single C–X bond lengths in the substituted neutral methanes H_3C–XH_2 decreases in the order N < P < As < Sb, ranging from 12.7% to 8.6%. The reference single bonds are calculated to be as follows: C–N 1.464 Å, C–P 1.887 Å, C–As 1.990 Å, C–Sb 2.193 Å. The angle $\angle CXH(3)$ approach 90 ° as X goes down the group from N to Sb. This is a direct consequence of the reluctance of the heavier p-block elements to maintain sp²-hybridization. The corresponding twisted isomers **X-2a** were optimized as open-shell biradicals in C_s symmetry. Frequence analyses identified these stationary points as minima on the triplet hypersurfaces. In principle, two geometries are possible with the carbon center pyramidalized cis ("tent") or trans ("plough") with respect to XH. However, Schoeller et al. [1997] showed that the energy differences

Table 2.1: C=X double bond systems. Energetics for neutral methylene pnictanes $H_2C=XH$, their protonated derivatives $[H_2C=XH_2]^+$ and related systems (X = N, P, As, Sb).[a]

		E_{opt}	ZPE	N	E_{ref}^1 [c]	E_{ref}^2 [d]	ΔE_{opt}	$\Delta E_{\mathrm{ref}}^1$ [c]	$\Delta E_{\mathrm{ref}}^2$ [d]
					CCSD(T)/BS(2,3)//QCISD/BS(1)[b]				
N-1a		−49.638509	25.6	0	−49.675571	−49.729306	0.0	0.0	0.0
N-2a	($^3A''$)	−49.534150	23.0	0	−49.567975	−49.620816	62.9	64.9	65.5
N-3a		−50.852995	41.4	0	−50.890355		0.0	0.0	
N-4a		−50.842167	40.2	1	−50.877797		5.7	6.8	
N-5a		−49.994310	34.9	0	−50.024762	−50.075402	0.0	0.0	0.0
N-7a	($^1A'$)	−49.872326	30.9	1	−49.905529	−49.958331	72.6	70.9	69.5
	($^3A''$)	−49.861628	30.7	0	−49.890139	−49.938311	79.1	80.3	81.9
N-8a	($^1A_1$)	−49.861247	36.1	1	−49.891106	−49.944759	84.7	85.1	83.2
	($^3B_1$)	−49.861561	30.3	1	−49.890043	−49.938228	78.7	79.9	81.5
P-1a		−46.236208	21.4	0	−46.274535	−46.340729	0.0	0.0	0.0
P-2a	($^3A''$)	−46.171964	19.4	0	−46.205920	−46.269792	37.6	40.0	41.4
P-3a		−47.461190	34.9	0	−47.499633		0.0	0.0	
P-4a		−47.401647	33.9	1	−47.441141		36.4	35.7	
P-5a		−46.534065	26.9	0	−46.571108	−46.635776	0.0	0.0	0.0
P-7a	($^1A'$)	−46.471588	25.3	1	−46.504794	−46.567220	37.6	40.0	41.4
	($^3A''$)	−46.469354	25.7	0	−46.502002	−46.564687	39.4	42.1	43.4
P-8a	($^1A_1$)	−46.382448	33.3	1	−46.415921	−46.479994	101.6	103.8	104.2
	($^3B_1$)	−46.463368	24.9	1	−46.496264	−46.558211	42.4	45.0	46.7
As-1a		−45.882527	20.5	0	−45.918918	−45.972115	0.0	0.0	0.0
As-2a	($^3A''$)	−45.826393	18.7	0	−45.857651	−45.909606	33.4	36.6	37.4
As-3a		−47.107578	33.7	0	−47.144217		0.0	0.0	
As-4a		−47.032927	33.0	1	−47.070541		46.2	45.6	
As-5a		−46.167680	25.6	1	−46.202717	−46.252974	−0.1	−0.1	−0.3
As-6a		−46.168022	25.8	0	−46.202944	−46.252895	0.0	0.0	0.0
As-7a	($^1A'$)	−46.123412	24.2	1	−46.153840	−46.203329	26.3	29.2	29.5
	($^3A''$)	−46.114416	24.6	0	−46.145102	−46.193403	32.4	35.1	36.1
As-8a	($^1A_1$)	−46.009237	24.6	1	−46.049076	−46.103680	98.4	95.3	92.4
	($^3B_1$)	−46.105052	23.9	1	−46.135819	−46.184251	37.6	40.2	41.1
Sb-1a		−45.079396	19.4	0	−45.120440	−45.173442	0.0	0.0	0.0
Sb-2a	($^3A''$)	−45.037806	17.9	0	−45.072971	−45.124763	24.6	28.3	29.1
Sb-3a		−46.307095	31.9	0	−46.349004		0.0	0.0	
Sb-4a		−46.227477	31.4	1	−46.269776		49.5	49.2	
Sb-5a		−45.357302	23.8	1	−45.399548	−45.449582	2.0	1.2	1.0
Sb-6a		−45.360810	24.0	0	−45.401865	−45.451533	0.0	0.0	0.0
Sb-7a	($^1A_1$)	−45.328150	22.6	1	−45.363288	−45.412438	19.0	22.7	23.1
	($^3A''$)	−45.323706	23.0	0	−45.361304	−45.410189	22.2	24.4	24.9
Sb-8a	($^1A_1$)	−45.223447	23.2	1	−45.270845	−45.325461	85.3	81.4	78.3
	($^3B_1$)	−45.310263	22.3	1	−45.347802	−45.396463	30.0	32.2	32.8

[a] Total energies E in Hartrees, ZPE and relative energies ΔE (including unscaled ZPE corrections) in $\mathrm{kcal\,mol}^{-1}$. N: number of imaginary frequencies. For a graphical representation of the structures see Fig. (2.1).

[b] BS(1): VDZP[1]; BS(2): VTZP[1]; BS(3): VTZP[2].

[c] Refined energies obtained using BS(2).

[d] Refined energies obtained using BS(3).

A

B
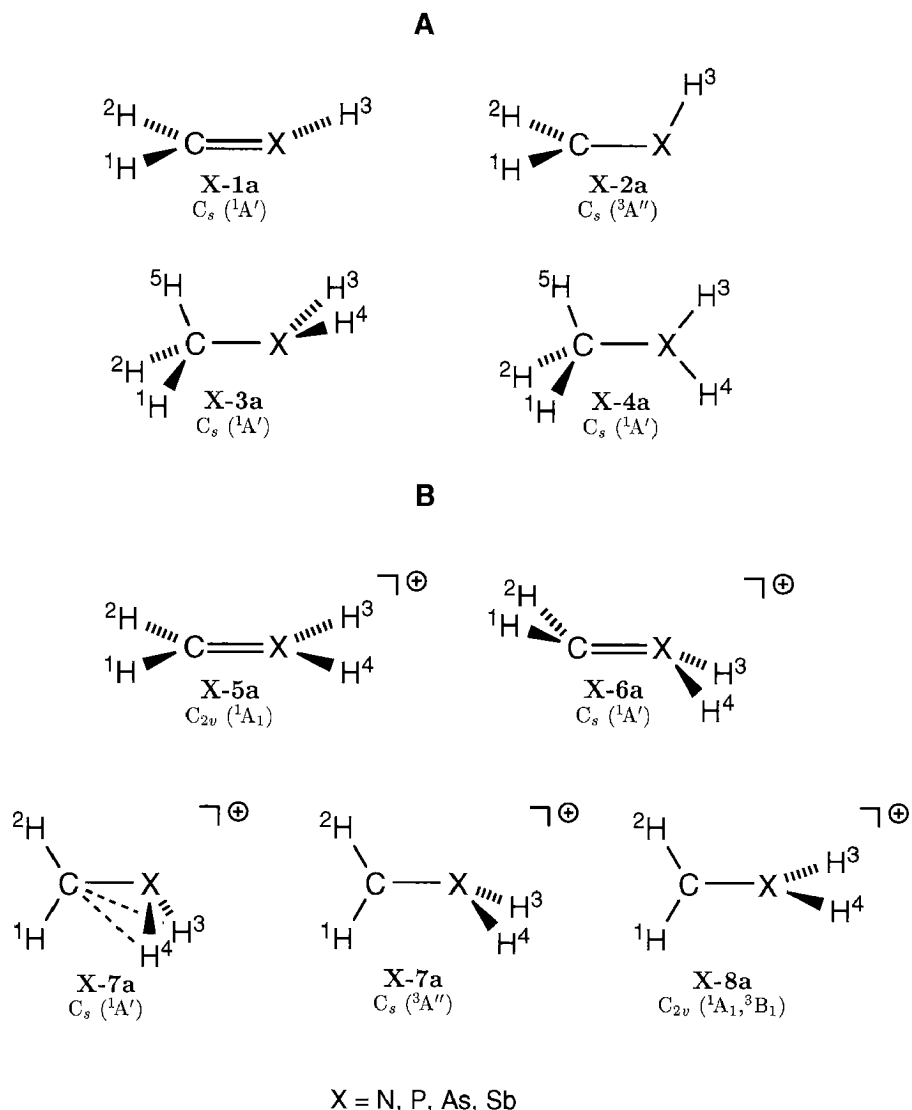
X = N, P, As, Sb

Figure 2.1:   Optimized structures for the neutral pnicto-alkenes CXH₃ (**A**), their protonated derivatives [CXH₄]⁺ (**B**) and related systems. For bonding parameters see Tab. (2.2).

between these isomers are marginal ($< 1.0\ \mathrm{kcal\,mol^{-1}}$) for all X = N, P, As, Sb. We therefore re-examined only the trans isomers. In **N-2a** the carbon center is strongly pyramidalized ($\phi_C = 34.4\ °$). In the heavier homologues **X-2a**, an almost planar geometry is preserved around the CH₂ moiety for all X = P, As, Sb ($\phi_C = 7.5\ °$, 5.8 °, 3.7 °). The C–X bonds are elongated compared to the corresponding C=X

Table 2.2: C=X double bond systems. Selected structural data for the neutral methylene pnictanes $H_2C=XH$ (**X-1a**) and related systems (X = N, P, As, Sb).[a]

symmetry/ state	parameters	X			
		N	P	As	Sb
X-1a C_s $^1A'$	CX	1.277	1.693	1.796	2.005
	XH(3)	1.021	1.432	1.525	1.720
	H(1)CH(2)	116.0	116.0	116.0	115.2
	H(1)CX	118.6	119.3	119.5	120.9
	H(2)CX	125.4	124.7	124.5	123.8
	CXH(3)	109.3	97.0	95.6	94.2
X-2a C_s $^3A''$	CX	1.394	1.820	1.931	2.141
	XH(3)	1.025	1.437	1.531	1.724
	H(1)CH(2)	116.3	117.4	117.1	116.3
	H(1)CX	115.8	121.0	121.3	121.8
	CXH(3)	111.6	97.8	95.8	94.4
	ϕ_C	34.4	7.5	5.8	3.7
X-3a C_s $^1A'$	CX	1.464	1.887	1.990	2.193
	XH(3)	1.013	1.425	1.518	1.713
	H(1)CX	109.0	108.6	108.6	109.1
	H(5)CX	115.4	112.7	112.3	110.8
	CXH(3)	109.1	97.0	95.3	94.0
	H(3)XH(4)	105.5	93.3	92.0	91.5
	ϕ_X	57.3	79.8	82.4	84.4
X-4a C_s $^1A'$	CX	1.434	1.851	1.945	2.154
	XH(3)	0.995	1.383	1.464	1.650
	CXH(3)	121.0	120.2	120.0	121.7
	H(3)XH(4)	117.9	118.0	118.2	118.3

[a] QCISD/VDZP[1] data. Bond lengths in Å, angles in degrees (°). The CH bond lengths are omitted (≈ 1.09 Å). Numbering as in Fig. (2.1).

bond distances in the planar isomers **X-1a**, and slightly shorter by $0.05 - 0.07$ Å than the reference C–X single bonds in H_3C–XH_2. This is mainly due to the broken π-bond in the **X-2a** isomers. The corresponding π-bond strengths are discussed in Sec. (2.2.1).

Protonation of the pnictogen lone-pair in $H_2C=XH$ is leading to the monocationic derivatives $[H_2C=XH_2]^+$. Formally, the core functional group, i.e. the double bond system, remains preserved in that process. In a recent study, Kapp et al. [1996] investigated these monocations at the MP2 level. At this level of theory, all

Table 2.3: C=X double bond systems. Selected structural data for the pnicto carbenium ions $[H_2C=XH_2]^+$ (**X-5a**/**X-6a**) and related systems (X = N, P, As, Sb).[a]

symmetry/ state		parameters	X			
			N	P	As	Sb
X-5a C_{2v} $^1A_1$		CX	1.281	1.656	1.749	1.952
		XH(3)	1.016	1.396	1.475	1.657
		H(1)CH(2)	121.0	120.0	120.5	120.0
		H(1)CX	119.5	120.0	119.7	120.0
		CXH(3)	121.6	121.1	121.1	121.5
		H(3)XH(4)	116.8	117.8	117.8	117.1
X-6a C_s $^1A'$		CX			1.765	2.008
		XH(3)			1.478	1.669
		H(1)CH(2)			119.4	116.8
		H(1)CX			119.6	120.0
		CXH(3)			117.5	110.5
		H(3)XH(4)			115.4	110.6
		ϕ_C			11.4	17.5
		ϕ_X			30.1	51.9
X-7a C_s $^1A'$		CX	1.359	1.846	1.965	2.217
		XH(3)	1.037	1.449	1.540	1.724
		H(1)CH(2)	117.5	115.4	114.8	113.4
		H(1)CX	124.1	122.3	122.2	121.3
		H(2)CX	118.4	122.3	123.1	125.3
		CXH(3)	107.4	85.5	83.8	82.1
		H(3)XH(4)	98.7	84.8	84.3	86.1
		ϕ_X	62.7	96.2	98.4	100.9
	$^3A''$	CX	1.409	1.785	1.888	2.093
		XH(3)	1.024	1.408	1.491	1.678
		H(1)CH(2)	123.5	121.8	122.3	121.5
		H(1)CX	116.9	118.6	118.2	118.4
		CXH(3)	121.4	115.2	113.5	111.7
		H(3)XH(4)	116.4	109.3	108.2	106.8
		ϕ_C	17.3	0.0	0.0	0.0
		ϕ_X	0.0	42.6	47.3	51.7
X-8a C_{2v} $^1A_1$		CX	1.343	1.850	1.713	1.926
		XH(3)	1.015	1.390	1.533	1.725
		H(1)CH(2)	116.3	115.6	121.2	124.0
		H(1)CX	121.8	122.2	119.4	118.0
		CXH(3)	121.4	113.3	129.8	131.2
		H(3)XH(4)	117.2	133.4	100.4	97.7
	$^3B_1$	CX	1.408	1.785	1.887	2.090
		XH(3)	1.024	1.401	1.480	1.662
		H(1)CH(2)	125.0	122.3	123.1	122.7
		H(1)CX	117.5	118.8	118.5	118.6
		CXH(3)	121.8	121.9	121.6	121.5
		H(3)XH(4)	116.4	116.1	116.7	117.0

[a] QCISD/VDZP[1] data. Bond lengths in Å, angles in degrees (°). The CH bond lengths are omitted ($\approx$ 1.09 Å). Numbering as in Fig. (2.1).

four structures prefer planar geometries. At the QCISD level, the global minimum of the methyleneammonium and methylenephosphonium cation, $[H_2C=NH_2]^+$ and $[H_2C=PH_2]^+$, indeed corresponds to the C_{2v} symmetric planar structures **N-5a** and **P-5a** respectively. In contrast, for $[H_2C=AsH_2]^+$ the frequence analysis revealed the trans-bent C_s-symmetric structure **As-6a** ($\phi_{As} = 30.1$ °, $\phi_C = 11.4$ °) to be the global minimum, whereas the planar isomer **As-5a** was identified as transition state. However, without ZPE correction **As-5a** is only 0.1 kcal mol^{-1} higher in energy than **As-6a**. Inclusion of the ZPE reverses this ordering making **As-5a** 0.1 kcal mol^{-1} lower in energy than **As-6a**. Refinement of the energies at the CCSD(T) level even pronounce this discrepancy. Optimization at the QCISD/6-311G(d,p) level shows the same energetic inconsistency but the trans-bent geometry is flattened ($\phi_{As} = 10.2$ °,$\phi_C = 4.2$ °). With the 6-311G(df,p) basis set $[H_2C=AsH_2]^+$ then re-converges to a planar minimum again. From this, we conclude that the hypersurface around the ground state minimum of $[H_2C=AsH_2]^+$ is difficult to describe accurately with respect to the geometrical distortion from planar C_{2v} to trans-bent C_s symmetry. Going from the arsenium to the stibonium system the trans bending increase ($\phi_C = 17.5$ °, $\phi_{Sb} = 51.9$ °) and **Sb-6a** was located as true minima on the hypersurface, 2.0 kcal mol^{-1} more stable than the planar transition state **Sb-5a**. Refinement of the total energies at the CCSD(T) level lower this energy difference to only 1.0 kcal mol^{-1}.

On the basis of these findings we can state that the monocationic systems $[H_2C=XH_2]^+$ become more stable towards a trans-bending with increasing atomic number: distortion from the the planar (**X-5a**, C_{2v}) to the trans-bent geometry (**X-6a**, C_s) stabilizes the heavier element C=X bonds at least for X = Sb. However, as the steric bulk of the substituents increases, the steric repulsion will drastically become larger compared to the stabilizing orbital interactions. Since the successful synthesis of such compounds certainly requires very bulky substituents we can expect that real, yet not known cations $[R_2C=AsR_2]^+$ or even $[R_2C=SbR_2]^+$ have

planar geometries. Iminium ions $[R_2C=NR_2]^+$ are already long known as "rock stable" planar structural motifs in molecular systems (for instance, see Ohla and Schleyer [1976]). Furthermore, all experimentally known methylenephosphonium cations adopt a planar ground state geometry. They are, however, twisted around the C=P bond by $11-22\,°$ owing to steric interaction of the bulky substituents, as shown by Grützmacher and Marchand [1997]. On the other hand, the frequency analysis of $[H_2C=PH_2]^+$ reveals low-energy vibrational modes towards pyramidalization of the pnictogen centers. At the QCISD/VDZP[1] level, these mode is calculated to $229\ cm^{-1}$ for X = P, compared to $967\ cm^{-1}$ for X =N. For the planar transition states **As-5a** and **Sb-5a**, the imaginary frequencies of the bending mode increase from $184i\ cm^{-1}$ to $317i\ cm^{-1}$. This indicates that the PES for the stibonium system is steeper along the bending coordinate than for the arsenium system. Notwithstanding, both PESs for $[H_2C=XH_2]^+$ (X = As, Sb) along the trans-bending mode are still much flatter than for $[H_2C=NH_2]^+$. Thus, the heavy element analogues of the imminium can be described as *soft double bonds*. Note the close relation to the neutral boron-pnictogen species R_2B-XR_2 due to the isoelectronic relationship between the units BR_2 and $\overset{\oplus}{C}R_2$. Driess and Grützmacher [1996] discussed a series of trans-bent boronphosphanyls, reported in [Pestana and Power 1991, Power 1990], for which the folding at the P center ($\phi_P = 2-60\,°$) is a function of the steric bulk.

We now turn to a discussion of the molecular structures for the twisted isomers of the monocations $[H_2C=XH_2]^+$. Both the C_s (**X-7a**), as well as the C_{2v} (**X-8a**) symmetric species, have been optimized as singlets and triplets (biradicals). The singlet closed-shell species **X-7a** ($^1A'$) and **X-8a** ($^1A_1$) were located as transition states on the ground state hypersurface of $[CXH_4]^+$. In the singlet C_s-symmetric structures **X-7a**, the XH_2 units are strongly pyramidalized and bent in such a way that the hydrogen atoms adopt semi-bridging positions between the X and carbon atoms (X = N: $\phi_N = 62.7\ Å$, $\angle CNH(3) = 107.4\ Å$; X = P: $\phi_P = 96.2\ Å$, $\angle CPH(3) = 85.5\ Å$; X = As: $\phi_{As} = 98.4\ Å$, $\angle CAsH(3) = 83.8\ Å$; X = Sb: $\phi_{Sb} = 100.9\ Å$, $\angle CSbH(3)$

$= 82.1$ Å). The reason for this is twofold. Firstly, the dative π-bond between the formally empty p orbital at the carbenium center and the pnictogen lone-pair is broken and cannot compensate the increasing inversion barrier for N $\ll$ P $<$ As $<$ Sb at the XH_2 centers anymore. Secondly, the singlet rotamers **X-7a** are further stabilized by positive hyperconjugative interaction between the overlapping twisted p orbital at the carbon center and the X–H σ bonds. The phenomenon of partial transfer of the XH_2 hydrogens to the carbon center in the 90 ° rotated forms has been previously discussed for $[H_2C=PH_2]^+$ by White et al. [1988]. Compared to the corresponding singlet C_{2v} symmetry restricted isomers **X-8a** they are more stable by 13.7 kcal mol^{-1} for X $=$ N, 62.8 kcal mol^{-1} for X $=$ P, 62.9 kcal mol^{-1} for X $=$ As, and 55.2 kcal mol^{-1} for X $=$ Sb. The high energy difference between the twisted singlet **X-8a** and $[H_2C=XH_2]^+$ should not be identified as their π-bond strengths, as is was done by Kapp et al. [1996], since these energy gaps also include contributions of the corresponding increasing planarization energies when X goes down the row from N to Sb.

In order to obtain suitable π-bond energies for the monocationic ground states of $[H_2C=XH_2]^+$, we also calculated the structures **X-7a** and **X-8a** in their triplet states. The C_s symmetric biradicals **X-7a** are true minima on the triplet hypersurface, which are close in energy to the singlet biradical transition states of the $[H_2C=XH_2]^+$ cis $\rightarrow$ trans isomerization. We will discuss the π-bond energies in the following section, together with the corresponding π-bond energies of the neutral ground state structures $H_2C=XH$. The XH_2 centers in the triplet minimum structures are less pyramidalized as in the corresponding singlet states (X $=$ N: $\phi_C =$ 17.3 Å, $\angle CNH(3) = 121.4$ Å; X $=$ P: $\phi_P = 42.6$ Å, $\angle CPH(3) = 115.2$ Å; X $=$ As: $\phi_{As} = 47.3$ Å, $\angle CAsH(3) = 113.5$ Å; X $=$ Sb: $\phi_{Sb} = 51.7$ Å, $\angle CSbH(3) = 111.7$ Å). Note that for triplet **N-7a** the pnictogen center remains planar, whereas the carbon center is pyramidalized. The C_{2v} symmetric triplets **X-8a** are located as transition

states of the XH_2 inversion (CH_2 for $X = N$) on the T^1 hypersurface. These barriers range from $0.4\,\mathrm{kcal\,mol^{-1}}$ ($X = N$) to $7.9\,\mathrm{kcal\,mol^{-1}}$ ($X = Sb$).

2.2   Properties of $H_2C{=}XH$ and their protonated derivatives $[H_2C{=}XH_2]^+$.

In Tab. (2.4) we compare our calculated $C{=}X$ bond lengths of the neutral and mono-cationic systems $H_2C{=}XH$ and $[H_2C{=}XH_2]^+$ at various levels of theory (this work) with a representative selection of other recent *ab initio* calculations (others) and experimental data (exp), where possible. For further information see the literature cited or [Power 1999 and references therein].

In general, our QCISD bond lengths for the neutral methylene pnictanes are only slightly shorter by $0.01 - 0.02$ Å, compared to the MCSCF results reported in [Schmidt et al. 1987, Schoeller et al. 1997], and in good agreement with experimental values, except for $H_2C{=}SbH$. However, the $C{=}Sb$ bond length in $Mes^*(O)C{-}Sb{=}C(OH)Mes^*$ is certainly elongated owing to substituent effects. Thus, $d_{C=Sb} = 2.078$ Å must be placed in the upper end of the scale of $C{=}S$ bond lengths. For the protonated derivatives $[H_2C{=}XH_2]^+$ the QCISD bond lengths for the planar structures **X-5a** are in good agreement with the MP2 values reported in [Kapp et al. 1996]. In $[H_2C{=}AsH_2]^+$ and $[H_2C{=}SbH_2]^+$ bond elongation is observed going from the planar (**X-5a**) to the trans-bent (**X-6a**) systems. With the increasing atomic number of X, the effect of bond lengthening also increases: 0.016 Å for $X = As$ and 0.056 Å for $X = Sb$, respectively. We also find their flap angle ϕ_X following the same trend, increasing from $30.1\,^\circ$ ($X = As$) to $51.9\,^\circ$ ($X = Sb$). Note that for $[H_2C{=}AsH_2]^+$ we observed that the folding is very sensitive with respect to the basis set used. Thus, the values for $\phi_{C,X}$ should be taken as a qualitative trend rather than absolute quantities.

Table 2.4: C=X double bond systems. Comparison of calculated and experimental equilibrium C=X bond lengths R_e and flap angles $\phi_{C,X}$ for the neutral methylene pnictanes $H_2C=XH$ (**X-1a**) and the pnicto carbenium ions $[H_2C=XH_2]^+$ (**X-5a/X-6a**).[a]

	this work[b]						others	exp
	6-31G(d,p)		6-311G(d,p)		VDZP			
	R_e	$\phi_{C,X}$	R_e	$\phi_{C,X}$	R_e	$\phi_{C,X}$	R_e	$d_{C=X}$
N-1a	1.279	0.0			1.277	0.0	1.289[c] 1.282[d]	1.273[i]
N-5a	1.283	0.0			1.281	0.0	1.281[d] 1.282[e]	
P-1a	1.680	0.0			1.693	0.0	1.700[c] 1.716[f]	1.671[j]
P-5a	1.646	0.0			1.656	0.0	1.624[g] 1.638[e]	1.683[k]
As-1a			1.792	0.0	1.796	0.0	1.823[f] 1.790[h]	1.794[l]
As-5a			1.750	0.0	1.749	0.0	1.746[e]	
As-6a			1.752	10.2 (4.2)	1.765	30.1 (11.4)		
Sb-1a					2.005	0.0	2.022[f] 2.010[h]	2.078[m]
Sb-5a					1.952	0.0	1.945[e]	
Sb-6a					2.008	51.9 (17.5)		

[a] Bond lengths in Å, angles in deg. ϕ_X denotes the fold angle for the XH_2 fragment. ϕ_C denotes the fold angle for the CH_2 fragment (given in parentheses). See Scheme 2.1 for graphical explanation. Experimental C=X distances are denoted as $d_{C=X}$.

[b] QCISD/VDZP[1] data.

[c] in [Schmidt et al. 1987] (MCSCF).

[d] in [Wang and Poirier 1997] (GVB).

[e] in [Kapp et al. 1996] (MP2).

[f] in [Schoeller et al. 1997] (MCSCF).

[g] in [Lohr et al. 1984] (HF).

[h] in [Dobbs et al. 1987] (HF).

[i] in [Harmony et al. 1979] ($H_2C=NH$).

[j] in [Brown et al. 1981] ($H_2C=PH$).

[k] in [Grützmacher and Marchand 1997] ($[Ph_2C=P(^tBu)_2]^+$).

[l] in [Decken et al. 1997] ($^tBu_2Fluorenyl=AsMes^*$).

[m] in [Jones et al. 1999] ($Mes^*(O)C-Sb=C(OH)Mes^*$).

With a consistently calculated set of equilibrium C=X bond lengths in hand, we can discuss the influence of the protonation reaction upon the C=X bond lengths for all X = N, P, As, Sb. Firstly, only the planar structures **X-1a** *vs.* **X-5a** are considered. In the imminium ion $[H_2C=NH_2]^+$ the C=N bond length is only *longer* by 0.004 Å than in the corresponding imine $H_2C=NH$. This lengthening is less pronounced than the reported HF value 0.024 Å in Bond [1991]. The bond lengthening was explained with the decrease in hyperconjugation in the protonated form. In contrast to these findings, the GVB calculations of Wang and Poirier [1997] predicted even a small decrease in the C=N bond length of 0.001 Å. However, they also investigated polyamines $H_2C=(CHCH=)_n NH$ (n = 1,2,3), for which protonation results in an increase of the C=N bond length up to 0.022 Å. Considering the protonation reaction **X-1a** → **X-5a** for the heavier congeners, the C=X bond lengths *decrease* significantly 0.036 Å for X = P, 0.047 Å for X = As, and 0.053 Å for X = Sb.

We continue our comparative discussion of the ground state structures $H_2C=XH$ and their protonated derivatives $[H_2C=XH_2]^+$ regarding the atom and group charges listed in Tab. (2.5). Charge separation between the atom centers of the C=X moiety is evidently correlated with the ordering of the electronegativities $\mathcal{X}_N > \mathcal{X}_C > \mathcal{X}_P > \mathcal{X}_{As} > \mathcal{X}_{Sb}$. As we expect from $\mathcal{X}_C < \mathcal{X}_N$ charge transfer in $H_2C=NH$ is going from N to C. As a result the nitrogen center is much more negatively charged $(-0.58\,e)$ than the carbon center $(-0.09\,e)$. On the other hand, the decrease of the electronegativities $\mathcal{X}_X < \mathcal{X}_C$ reverses the direction of $\sigma + \pi$ charge transfer from X to C in the heavier systems $H_2C=XH$ with X = P, As, Sb. Thus, negative charge is accumulated at the carbon atom $(\approx -0.80\,e)$, whereas the pnictogen centers are positively charged in the order P $(0.43\,e)$ < As $(0.50\,e)$ < Sb $(0.66\,e)$. The differences in the charge distribution between the imine and its heavier congeners is also reflected in the group charges of CH_2 *vs.* XH. In the imine $H_2C=NH$ the charge is less polarized between the main molecule fragments with NH group bearing a negative charge of $-0.24\,e$. In the heavier homologues $H_2C=XH$ with X =

Table 2.5: C=X double bond systems. Atomic and group charges for neutral methylene pnictanes $H_2C=XH$ (**X-1a**) and their protonated derivatives $[H_2C=XH_2]^+$ (**X-5a**/**X-6a**) (X = N, P, As, Sb).[a]

atoms/	X			
groups	N	P	As	Sb
X-1a C	−0.09	−0.79	−0.81	−0.86
X	−0.58	0.43	0.50	0.66
H(1)	0.18	0.22	0.22	0.21
H(2)	0.16	0.22	0.22	0.22
H(3)	0.33	−0.08	−0.12	−0.22
CH_2/XH	±0.24	∓0.35	∓0.38	∓0.43
X-5a C	0.19	−0.66	−0.69	−0.76
X	−0.17	0.87	0.98	1.29
H(1)	0.29	0.30	0.29	0.28
H(3)	0.20	0.09	0.06	−0.05
CH_2	0.76	−0.06	−0.10	−0.19
XH_2	0.24	1.06	1.10	1.19
X-6a C			−0.64	−0.61
X			0.95	1.22
H(1)			0.29	0.27
H(3)			0.05	−0.07
CH_2			−0.06	−0.08
XH_2			1.06	1.08

[a] QCISD/VDZP[1] data derived from NBO analyses. Numbering as in Fig. (2.1).

P, As, Sb charge separation increases with the negative charge accumulated in the CH_2 group, ranging from $-0.35\,e$ to $-0.44\,e$.

For the charges of the monocationic derivatives of $H_2C=XH$ we consider the planar structures **X-5a** for all X = N, P, As, Sb. As shown in Tab. (2.5) trans-bending only has a marginal effect on the atom and group charges for $[H_2C=AsH_2]^+$ and $[H_2C=SbH_2]^+$, respectively. Protonation of methylene phosphane HP=PH and its heavier congeners results in a significant increase of the positive charge at P (0.87 e) < As (0.98 e) < Sb (1.29 e). The increase of q^+ at these centers with respect to the

Table 2.6: C=X double bond systems. σ and π populations for the neutral methylene pnictanes $H_2C=XH$ (**X-1a**) and the planar pnicto carbenium ions $[H_2C=XH_2]^+$ (**X-5a**) (X = N, P, As, Sb).[a]

atoms		X							
		N		P		As		Sb	
		p_σ	p_π	p_σ	p_π	p_σ	p_π	p_σ	p_π
X-1a	C	3.17	0.87	3.72	1.03	3.73	1.03	3.79	1.02
	X	4.40	1.11	3.52	0.95	3.47	0.95	3.32	0.96
	H(1)	0.82		0.77		0.78		0.78	
	H(2)	0.84		0.77		0.77		0.78	
	H(3)	0.66		1.07		1.12		1.21	
X-5a	C	3.21	0.61	3.74	0.88	3.73	0.92	3.77	0.95
	X	4.16	1.37	2.95	1.09	2.90	1.06	2.64	1.02
	H(1)	0.74		0.69		0.71		0.73	
	H(3)	0.53		0.90		0.94		1.06	

[a] QCISD/VDZP[1] data derived from NBO analyses. Numbering as in Fig. (2.1).

neutral species $H_2C=XH$ is much higher ($> 0.39\,e$) than the concomitant decrease of negative charge at carbon ($< 0.13\,e$). This can be explained by additional X $\rightarrow$ C charge transfer through dative π bonding, i.e. lone-pair donation from X to the carbenium center via π_{pp} orbital overlap. According to the differences between $\mathcal{X}_X$ and $\mathcal{X}_C$, σ and π charge transfer is expected to occur in opposite directions for X $=$ N ($\mathcal{X}_N > \mathcal{X}_C$) on one side, and in the same direction from X to the CH_2 fragment for X $=$ P, As, Sb ($\mathcal{X}_X < \mathcal{X}_C$) on the other side. Thus, in the iminium ion $[H_2C=NH_2]^+$ charge is less separated between nitrogen and carbon due to the fact that N $\rightarrow$ C π backdonation partially counterbalances the C $\rightarrow$ N σ charge transfer. The situation encountered in the monocations $[H_2C=XH_2]^+$, as shown graphically in Scheme 2.2, is reminiscent of the charge dispersal found in $[HOCH_2]^+$ vs. $[HSCH_2]^+$ by Bernardi et al. [1975].

$$0 < q(\text{CH}_2) > q(\text{XH}_2) \qquad\qquad 0 > q(\text{CH}_2) \ll q(\text{XH}_2)$$
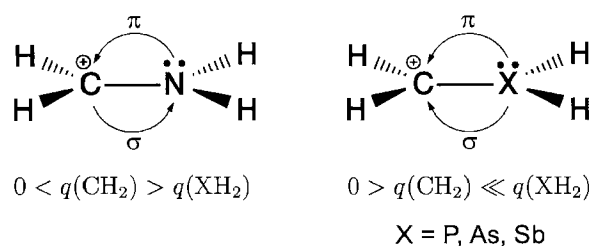
X = P, As, Sb

Scheme 2.2

A considerable increasing amount of negative charge is also shifted to the hydrogens H(3,4) when X goes from N to Sb. For the hydrogens H(1,2) bonded to carbon the positive charge remains almost constant ($\approx 0.29\,e$) for all X = N, P, As, Sb. If the charges at H(1,2) and H(3,4) are taken into account, the XH$_2$ and CH$_2$ group charges show little variation for the heavier monocations [H$_2$C=XH$_2$]$^+$ with X = P,

Table 2.7: C=X double bond systems. Stretching frequencies $\nu_{\text{C=X}}^{\text{calc}}$ for the neutral methylene pnictanes H$_2$C=XH (**X-1a**) and their protonated derivatives [H$_2$C=XH$_2$]$^+$ (**X-5a/X-6a**) (X = N, P, As, Sb).[a]

	this work[b]		others	$\nu_{\text{C=X}}^{\text{exp}}$
N-1a	1665		1638[c], 1628[d]	1638[f], 1660[g]
N-5a	1737		1738[d]	
P-1a	931		1109[e]	
P-5a	975			
As-1a	791			
As-5a (6a)	846	(828)		
Sb-1a	668			
Sb-5a (6a)	711	(661)		

[a] Frequencies in cm^{-1}.
[b] QCISD/VDZP[1] data scaled by 0.96.
[c] in [Hout et al. 1982] (MP2, scaled).
[d] in [Wang and Poirier 1997] (GVB, unscaled).
[e] in [Schmidt et al. 1987] (SCF, unscaled).
[f] in [Hamada et al. 1984] (H$_2$C=NH).
[g] in [Findeisen et al. 1981] (Me$_2$C=NMe).

As, Sb with a slightly negative group charge for the CH_2 unit, ranging from $(-0.06\,e)$ to $(-0.19\,e)$. Conversely, the imminium ion $[H_2C=NH_2]^+$ is opposite to this trend, with a highly positive charged carbon center $(0.76\,e)$.

In Tab. (2.7) we present C=X stretching frequencies for $H_2C=XH$ and $[H_2C=XH_2]^+$ with X = N, P, As, Sb, scaled by 0.96. Firstly, only the planar systems for both series of molecules **X-1a** and **X-5a** are considered. The drop in the C=X stretching frequencies in going from the imine $(H_2C=NH)$ and iminium ion $([H_2C=NH_2]^+)$ to the corresponding heavier heteronuclear systems reveals that the C=X bond becomes increasingly weaker in the order C=N $\ll$ C=P $<$ C=As $<$ C=Sb. For all neutral systems $H_2C=XH$ protonation is leading to an increase in the C=X stretching frequencies in the order X = N $(82\ \mathrm{cm^{-1}})$ > X = P $(44\ \mathrm{cm^{-1}})$ $\approx$ X = As $(55\ \mathrm{cm^{-1}})$ $\approx$ X = Sb $(43\ \mathrm{cm^{-1}})$. However, for $[H_2C=AsH_2]^+$ and $[H_2C=SbH_2]^+$ bending distortion from the planar C_{2v} to the trans-bent C_s geometries **As-6a** and **Sb-6a** diminishes the stretching frequencies by $18\ \mathrm{cm^{-1}}$ and $50\ \mathrm{cm^{-1}}$, respectively. Taking this into consideration, protonation shifts up the C=X stretching frequencies for X = N, P, As on one side and down for X = Sb on the other side. This parallels the effect of protonation observed for the double bond strengths, as is discussed in the next section.

2.2.1   Bonding energies

In this section we present an analysis of the double bond strengths for the systems $H_2C=XH$ and their protonated derivatives $[H_2C=XH_2]^+$. Total bond energies ΔE_{TBE} are obtained from ZPE corrected enthalpies D_0 of the dissociation reactions of $H_2C=XH$ and $[H_2C=XH_2]^+$ into their singlet and triplet ground state fragments according to (Rxn. 2.1) and (Rxn. 2.2), respectively. The results are presented in Tab. (2.10). Note that we refer our D_0 values for $[H_2C=XH_2]^+$ to the planar geome-

tries **X-5a** for all X = N, P, As, Sb. Corresponding π-bond energies are obtained by rotational barriers according to Schmidt et al. [1987] and presented in Tab. (2.12).

$$H_2C{=}XH \quad \longrightarrow \quad CH_2 \;+\; XH \qquad\qquad \text{(Rxn. 2.1)}$$

$$[H_2C{=}XH_2]^+ \quad \longrightarrow \quad CH_2 \;+\; XH_2^+ \qquad\qquad \text{(Rxn. 2.2)}$$

We briefly discuss first the outcome of the calculations for the various hydride fragments since the singlet-triplet splitting energies $\Delta E_{s\to T}$ are crucial for the bonding analysis and a good test for gauging the quality of the method used.

The energies of the singlet and triplet ground states of the group 15 monohydrides XH, as well as for dihydrides CH_2 and XH_2^+, are collected in Tab. (2.8) for all X = N, P, As, Sb. The corresponding singlet-triplet energy gaps $\Delta E_{s\to T}$ of the group 15 hydrides are compared with the literature in Tab. (2.9). Note that we only present a small selection of the data available. For all monohydrides XH, the energy ordering remains the same for all X = N, P, As, Sb, i.e. $^3\Sigma^- < {}^1\Delta$. The calculated $^1\Delta$–$^3\Sigma^-$ energy gaps are far away from chemical accuracy (± 1.0 kcal mol^{-1}), compared to the experimental data given by Huber and Herzberg [1979], but in good agreement with the previously reported CASSCF values in [Mahé and Barthelat 1995]. On the other hand, for methylene and the cationic dihydrides XH_2^+ a different picture arises. Here, our values are comparable with the results from high level calculations such as [Cramer et al. 1994] and in excellent accord with the experimental data (see Tab. (2.9)). The valence-isoelectronic dihydrides of the second row, i.e. CH_2 and NH_2^+ have a triplet to be the more stable state, whereas for the heavier carbenic homologues XH_2^+ with X = P, As, Sb the opposite ordering is observed, i.e. $^1A_1 < {}^3B_1$. This is due to the fact that the valence s and p orbitals in the higher dihydrides are no longer localized in the same region of space. The reason for this stems from the essential difference between second and higher row elements pointed out by Kutzelnigg [1984]: the cores in the former contains only s orbitals whereas the cores in the latter includes at least s an p orbitals.

Table 2.8: C=X bonding energies. Energetics of the carbon hydride CH_2 together with the group 15 hydrides XH and XH_2^+ including singlet-triplet splitting energies $\Delta E_{s \to T}$ (X = N, P, As, Sb).[a]

| | state | \multicolumn{4}{CCSD(T)/BS(2,3)//QCISD/BS(1)[b]} | | | \multicolumn{3}{$\Delta E_{s \to T}$} | |
		E_{opt}	ZPE	E^1_{ref} [c]	E^2_{ref} [d]	ΔE_{opt}	ΔE^1_{ref}	ΔE^2_{ref}
CH_2	$^1A_1$	−39.013458	10.6	−39.036025	−39.059138			
	$^3B_1$	−39.037650	11.2	−39.055760	−39.075142	−15.2	−12.4	−10.0
NH	$^1\Delta$	−10.281891	4.8	−10.299527	−10.327193			
	$^3\Sigma^-$	−10.362808	4.7	−10.375403	−10.399687	−50.8	−47.6	−45.5
NH_2^+	$^1A_1$	−10.564212	11.6	−10.578142	−10.601278			
	$^3B_1$	−10.618245	11.0	−10.628875	−10.649117	−33.9	−31.8	−30.0
PH	$^1\Delta$	−6.976722	3.3	−6.991708	−7.028314			
	$^3\Sigma^-$	−7.030444	3.3	−7.041866	−7.073748	−33.7	−31.5	−28.5
PH_2^+	$^1A_1$	−7.290868	8.5	−7.305446	−7.337987			
	$^3B_1$	−7.268070	8.4	−7.281801	−7.310947	14.3	14.8	17.0
AsH	$^1\Delta$	−6.643712	3.1	−6.655960	−6.682538			
	$^3\Sigma^-$	−6.695677	3.1	−6.703900	−6.726070	−32.6	−30.1	−27.3
AsH_2^+	$^1A_1$	−6.963563	7.9	−6.975185	−6.995927			
	$^3B_1$	−6.927532	7.7	−6.939104	−6.958264	22.6	22.6	23.6
SbH	$^1\Delta$	−5.872440	2.7	−5.887796	−5.913069			
	$^3\Sigma^-$	−5.919377	2.7	−5.930881	−5.952147	−29.5	−27.0	−24.5
SbH_2^+	$^1A_1$	−6.198504	7.0	−6.216440	−6.236825			
	$^3B_1$	−6.157339	6.8	−6.175617	−6.194625	25.8	25.6	26.5

[a] Total energies E in Hartrees, ZPE and relative energies ΔE (without ZPE corrections) in kcal mol^{-1}. XH are optimized in $C_{\infty v}$ symmetry. XH_2^+ (CH_2) are optimized in C_{2v} symmetry. A negative $\Delta E_{s \to T}$ indicates the triplet to be the more stable multiplicity.

[b] BS(1): 6-31G(d,p); BS(2): 6-311G(d,p); BS(3): 6-311G(3df,2p) for CH_2. BS(1): VDZP^1; BS(2): VTZP^1; BS(3): VTZP^2.

[c] Refined energies obtained using BS(2).

[d] Refined energies obtained using BS(3).

The total energies obtained for the hydrides were used to calculate the dissociation energies D_0 for the double bond systems $H_2C=XH$ and $[H_2C=XH_2]^+$ according to (Rxn. 2.1) and (Rxn. 2.2), respectively (vide supra). As shown in Tab. (2.10), the ZPE uncorrected D_e values increase when going from VTZP^1 to VTZP^2 signifi-

Table 2.9: C=X bonding energies. Comparison of the singlet-triplet exitation energies $\Delta E_{S \to T}$ of group 15 hydrides XH and XH$_2^+$ (X = N, P, As, Sb).[a]

X	XH			XH$_2^+$		
	this work[b]	Mahé[c]	exp	this work[b]	Cramer[d]	exp
N	−45.5	−42.7	−35.9[f]	−30.0	−30.5	−30.1 ± 0.2[g]
P	−28.5	−29.4 (−22.0[e])	−21.9[f]	17.0	16.3	17.3 ± 1.2[h]
As	−27.3	−28.5		23.6	21.0	23.8 ± 9.9[i]
Sb	−24.5	−25.3		26.5		

[a] If necessary, literature values have been transformed and rounded. Theoretical as well as experimental values for $\Delta E_{S \to T}$ (CH$_2$) are -10.0 kcal mol^{-1} (this work, Cramer[d]) and -9.00 ± 0.01 kcal mol^{-1} ([Schaefer III 1986]), respectively.

[b] CCSD(T)/VTZP^2 data. $\Delta E_{S \to T}$ (without ZPE corrections) in kcal mol^{-1} taken from Tab. (2.8). Negative values indicate the triplet to be the more stable multiplicity.

[c] in [Mahé and Barthelat 1995] (CASSCF).

[d] in [Cramer et al. 1994] (MRCISD).

[e] in [Cade 1968] (CI).

[f] in [Huber and Herzberg 1979].

[g] in [Gibson et al. 1985].

[h] in [Berkowitz and Cho 1989].

[i] in [Berkowitz 1988].

cantly by $6 - 10$ kcal mol^{-1}. Corresponding calculations for X = P with all electron basis sets revealed that this improvement of the dissociation energies can be mainly attributed to the inclusion of the f polarization function. Nevertheless, the dissociation energies obtained at the CCSD(T)/VTZP^2 level are still systematically lower by $6 - 9$ kcal mol^{-1} compared with the G2 values obtained for all structures with X = N, P, As. Total bond energies have been reported for H$_2$C=NH and H$_2$C=PH [Schleyer and Kost 1988] as well as for [H$_2$C=NH$_2$]$^+$ [Bond 1991]. The values are obtained with Schleyer's method which employs the difference in heats of hydrogenation of the single and double bonds to the extent to which the π-bond is stronger

Table 2.10: C=X bonding energies. Dissociation energies D_0 for the neutral methylene pnictanes $H_2C{=}XH$ (**X-1a**) and their protonated derivatives $[H_2C{=}XH_2]^+$ (**X-5a**)(X = N, P, As, Sb).[a]

| | D_e [b] | corrections | | D_0 | | |
		ΔZPE[c]	ΔBS[d]	this work[e]	others	exp
N-1a	153.4	−9.7	6.3	150.0 (158.2)	160.2[f] 157.6[g]	156.0[g]
N-5a	213.4	−12.6	6.9	207.7 (216.2)	194.5[g]	213.7[g]
P-1a	111.0	−6.9	9.4	113.5 (122.2)	115.4[f]	
P-5a	131.7	−7.2	8.0	132.5 (139.0)		
As-1a	99.9	−6.3	7.3	101.0 (106.5)		
As-5a	107.8	−6.4	6.3	107.7 (114.4)		
Sb-1a	84.0	−5.5	7.8	86.3		
Sb-5a	79.9	−5.6	6.4	80.7		

[a] Results in $kcal\,mol^{-1}$ calculated from total and zero-point energies presented in Tab. (2.1) ($H_2C{=}XH$, $[H_2C{=}XH_2]^+$) and Tab. (2.8) (CH_2, XH, XH_2^+).

[b] $CCSD(T)/VTZP^1//QCISD/VDZP^1$ data.

[c] Difference for ZPE (unscaled) between doubly bonded species and their constituting ground state fragments.

[d] Difference between the D_e values in the $VTZP^1$ and $VTZP^2$ basis sets.

[e] ZPE corrected $CCSD(T)/VTZP^2$ data: $D_e + \Delta ZPE + \Delta BS$. (G2 values in parentheses).

[f] in [Schleyer and Kost 1988].

[g] in [Bond 1991].

than the σ bond. Although there are some differences compared with our values the overall agreement is acceptable.

For the neutral ground state systems $H_2C{=}XH$, the dissociation energies D_0 decrease in steps of $36.5\,kcal\,mol^{-1}$ (N $\to$ P), $12.5\,kcal\,mol^{-1}$ (P $\to$ As) and $14.7\,kcal\,mol^{-1}$ (As $\to$ Sb), ranging from $150.0\,kcal\,mol^{-1}$ to $86.3\,kcal\,mol^{-1}$. For the corresponding protonated derivatives $[H_2C{=}NH_2]^+$ and its higher congeners the same trend in D_0 is observed, with a much wider range from $207.7\,kcal\,mol^{-1}$ to $80.7\,kcal\,mol^{-1}$. Now, D_0 drops down in steps of $75.2\,kcal\,mol^{-1}$ (N $\to$ P),

24.8 kcal mol^{-1} (P $\rightarrow$ As) and 27.0 kcal mol^{-1} (As $\rightarrow$ Sb), respectively. The reason for the rapid fall off in the total bond energies between the protonated species $[H_2C{=}NH_2]^+$ and its higher congeners refers basically to the fact that the fragment NH_2^+ and its higher homologues have different electronic ground states. As a result, the dissociation of $[H_2C{=}XH_2]^+$ with X = P, As, Sb involves relaxation of the XH_2^+ fragment into its singlet ground state minimum. Thus, the corresponding D_0 values include contributions from the singlet-triplet splitting energy $\Delta E_{S\rightarrow T}$. In other words, the attractive decreasing π_{pp} interaction energies in methylenephosphonium and its heavier homologues are due to the increasing preparation energies $(\Delta E_{S\rightarrow T})$ of the carbenoid XH_2^+ fragments, diminishing the respective total bond strengths ΔE^0_{TBE} accordingly.

In agreement with Bond [1991], the C=N double bond in the protonated imminium ion $[H_2C{=}NH_2]^+$ is calculated to be 57.7 kcal mol^{-1} more stable than in $H_2C{=}NH$. However, the gain in stability upon protonation declines from 19.0 kcal mol^{-1} for $[H_2C{=}PH_2]^+$ to 6.7 kcal mol^{-1} for $[H_2C{=}AsH_2]^+$, respectively. For $[H_2C{=}SbH_2]^+$ the C=Sb double bond in (**Sb-5a**) is even weaker (80.7 kcal mol^{-1}) than in **Sb-1a** (86.3 kcal mol^{-1}). The reason for this can be found in the property of higher period elements to avoid hybridization due to the fact that the valence s and p orbitals are spatially more separated (non-orbital hybridization (NOH) effect, see in [Schoeller 1990]). In the neutral systems $H_2C{=}XH$, the heavier pnictogen centers can participate in a classical double bonding with their p orbitals alone so that the lone pair are free to retain mostly s character. This trend is reflected in the $\angle$CXH(3), which approaches 90 $^\circ$ when X goes down the row from N to Sb. Conversely, in the monocations $[H_2C{=}XH_2]^+$, rehybridization at the X center forces the lone pair into a strong dative π_{pp} interaction with the formally empty 2p valence orbital of carbon. As a consequence, the lone pair at X has a strong p character which is increasingly unfavorable (in an energy sense) when going from the nitrogen to the antimony system. Thus, in the heavier systems of $[H_2C{=}XH_2]^+$, the

dative π-bond competes with the increasing energy required to planarize the XH_2 centers. As a result, the dropping of the double bond strength is much steeper in the series of protonated derivatives $[H_2C=XH_2]^+$ than in the series of the neutral species $H_2C=XH$.

Table 2.11: C=X bonding energies. Application of the CGMT model to the pnicto carbenium ions $[H_2C=XH_2]^+$ (X = N, P, As, Sb) according to the inequalities (1.2)–(1.4) (cf. Sec. (1.1.1) on page 4).[a]

system	$\Sigma\Delta E_{S\to T}$	$\frac{1}{2}\Delta E^0_{TBE}$	$\frac{1}{2}E_{\sigma+\pi}$	structure
$[H_2C=NH_2]^+$	-55.5	103.9	103.9	p
$[H_2C=PH_2]^+$	7.0	66.3	74.8	p
$[H_2C=AsH_2]^+$	13.7	53.9	65.7	p
$[H_2C=SbH_2]^+$	16.5	40.4	53.6	p

[a] All energies in $kcal\,mol^{-1}$. $\Sigma\Delta E_{S\to T}$ refers to the sum of the singlet-triplet splitting energies, taken from Tab. (2.8). ΔE^0_{TBE} refers to D_0, taken from Tab. (2.10). $E_{\sigma+\pi}$ refers to the ZPE uncorrected reaction enthalpy for the dissociation of the planar double bond systems into their triplet fragments. p = planar , tb = trans-bent.

Which geometries are expected according to the CGMT model? The condition required for a trans-bent double bond is $\Sigma\Delta E_{S\to T} > 1/2 E_{\sigma+\pi}$, according to inequality Eq. (1.3). Obviously, the $H_2C=XH$ double bond systems adapt classical planar geometries, since both fragments CH_2, as well as XH, have triplet ground states, and thus $\Sigma\Delta E_{S\to T} < 0$. On the other hand, for the protonated derivatives $[H_2C=XH_2]^+$ the XH_2^+ fragments of the higher row elements have a singlet ground state so that $\Sigma\Delta E_{S\to T}$ becomes positive, ranging from $7.0\,kcal\,mol^{-1}$ to $16.5\,kcal\,mol^{-1}$ when X goes from P to Sb. Nevertheless, the gain in stability, when forming a classical planar double bond, is significantly higher than $\Sigma\Delta E_{S\to T}$ for all monocations with X = N, P, As, Sb, as seen in Tab. (2.11). Even comparison of $\Sigma\Delta E_{S\to T}$ with the considerable smaller values of ΔE^0_{TBE}, which is a lower-limit criterion, the same

prediction results: within the CGMT-Model, the planar structures **X-5a** are the more favored geometries for all monocationic double systems $[H_2C=XH_2]^+$.

For both series of systems $H_2C=XH$ as well as $[H_2C=XH_2]^+$ the corresponding π-bond energies are gathered in Tab. (2.12) together with previously reported theoretical values from the literature. Comparison with a complete set of experimental data is apparently not possible. All rotational barriers have been estimated by the singlet-triplet differences between the planar ground state systems **X-1a** and **X-5a** and their corresponding twisted triplets **X-2a** and **X-7a**, respectively. According to Hund's rule, it is not surprising that our values for the $H_2C=XH$ systems are slightly lower than those reported by Schmidt et al. [1987] (X = N, P) and Schoeller et al. [1997] (X = P, As, Sb). On the other hand, π-bond strengths reported for $H_2C=NH$ (80.8 kcal mol^{-1}) and $H_2C=PH$ (49.4 kcal mol^{-1}) according to Schleyer's

Table 2.12: C=X bonding energies. π-bond energies for the planar methylene pnictanes $H_2C=XH$ (**X-1a**) and their protonated derivatives $[H_2C=XH_2]^+$ (**X-5a**) (X = N, P, As, Sb).

	this work[a]	Schmidt[b]	Schoeller[c]	Schleyer[d]	others
N-1a	65.5	63.3		80.8	
N-5a	81.9				87.1[e]
P-1a	41.4	43.1	44.2	49.4	
P-5a	43.4				
As-1a	37.4		39.2		
As-5a	36.4				
Sb-1a	29.1		30.3		
Sb-5a	23.9				

[a] CCSD(T)/VTZP^2 data. ZPE correted values in kcal mol^{-1} taken from Tab. (2.1).

[b] in [Schmidt et al. 1987] (SOCI).

[c] in [Schoeller et al. 1997] (MRCI).

[d] in [Schleyer and Kost 1988] (MP4).

[e] in [Bond 1991] (MP4).

method [Schleyer and Kost 1988] are considerable higher compared to the values derived from rotational barriers. Nevertheless, neither method are free from flaws. Rotational barriers must be certainly regarded as lower-limits for π-bond strengths simply due to possible residual π interactions in the twisted isomer. This is certainly true for $H_2C=NH$ where the CH_2 fragment in the triplet **N-2a** is strongly pyramidalized ($\phi_C = 34.4\,°$). Rotation of the NH group around 90 $°$ brings the nitrogen lone pair into conjugation with the singly occupied p orbital located at the carbon center. This gives rise to a 3e-2c (p_C-n_N) interaction, which is even further enhanced under pyramidalization of the CH_2 fragment (Scheme 2.3). The reason for this is that under geometric distortion from C_{2v} to C_s symmetry, the energy gap between the C-centered SOMO and the lone pair at nitrogen is diminished. This interaction is certainly much smaller in the triplet isomers **X-2a** containing the higher row elements X = P, As, Sb ($\phi_C < 8.0\,°$). Therefore, the rotational barriers become a better approximation for the π-bond strengths of $[H_2C=XH_2]^+$ when X goes down the row from N to Sb.
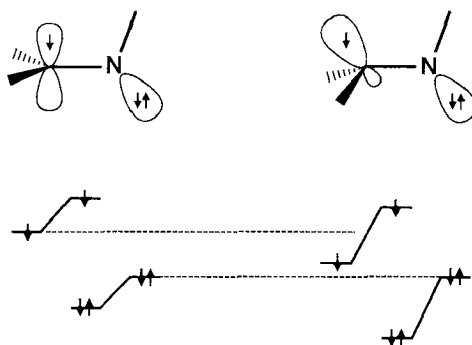
Scheme 2.3

On the other hand, in the twisted triplets **X-7a** of the protonated derivatives $[H_2C=XH_2]^+$, pyramidalization around X increase in the order $NH_2 \ll PH_2 < AsH_2 < SbH_2$. The concomitant rehybridization of the σ-bond results presumably in an increasing error in the π-bond strengths for the heavier monocations $[H_2C=XH_2]^+$. For the protonated imminium ion $[H_2C=NH_2]^+$ our π-bond strength is compara-

ble with the one reported in Bond [1991] also calculated with Schleyer's method according to Schleyer and Kost [1988].

From the double bond energies $E_{\sigma+\pi}$ and the π-bond strengths presented above, σ-bond values are readily obtained. The $E_{\sigma+\pi}$ values are used instead $\Delta E_{\mathrm{TBE}}^{0}$ simply to compare the σ and π increments of the double bond strengths of the neutral and monocationic systems $H_2C=XH$ and $[H_2C=XH_2]^+$ on an equal footing. It should be mentioned here that we are not concerned in *absolute* σ and π contributions, but rather in the changes of the relative σ/π proportioning upon protonation. The values for $E_{\sigma+\pi}$ and its σ/π contributions are presented in Tab. (2.13).

Table 2.13: C=X double bond systems. σ and π increments of the double bond interaction energy $E_{\sigma+\pi}$ for the neutral methylene pnictanes $H_2C=XH$ and their protonated derivatives $[H_2C=XH_2]^+$ $(X = N, P, As, Sb)$.[a]

X	$H_2C=XH$		$[H_2C=XH_2]^+$	
	$E_{\sigma+\pi}$	σ/π	$E_{\sigma+\pi}$	σ/π
N	160	94/66 (70/65)[b] (79/81)[c]	220	138/82 (107/87)[d]
P	120	79/41 (64/48)[b] (66/49)[c]	157	114/43
As	107	70/37	138	102/36
Sb	92	63/29	113	89/24

[a] CCSD(T)/VTZP[2] data. $E_{\sigma+\pi}$ refers to the ZPE uncorrected reaction enthalpy for the dissociation of the planar double bond systems into their triplet fragments. The π-bond increments are taken from Tab. (2.12). The σ-bond increments are readily derived from $E_{\sigma+\pi}$-E_{π}.

[b] in [Kutzelnigg 1984].

[c] in [Schleyer and Kost 1988].

[d] in [Bond 1991].

The results for the neutral imine $HN=NH$ and its higher congener, the diphosphene $HP=PH$, can be compared with the σ and π contributions reported

by Kutzelnigg [1984] and Schleyer and Kost [1988]. The high σ-bond strength for the imine is certainly due to the much too low estimate for the π-bond strength, as discussed above. Considering this, a σ:π ratio of approximately 1:1 can be expected, as reported in the literature. For the phosphorus system **P-1a**, the results are in acceptable accordance with the values cited, given a σ:π of 2:1. For the higher congeners **As-1a** and **Sb-1a** similar ratios $\approx$ 2:1 are obtained, while the corresponding net double bond energies $E_{\sigma+\pi}$ further decrease. Going from the neutral systems to the protonated derivatives $H_2C=XH$, the corresponding $E_{\sigma+\pi}$ values are strongly shifted to higher values for all X = N, P, As, Sb. This is so, because the decrease in the double bond strength for the heavier monocations is less steep than in the corresponding D_0 values, since the contributions from $\Delta E_{S\to T}$ of the singlet fragments XH_2^+ (X = P, As, Sb) are excluded. Comparison of the σ and π increments between the neutral and cationic forms shows that the π strengths only slightly change, whereas the σ contributions are strongly increased upon protonation. This can be rationalized with the increased degree of hybridization in the planar XH_2 fragments. For the higher congeners of the imminium ion $[H_2N=NH]^+$, the enhanced σ-bond strengths are not for free: the increasing energies required to planarize the higher row X centers in $[H_2C=XH_2]^+$ are in the range of $36 - 49\ \mathrm{kcal\,mol^{-1}}$ for X = P, As, Sb, in contrast to $\approx 7\ \mathrm{kcal\,mol^{-1}}$ for X =N.

2.2.2 Bader Analysis

The properties of the electron density at the (3,-1) bond critical points for the double bond systems $H_2C=XH$ and $[H_2C=XH_2]^+$ are listed in Tab. (2.14). Again, for the heavier systems of the monocations $[H_2C=XH_2]^+$ with X = As, Sb, we present results for both, the planar (**X-5a**) and the trans-bent (**X-6a**) structures. In Fig. (2.2) and Fig. (2.3) two-dimensional plots of the *negative* Laplacian $-\nabla^2\rho(\mathbf{r})$ are shown for the systems $H_2C=XH$ and $[H_2C=XH_2]^+$. Furthermore, contour lines of the zero flux surfaces are included which define the space taken by atoms within molecules.

Table 2.14: C=X topographical analysis. Bond critical point data for the C=X double bond for the methylene pnictanes $H_2C=XH$ (**X-1a**) and their protonated derivatives $[H_2C=XH_2]^+$ (**X-5a**/**X-6a**) (X = N, P, As, Sb).[a]

	bond	R_b (Å)	C–r_b (Å)	r_b	ρ_b (e Å^{-3})	$\nabla^2\rho_b$ (e Å^{-5})	$H(r)$ (Hartree Å^{-3})	ϵ_b
X-1a	C=N	1.277	0.431	0.338	2.591	−17.700	−4.619	0.274
	C=P	1.693	1.049	0.619	1.187	11.041	−1.024	0.421
	C–As	1.795	0.930	0.518	1.133	4.307	−0.789	0.270
	C=Sb	2.004	1.003	0.501	0.848	6.418	−0.407	0.237
X-5a	C=N	1.281	0.423	0.331	2.476	−10.140	−4.309	0.064
	C=P	1.656	1.028	0.615	1.297	10.403	−1.195	0.777
	C=As	1.749	0.866	0.505	1.255	1.792	−0.950	0.364
	C=Sb	1.952	0.996	0.510	0.948	5.477	−0.515	0.290
X-6a	C=As	1.765	0.897	0.508	1.225	2.056	−0.908	0.309
	C=Sb	2.007	1.009	0.503	0.864	5.219	−0.435	0.189

[a] Derived from QCISD/6-31G(d,p) (X = N, P) and QCISD/DZP(AE) (X = As, Sb) wavefunctions on the QCISD/VDZP[1] optimized geometries. For a graphical presentation of the negative Laplace $-\nabla^2\rho(r)$, see Fig. (2.2) ($H_2C=XH$) and Fig. (2.3) ($[H_2C=XH_2]^+$).

In the neutral methylene pnictogens $H_2C=XH$, the shift of the electron charge towards the carbon atom is revealed by the location of the BCP r_b, which is given as ratio between the distances X_α–r_b/R_e. The values of r_b increase when X goes down from N to Sb demonstrating the *Umpolung* of the C=X bond and the very different sizes of the carbon atom in $H_2C=NH$ ($r_b < 0.5$), on one side and in $H_2C=XH$ ($r_b > 0.5$, X = P, As, Sb), on the other side. The shift of r_b towards the X center is graphically displayed in Fig. (2.2). The ρ_b value is indicative of charge concentration within the C=X bond and is highest for $H_2C=NH$, decreasing in the order N=N $\ll$ P=P $\approx$ As=As < Sb=Sb from 2.6 e Å^{-3} to 0.8 e Å^{-3}. The corresponding Laplacian is highly negative (-17.7 e Å^{-5}) for the imine **1a**, while the higher congeners **X-1a** have *positive* $\nabla^2\rho(r)$ values, decreasing in the order P (11.0 e Å^{-5}) > As (4.3 e Å^{-5}) < Sb (6.4 e Å^{-5}). However, the local energy density H_b remains negative for all $H_2C=XH$, ranging from -4.6 Hartree Å^{-3} to -0.4 Hartree Å^{-3}. Remember that

negative values for $\nabla^2\rho(\mathbf{r})$ and H_b can be attributed to shared interactions, i.e. covalent bonds, whereas positive values refer to closed shell interactions, such as ionic or van der Waals bonding. As a result, the bond critical point data for the C=N bond in the imine **X-1a** indicates a highly covalent character with the valence electrons concentrated in the nitrogen basin along the C–N bond path. Conversely, the C=X bond in the higher homologues can be classified as polar ($\nabla^2\rho(\mathbf{r}) > 0$) but still covalent ($H_b < 0$) with ρ_b less contracted along the C–X path. The ellipticity value ϵ_b, defining the π character of the C=X bond is largest for the carbon phosphorus bond (0.42). This is comparable with the ellipticity found for ethylene (≈ 0.45). In the other structures H_2C=XH with X = N, As, Sb, the value of ϵ_b is smaller (0.27–0.24).

Protonation of H_2C=NH results in an significant decrease in the magnitude of $\nabla^2\rho(\mathbf{r})$ by $7.2 \, e\,\text{Å}^{-5}$. This indicates an increased charge separation along the C–N bond path in the still highly covalent C=N double bond of **N-5a**. On the other hand, in the heavier systems $[H_2C$=XH$_2]^+$ with X = P, As, Sb, protonation alters the bond critical point data in the opposite direction. Now, electron density is more cumulated at the BCP compared to the corresponding deprotonated forms H_2C=XH. Furthermore, the Laplacians $\nabla^2\rho(\mathbf{r})$ are less positive whereas the local density H_b is more negative. Thus, it appears that protonation increases the covalent character of the C=X bond in the heavier systems. Remarkably, the ellipticity in **N-5a** is only 0.06! A possible explanation for this apparently contradictory result, may be found in the mutual σ and π charge transfer as shown in Scheme 2.2. As a consequence, the increased positive charge at carbon ($0.19\,e$ from Tab. (2.5)), also reflected in the smaller value of r_b, is leading to a density contraction in the "π space" perpendicular to the molecular plane, as seen in the change of the magnitude of λ_2 from 0.72 to 0.79 au. Concomitantly, charge is depleted along the bond path as seen in the magnitude of λ_1 ("σ space" within the molecular plane) which changes from 0.92 to 0.84 au. On the other hand, within the heavier monocationic systems

N-1a   P-1a

As-1a   Sb-1a
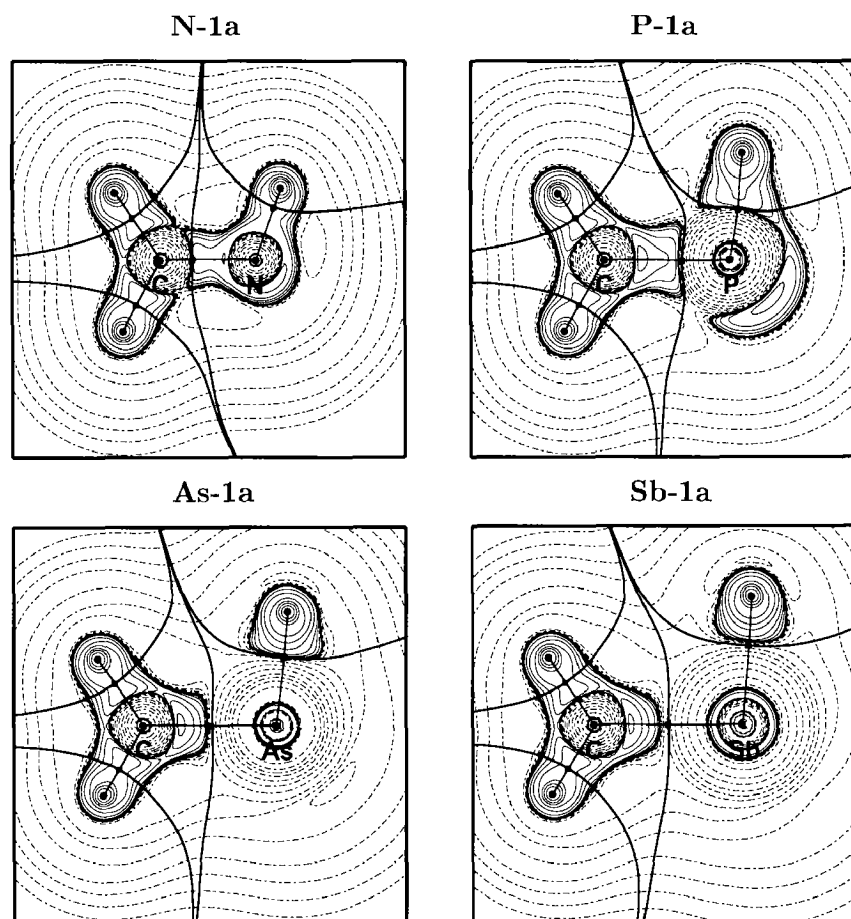
Figure 2.2: Two-dimensional contour plots of the negative Lapla-
cians $-\nabla^2\rho(\mathbf{r})$ (in au) for the neutral double bond systems $H_2C{=}XH$
(**X-1a**) within the molecular plane. Solid contour lines indicate re-
gions of charge concentration $(-\nabla^2\rho(\mathbf{r}) > 0)$, dashed contour lines
indicate regions of charge depletion $(-\nabla^2\rho(\mathbf{r}) < 0)$. Contour lines
of the interatomic surfaces (—) and bond paths (—) are shown as
solid bold lines. Bond critical points are indicated by black squares
(■). For the corresponding BCP data of the C=X double bonds see
Tab. (2.14).

the ellipticity increases due to protonation. The ellipsoidal shape of the C=X bond
given by ϵ_b is largest for the phosphorus containing structure **P-5a** and decreases in
the order C=P $\gg$ C=As $>$ C=Sb $\gg$ C=N. For the former three bonds, the increase
in ϵ_b is primarily a result of an increased contraction of the density towards the bond
path, as seen from the increasing magnitude of λ_1 (e.g. from 0.26 to 0.31 au for X
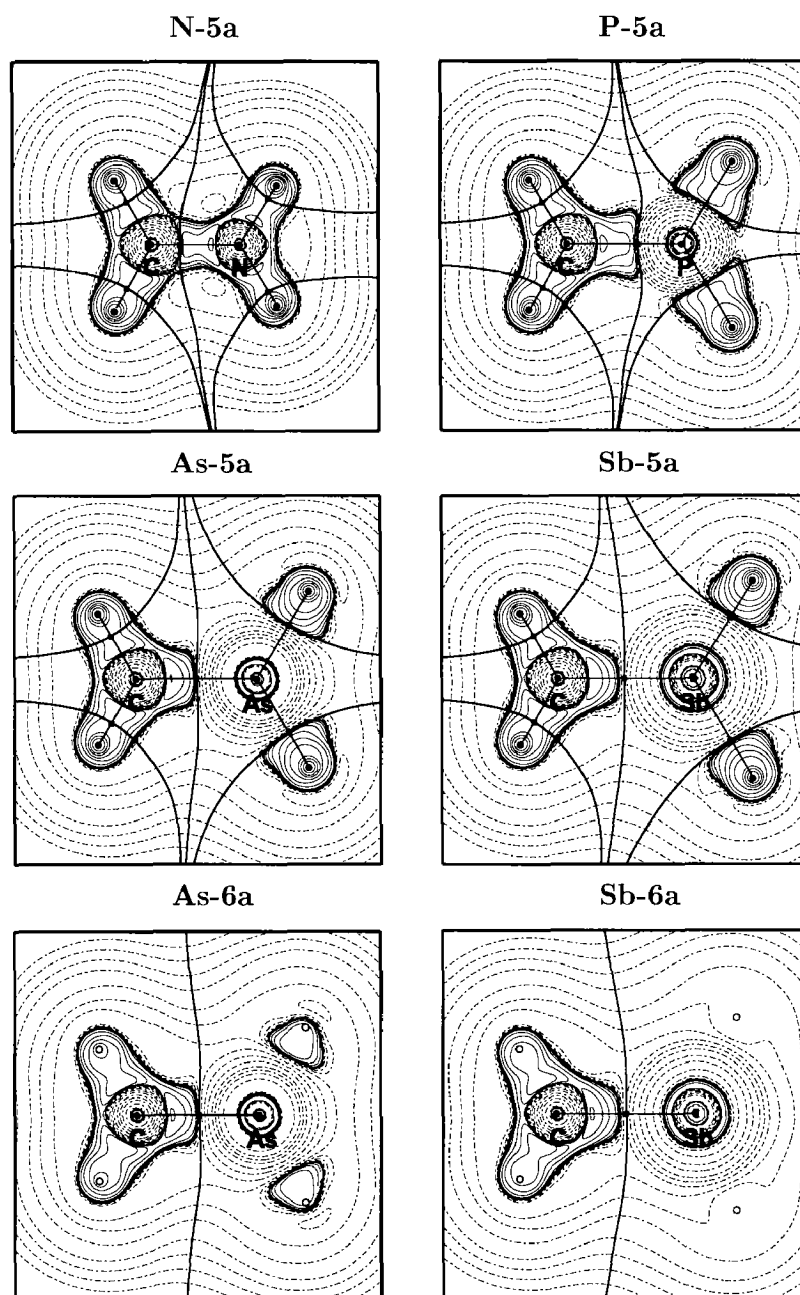
Figure 2.3: Two-dimensional contour plots of the negative Laplacians $-\nabla^2\rho(\mathbf{r})$ for the monocationic double bond systems $[\mathrm{H_2C{=}XH_2}]^+$ (**X-5a**) within the molecular plane. In the trans-bent structures **As-6a** and **Sb-6a**, the C–X axis lies in the plotting plane perpendicular to the σ_v symmetry plane. Solid contour lines indicate regions of charge concentration $(-\nabla^2\rho(\mathbf{r}) > 0)$, dashed contour lines indicate regions of charge depletion $(-\nabla^2\rho(\mathbf{r}) < 0)$. Contour lines of the interatomic zero-flux surfaces (—) and bond paths (—) are shown as solid bold lines. Bond critical points are indicated by black squares (■). Small black circles indicate hydrogen atoms above (solid) and below (dashed) the plot plane. For the corresponding BCP data of the C=X double bonds see Tab. (2.14).

= P), whereas little variation is observed in the charge dispersal perpendicular to the molecular plane (λ_2 (**X-1a**) $\approx \lambda_2$ (**X-5a**)).

2.2.3 ELF

In Fig. (2.4) and Fig. (2.5) two-dimensional plots of the ELF for the neutral ground states $H_2C=XH$ and their protonated derivatives $[H_2C=XH_2]^+$ are shown. The molecules lie with the C–X axis in the paper plane and the hydrogen atoms above and below that plane. The local ELF maxima (bond attractors) M^1 and M^2 of the C=X bond regions are indicated by black dots within a grey colored ELF region in which both maxima are found. Additionally, each plot is overlaid with the C–X bond path, its BCP and the corresponding trace of the interatomic surface $S(\mathbf{r_s})$ (dotted line) derived from the Bader Analysis.

In $H_2C=XH$ the C=X double bond domains are characterized by a distorted dumb-bell shaped region (ELF > 0.88). For lower values (0.8), ELF also surrounds the pnictogen centers, i.e. the ELF for the lone pair at X and ELF for the C=X double bond merge already at high values. For all four species two bond attractors are localized above (M^1) and below (M^2) the C–X bond path on a line perpendicular to the molecular plane. According to Grützmacher and Fässler [2000], finding two weakly separated ELF maxima M^1 and M^2 within one region of high electron localization is proposed to be a criterion for a double bond. This goes back to Silvi and Savin [1994] who first introduced the possibility to classify chemical bonds according to their bonding attractors. Thus, all C=X bonds in $H_2C=XH$ are identified as double bonds in a very simple topographical analysis of the ELF contribution. In **N-1a** and **P-1a**, the two maxima are only weakly separated in contrast to the maxima encountered in the higher homologues **As-1a** and **Sb-1a**. Noteworthy, the separation is higher for the C=As bond than for the C=Sb bond! It is informative to compare the location of the double bond attractors with respect to the position

of the BCP associated with the C–X bond path. Going from the nitrogen to the antimony systems r_b shifts towards the pnictogen center. Concomitantly, M^1 and M^2 are moving in the opposite direction and are always located in the atomic basin of the more electronegative atom.

In the protonated planar derivatives **X-5a** (see Fig. (2.5)) the C=X double bond domains (ELF > 0.80) can be described as a dumb-bell shaped region bended around the pnictogen centers. The absence of the lone pair is seen in the shape of the 0.8 contour lines which do not envelope the X center anymore, at least for X = P, As, Sb. The double bond attractors are more separated from each other compared to the corresponding neutral systems $H_2C=XH$. Again, the separation is largest for the C=As bond decreasing in the order C=As > C=P > C=Sb > C=N. Allowing the planar geometries of the higher monocations $[H_2C=AsH_2]^+$ and $[H_2C=SbH_2]^+$ to trans-bent causes a significant change in the ELF distribution in the C_s symmetry plane of **As-6a** and **Sb-6a**, respectively. The local ELF maximum M^1 above the C–X bond path is shifted towards the outer regions of the heavy atom center. On the other hand, the second maximum M^2 is hardly moved and still located near the C–X bond path. Can these two maxima still be regarded as the two bonding attractors associated with a double bond? Evidently, the ELF region containing both maxima (grey colored area with ELF > 0.80 in Fig. (2.5)) is enlarged and high values of ELF are found above the X center As and Sb. However, the two maxima remain only weakly separated as indicated by the high ELF value in the C–X bond region. Grützmacher and Fässler [2000] derived their double bond criterion by means of homopolar systems in which, for symmetry reasons, the two bond attractors are always equidistantly distributed around the molecular inversion center. For heteropolar systems such as $[H_2C=XH_2]^+$, distortion from planarity reduces the symmetry from C_{2v} to C_s. As a result, the electron density distribution above and below the C–X axis is not equal anymore. Consequently, the bond attractors M^1 and M^1 are distributed accordingly within the C_s symmetry plane, reflecting the

N-1a   **P-1a**

As-1a   **Sb-1a**
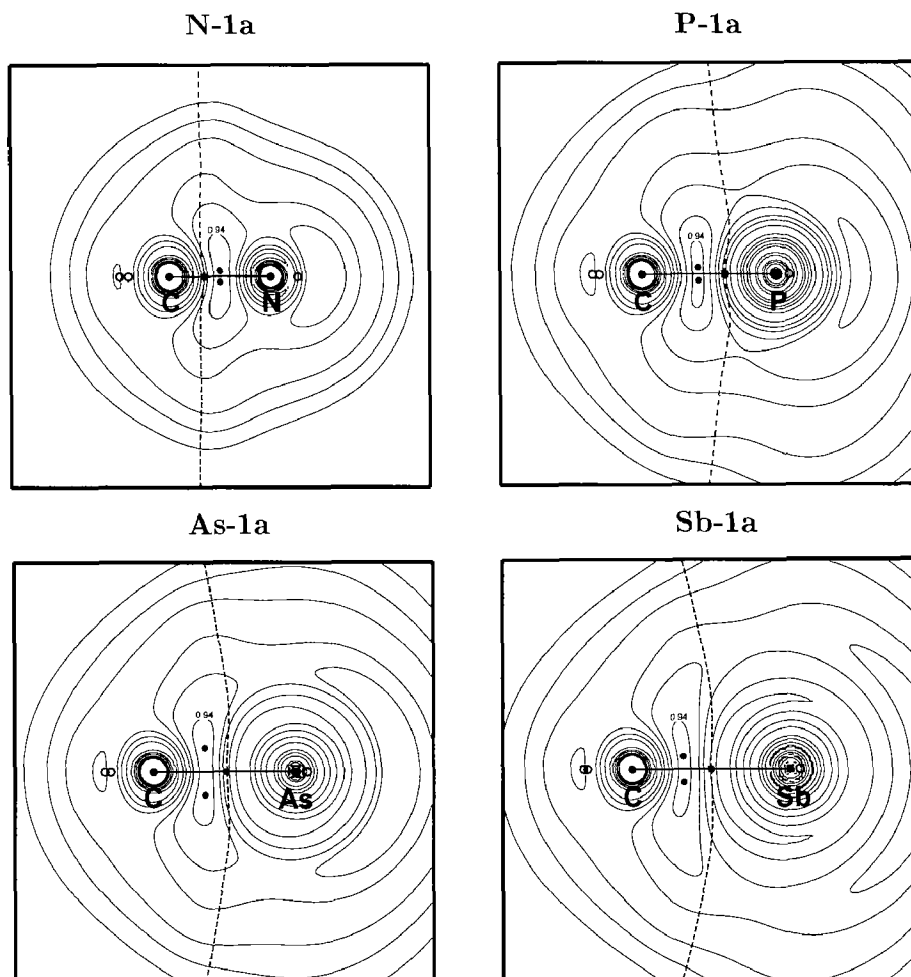
Figure 2.4: Two-dimensional contour plots (perpendicular to the molecular plane) of the ELF distribution in the neutral double bond systems $H_2C=XH$, overlayed with the BPs (—), the BCPs (■) and IASs (- -) from the Bader Analyses of the C=X double bonds. The inner contour lines (—) correspond to ELF = 0.8, 0.88, 0.94. Local ELF maxima > 0.94 , i.e. the bond attractors above (M^1) and below (M^2) the C–X bond paths are indicated as black dots (●). The grey colored regions represent domains within both maxima, M^1 and M^2, are found (ELF > 0.94). Nuclei above and below the plot plane are indicated by black circles (○).
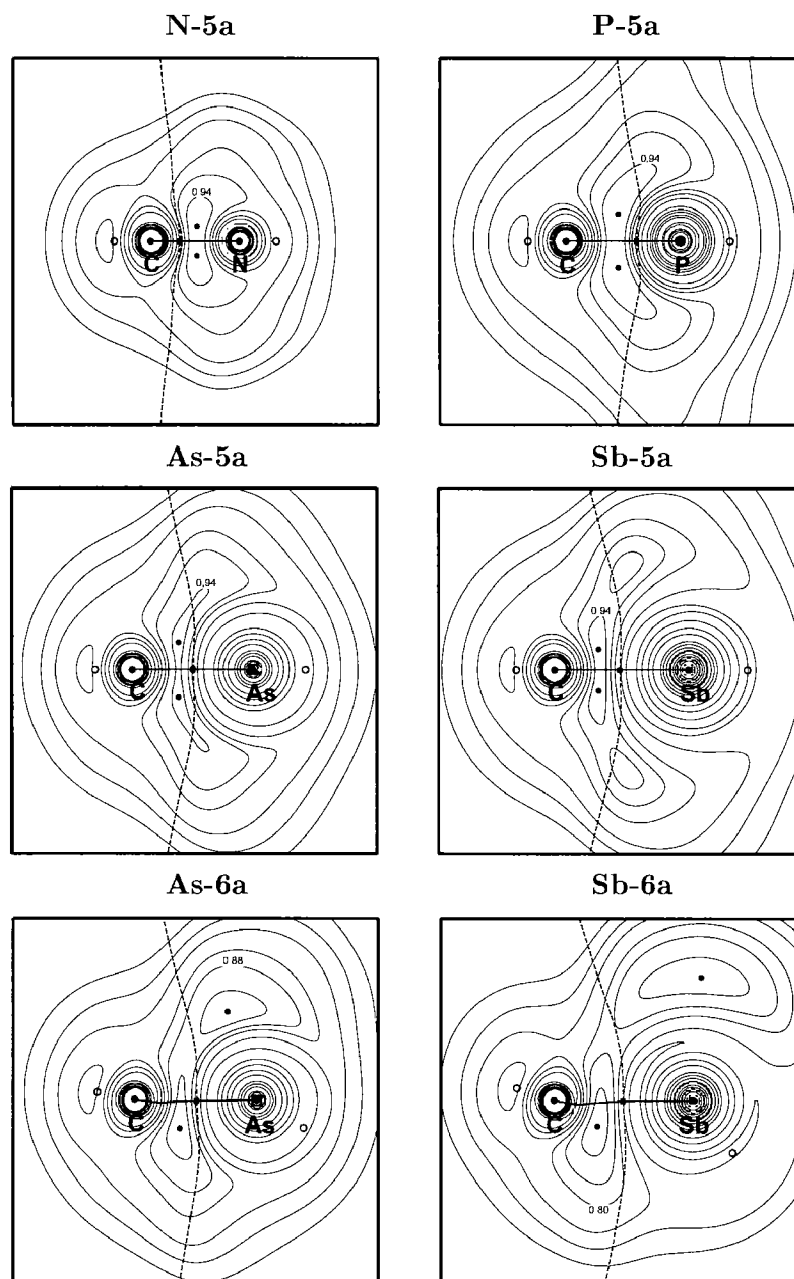
N-5a

P-5a

As-5a

Sb-5a

As-6a

Sb-6a

Figure 2.5: Two-dimesional contour plots (within the σ_v symmetry plane) of the ELF distribution in the monocationic double bond systems $[H_2C=XH_2]^+$ (**X-5a**/**X-6a**) overlayed with the BPs (—), BCPs (■) and the IAS (- -) from the Bader Analyses of the C=X double bonds. The inner contour lines (—) correspond to ELF = 0.8, 0.88, 0.94. Local ELF maxima > 0.94, i.e. the bond attractors above (M^1) and below (M^2) the C–X bond path, are indicated as black dots (●). The grey colored regions represent domains within both maxima, M^1 and M^2, are found (ELF > 0.94 for **X-5a**; ELF > 0.88 for **As-6a**; ELF > 0.80 for **As-6a**). Nuclei above and below the plot plane are indicated by black circles (○).

different nature of the core attractors C and X. In **As-6a** and **Sb-6a** it is evident that M^1 is associated with the pnictogen centers As and Sb respectively, moving over the top of the X atom when ϕ_X goes from 31.1 ° to 51.9 °. However, the angle $\angle CXM^1$ is $\leq$ 90 °. According to the VSEPR theory the maximum for a sole lone pair in such a system would be expected to make an angle $\gg$ 90 ° with respect to the C–X axis. As a result, M^1 and M^2, in **As-6a** and **Sb-6a**, can be seen as still associated with each other forming a attractor pattern for *slipped heteropolar double bonds*. However, from this topographical classification it is not possible to determine whether the planar or the trans-bent geometry is more favorable energetically.

2.3 Protonation of $[H_2C{=}XH_2]^+$

The structures taken into consideration are presented in Fig. (2.6). All dications $[CXH_5]^{2+}$ were optimized under C_s symmetry in the $^1A_1$ electronic ground state, with X = N, P, As, Sb. The corresponding structural data is given in Tab. (2.16). Calculated total and relative energies for minima and transition states of the ylide dications $[H_2C{-}XH_3]^{2+}$ and related systems are presented in Tab. (2.15). As shown in Tab. (2.5) on page 37, the carbon atoms in $[H_2C{=}XH_2]^+$ are considerable negatively charged for the heavier pnictogens X = P, As, Sb. Therefore, we calculated X-site protonation as well as C-site protonation of $H_2C{=}XH$, leading to $[H_2C{-}XH_3]^{2+}$ (**X-9a**) and $[H_3C{-}XH_2]^{2+}$ (**X-11a**), respectively.

If *positive* hyperconjugation contributes to the stability of $[H_2C{-}XH_3]^{2+}$ and $[H_3C{-}XH_2]^{2+}$, pyramidalization of the trigonal coordinated C or X center and narrowing of the angle $\angle H(5)XC$ and $\angle XCH(5)$ are expected. The methylene ammonium dication $[H_2C{-}NH_3]^{2+}$ and its heavier congeners all have a preferred staggered conformation with planar carbenium centers (**X-9a**). The angles $\angle XCH$ decrease from 108.2 ° (X = N) to 100.6 ° (X = P) and 100.5 ° (X = As) to 99.4 ° (X = Sb), and there is no significant bond angle variation within each species. The π popu-

Table 2.15: C–X dications. Energetics for ylide dications $[H_2C\text{-}XH_3]^{2+}$ and related structures (X = N, P, As, Sb).[a]

	CCSD(T)/BS(2,3)//QCISD/BS(1)[b]							
	E_{opt}	ZPE	N	E^1_{ref} [c]	E^2_{ref} [d]	ΔE_{opt}	ΔE^1_{ref}	ΔE^2_{ref}
N-9a	−49.960272	40.0	0	−49.988390	−50.035924	0.0	0.0	0.0
N-10a	−49.960234	39.9	1	−49.988323		−0.1	0.0	
N-14a[TS]	−49.829973	34.6	1	−49.885470	−49.926450	76.4	59.2	63.3
P-9a	−46.548772	31.8	0	−46.580407	−46.640470	0.0	0.0	0.0
P-10a	−46.548668	31.7	1	−46.580288		0.0	0.0	
P-11a	−46.541354	31.8	0	−46.579249	−46.640668	4.6	0.7	−0.1
P-12a	−46.540652	31.8	1	−46.577662		5.1	1.7	
P-13a[TS]	−46.532815	31.2	1	−46.569422	−46.632304	9.4	6.3	4.5
P-14a[TS]	−46.447602	27.7	1	−46.502753	−46.554751	59.4	44.6	49.7
P-15a[TS]	−46.514084	31.6	2[e]	−46.545892	−46.599573	21.5	21.4	25.4
As-9a	−46.194271	30.6	0	−46.224112	−46.269899	0.0	0.0	0.0
As-10a	−46.194216	30.5	1	−46.224045		−0.1	−0.1	
As-11a	−46.205742	31.5	0	−46.240381	−46.288961	−6.2	−9.2	−11.0
As-12a	−46.205642	31.5	1	−46.240181		−6.2	−9.2	
As-13a[TS]	−46.177484	29.9	1	−46.212716	−46.260567	9.9	6.5	5.2
As-14a[TS]	−46.099758	26.6	2[e]	−46.152417	−46.191579	55.4	41.1	45.2
As-15a[TS]	−46.189712	30.9	1	−46.218699	−46.262579	3.2	3.7	4.9
Sb-9a	−45.405071	28.1	0	−45.444362	−45.491339	0.0	0.0	0.0
Sb-10a	−45.405050	28.1	1	−45.444343		0.0	0.0	
Sb-11a	−45.449627	30.7	0	−45.491649	−45.540361	−25.4	−27.1	−28.2
Sb-12a	−45.449621	30.7	1	−45.491630		−25.4	−27.1	
Sb-13a[TS]	−45.387636	27.8	1	−45.432254	−45.481250	10.6	7.2	6.0
Sb-14a[TS]	−45.318806	24.6	2[e]	−45.380621	−45.419593	50.6	36.5	41.5
Sb-15a[TS]	−45.436667	29.5	1	−45.472255	−45.515574	−18.5	−16.2	−13.9

[a] Total energies E in Hartrees, ZPE and relative energies ΔE (including unscaled ZPE corrections) in kcal mol^{-1}. N: Number of imaginary frequencies. For a graphical representation of the structures see Fig. (2.6).

[b] BS(1): VDZP^1; BS(2): VTZP^1; BS(3): VTZP^2.

[c] Refined energies obtained using BS(2).

[d] Refined energies obtained using BS(3).

[e] The second imaginary frequencies are small: 5.4i cm^{-1} (**P-15a**[TS]), 17.8i cm^{-1} (**As-14a**[TS]), 4.6i cm^{-1} (**Sb-14a**[TS]).
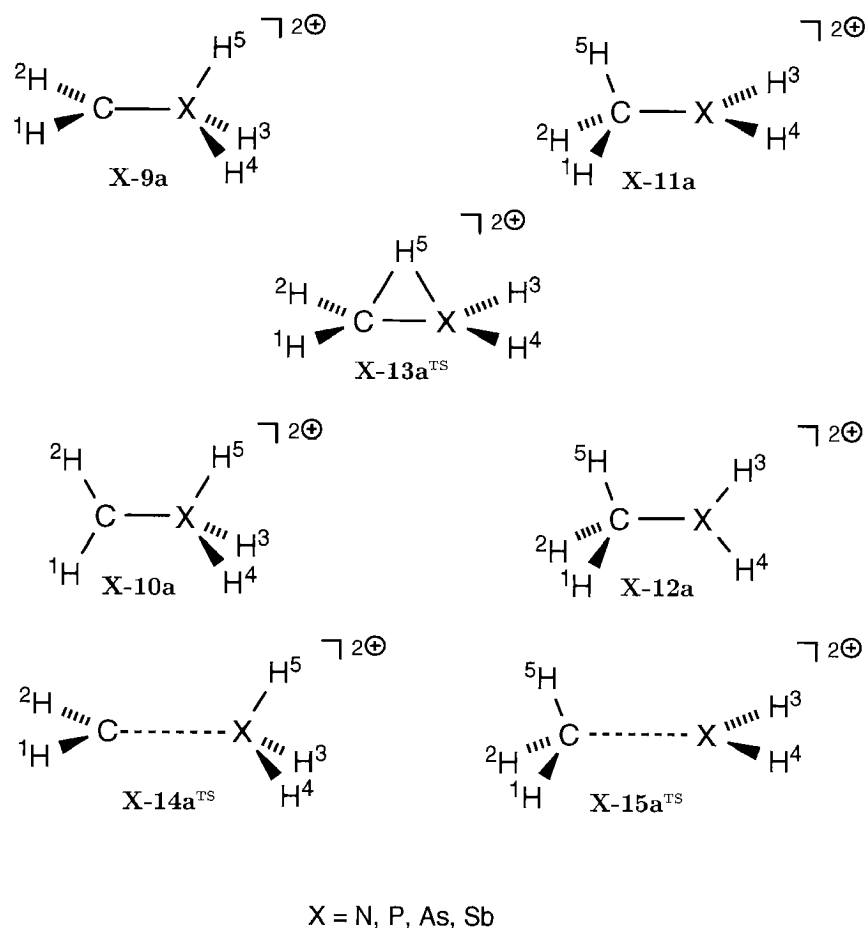
X = N, P, As, Sb

Figure 2.6: Singlet ground state minima and transition states of the C_s symmetric dications $[CXH_5]^{2+}$. For bonding parameters see Tab. (2.3).

lation of the carbon atom in the dication ylides $[H_2C–XH_3]^{2+}$ is almost zero for all X = N, P, As, Sb, indicating that there is no significant π charge transfer in **X-9a** (see Tab. (2.19)). In this context, it is interesting to note that in neutral ylides $H_2C–XH_3$ (X = P, As, Sb), which possess two electrons more, *negative* hyperconjugation leads to pyramidalization of the carbon center [Gilheany 1994].

As reported by Yates et al. [1986], we found that the methylamine dication $[H_3C–NH_2]^{2+}$ is unstable with respect to the 1,2-hydrogen shift that yields **N-9a**. In contrast, the heavier homologues $[H_3C–XH_2]^{2+}$ (**X-11a**) with X = P, As and Sb are all true minima with a preferred staggered conformation. For these three compounds

Table 2.16: C–X dications. Selected structural data for the ylide dications $[H_2C–XH_3]^{2+}$ (**X-9a**) and related systems (X = N, P, As, Sb).[a]

	symmetry/ state	parameters	N	P	As	Sb
X-9a	C_s $^1A_1$	CX	1.426	1.889	1.997	2.235
		XH(3)	1.043	1.411	1.486	1.666
		XH(5)	1.056	1.421	1.495	1.670
		H(1)CH(2)	123.0	112.4	118.1	116.1
		H(1)CX	118.5	120.6	120.9	121.9
		CXH(3)	113.6	107.3	105.8	103.4
		CXH(5)	108.2	100.6	100.5	99.4
		H(3)XH(4)	110.4	115.5	113.4	115.1
X-11a	C_s $^1A_1$	CX		1.739	1.887	2.152
		XH(3)		1.427	1.507	1.686
		H(1)CH(2)		118.5	109.0	111.7
		H(1)CX		115.4	109.6	106.6
		H(5)CX		89.1	102.2	104.2
		CXH(3)		121.1	122.6	123.6
		H(3)XH(4)		116.6	114.7	112.7
		ϕ_X		11.0	3.5	0.0
X-13a^{TS}	C_s $^1A_1$	CX		1.745	1.853	2.078
		CH(5)		1.663	1.778	1.938
		XH(3)		1.417	1.491	1.668
		XH(5)		1.538	1.605	1.779
		H(1)CH(2)		120.6	120.2	118.4
		H(1)CX		119.3	119.2	119.5
		H(5)CX		53.6	52.4	52.4
		H(5)XC		60.5	61.4	59.8
		CXH(3)		117.8	116.7	115.3
		H(3)XH(4)		123.6	124.9	125.9
X-14a^{TS}	C_s $^1A_1$	CX	3.033	3.679	3.816	4.142
X-15a^{TS}	C_s $^1A_1$	CX		2.507	2.611	3.006

[a] QCISD/VDZP[1] data. Bond lengths in Å, angles in degree (°). The CH bond lenghts are omitted ($\approx$ 1.09 Å). Numbering as in Fig. (2.6).

only $[H_3C–PH_2]^{2+}$ shows a noteworthy hyperconjugative interaction, as indicated by the narrow angle $\angle H(5)CP = 89.1$ ° and the pyramidalization of the PH_2 center ($\phi_P = 11.0$ °).[1] In the corresponding homologues $[H_3C–AsH_2]^{2+}$ and $[H_3C–SbH_2]^{2+}$,

---

[1]The resulting geometry is very much dependent on the basis set used. QCISD/6-31G(d,p) data: $\angle H(5)CP = 100.8$ °, $\phi_P = 4.8$ °; QCISD/6-311G(d,p) data: $\angle H(5)CP = 75.5$ °(!), $\phi_P = 14.6$ °. From this, we suggest that some hyperconjugative stabilization is active in $[H_3C–PH_2]^{2+}$.

the angles $\angle$H(5)CX are equal to 102.2 ° and 104.2 °, respectively. Within the chemical accuracy of the calculations, the XH$_2$ units therein can be considered as planar ($\phi_{As} = 3.5$ °, $\phi_{Sb} = 0.0$ °). The loss of hyperconjugation is also seen in the decreasing π populations at X from 0.31 (X = P), to 0.14 (X = As), and 0.06 (X = Sb). The C–X bond lengths in the X-site protonated dications [H$_3$C–XH$_2$]$^{2+}$ are all considerable shorter than in the corresponding isomers [H$_2$C–XH$_3$]$^{2+}$ by 0.015, 0.011 and 0.08 Å for X = P, As, Sb.

The alternative eclipsed structures **X-10a** and **X-12a**, in which the CH$_2$ groups are rotated by 90 ° (see Fig. (2.1)), are all located as saddle points on the PES, i.e they represent the transition structures for internal rotation. The very small energy differences (< 0.1 kcal mol^{-1}), compared to their minimum structures, indicate free rotation around the C–X bond within the dications [CXH$_5$]$^{2+}$ (X = P, As, Sb), for both isomers **X-9a** and **X-11a**.

According to the protonation reactions (Rxn. 2.3) – (Rxn. 2.5), proton affinities (PAs) for the neutral and monocationic minimum ground states H$_2$C=XH and [H$_2$C=XH$_2$]$^+$ (X = N, P, As, Sb) are presented in Tab. (2.17).

$$\text{H}_2\text{C=XH} \quad + \quad \text{H}^+ \quad \longrightarrow \quad [\text{H}_2\text{C=XH}_2]^+ \qquad \text{(Rxn. 2.3)}$$

$$[\text{H}_2\text{C=XH}_2]^+ \quad + \quad \text{H}^+ \quad \longrightarrow \quad [\text{H}_2\text{C–XH}_3]^{2+} \qquad \text{(Rxn. 2.4)}$$

$$[\text{H}_2\text{C=XH}_2]^+ \quad + \quad \text{H}^+ \quad \longrightarrow \quad [\text{H}_3\text{C–XH}_2]^{2+} \qquad \text{(Rxn. 2.5)}$$
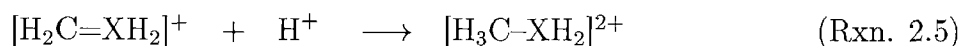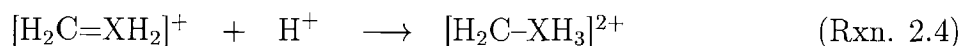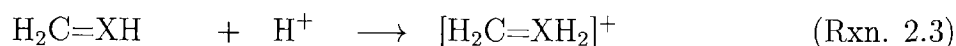
For all methylene pnictanes **X-1a**, protonation is highly exothermic resulting in positive PA values ranging from 170.0 kcal mol^{-1} to 210.0 kcal mol^{-1}, in the order N $>$ P $>$ As $>$ Sb. On the other hand, protonation of the monocationic [H$_2$C=XH$_2$]$^+$, i.e superelectrophilic activation, brings up quite a different picture. According to (Rxn. 2.4) N-site protonation is endothermic resulting in a negative PA value of -28.9 kcal mol^{-1} for the imminium ion [H$_2$C=NH$_2$]$^+$. However, for the heavier congeners of [H$_2$C=NH$_2$]$^+$ the PA values *increase* in the order P $<$ As $<$ Sb, regardless

Table 2.17: C=X double bond systems. Proton affinities PA for the planar methylene pnictanes and their protonated derivatives $[H_2C=XH_2]^+$ according to the protonation reactions reactions (Rxn. 2.3) – (Rxn. 2.5) (X = N, P, As, Sb).[a]

X	(Rxn. 2.3)	(Rxn. 2.4)	(Rxn. 2.5)
N	209.4	−28.9	
P	180.7	−0.7	3.1
As	172.6	6.5	22.6
Sb	170.9	21.9	55.7

[a] CCSD(T)/VTZP^2 data.

of C-site or X-site protonation. At the QCISD/VDZP^1 level, the methylphosphine dication $[H_3C-PH_2]^{2+}$ (P-11a) is 4.6 kcal mol^{-1} higher in energy than the methylene phosphonium dication $[H_2C-PH_3]^{2+}$ (P-11a). However, refinement at the CCSD(T) level of theory reverses this energy difference to −0.1 kcal mol^{-1}. Thus, according to the protonation reactions (Rxn. 2.4) and (Rxn. 2.5), PA values for P-5a of −0.7 kcal mol^{-1} and 3.1 kcal mol^{-1} are obtained, slightly favoring C-site protonation by 3.8 kcal mol^{-1}. For the heavier isomers $[H_2C=AsH_2]^+$ and $[H_2C=SbH_2]^+$, C-site protonation becomes even more favored over X-site protonation by 16.1 kcal mol^{-1} and 33.8 kcal mol^{-1}, respectively. This trend can be simply explained by the differences in the X-H bond energies which sharply decrease in the order P > As > Sb.

The charge distributions in the dications have been calculated from the NBO analyses. The values for atom and group charges are summarized in Tab. (2.18). In comparison to $[H_2C=XH_2]^+$, where the carbon centers are negatively charged for X = P, As, Sb ($\approx$ −0.63 e, see Tab. (2.5)), the atomic charges of the carbon centers in the ylide dications X-9a decrease from 0.57 e (X = N), over 0.11 e (X = P), and 0.08 e (X = As), to −0.01 e (X = Sb). Concomitantly, the atomic charge of X increases

Table 2.18: C–X dications. Atomic and group charges for the dications $[H_2C–XH_3]^{2+}$ (**X-9a**) and $[H_3C–XH_2]^{2+}$ (**X-11a**).[a]

	atoms/ groups	X			
		N	P	As	Sb
X-9a	C	0.57	0.11	0.078	−0.01
	X	−0.90	0.76	0.93	1.41
	H(1)	0.32	0.31	0.30	0.28
	H(3)	0.56	0.17	0.13	0.01
	H(5)	0.58	0.18	0.14	0.01
	CH_2	1.21	0.72	0.67	0.56
	XH_3	0.79	1.28	1.33	1.44
X-11a	C		−1.04	−1.06	−1.00
	X		1.52	1.72	2.04
	H(1)		0.40	0.37	0.34
	H(3)		0.16	0.10	−0.04
	H(5)		0.42	0.40	0.35
	CH_3		0.17	0.08	0.03
	XH_2		1.83	1.92	1.97

[a] QCISD/VDZP[1] data. Numbering as in Fig. (2.6).

from $−0.87\,e$ for N, $0.76\,e$ for P, $0.93\,e$ for As and $1.41\,e$ for Sb, as expected from the decreasing electronegativities. The charge distributions in the C-site protonated dications **X-11a** are unexpected at first glance. The carbon centers become considerably more negatively charged, when compared to the monocations $[H_2C=XH_2]^+$, while the X-centers bear highly positive charges which increase in the order X = P < As < Sb. However, including the charges residing at the hydrogen centers in $[H_2C=XH_2]^+$, $[H_2C–XH_3]^{2+}$ and $[H_3C–XH_2]^{2+}$, a somewhat different picture is obtained when the group charges are compared. The CH_2 group in $[H_2C=XH_2]^+$ remains slightly negatively charged for X = P, As, Sb, while the CH_3^+ groups in **X-11a** bear small positive charges. The +2 charge in these cations is mainly located on the X centers. In the X-site protonated dications **X-9a**, the charge is more uniformly distributed over the skeleton, but the larger portion of the positive charge

Table 2.19: C–X dications. Calculated σ and π populations at the CH_2 and XH_2 centers of the ylide dications $[H_2C–XH_3]^{2+}$ (**X-9a**) and their isomers $[H_3C–XH_2]^{2+}$ (**X-11a**) (X = N, P, As, Sb).[a]

	atoms	X = N		X = P		X = As		X = Sb	
		p_σ	p_π	p_σ	p_π	p_σ	p_π	p_σ	p_π
X-9a	C	3.30	0.09	3.79	0.07	3.83	0.06	3.92	0.05
X-11a	X			3.09	0.31	3.08	0.14	2.85	0.06

[a] $QCISD/VDZP^1$ data derived from NBO analyses. Numbering as in Fig. (2.1).

remains located at the XH_3^+ groups, as expected. In summary, the trigonal planar CH_2 units in **X-9a** bear the most positive charge of the hydrocarbon units of all cations studied here, and thus may be designed as activated for nucleophilic attack. In general, in each homologous series of mono- and dications, the positive charges at the XH_n groups increase in the order Sb > As > P ≫ N as electron density is accumulated at the corresponding CH_m units. (see Tab. (2.5) and Tab. (2.18))

Following previous studies by Bernardi et al. [1986] and Kapp et al. [1996] focusing on the stability of the monocations $[H_2C=XH_2]^+$, we examined the methyl stabilization energies (MSEs) of the X-site protonated dications $[H_3C–XH_2]^{2+}$ (**X-9a**) by application of the isodesmic reaction (Rxn. 2.6) and (Rxn. 2.7). The MSE values are presented in Tab. (2.20).

$$[H_2C=XH_2]^+ \quad + \quad CH_4 \quad \longrightarrow \quad H_3C–XH_2 \quad + \quad CH_3^+ \qquad \text{(Rxn. 2.6)}$$

$$[H_2C–XH_3]^{2+} \quad + \quad CH_4 \quad \longrightarrow \quad [H_3C–XH_3]^+ \quad + \quad CH_3^+ \qquad \text{(Rxn. 2.7)}$$
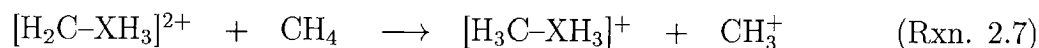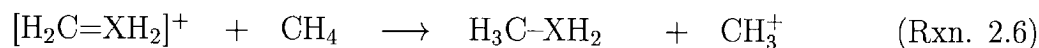
We re-examined, at the QCISD level, the stabilization energies for the monocations $[H_2C=XH_2]^+$ which are positive, decreasing from 97.7 $kcal\,mol^{-1}$ for NH_2 over 59.7 $kcal\,mol^{-1}$ for PH_2 and 51.7 $kcal\,mol^{-1}$ for AsH_2 to 47.9 $kcal\,mol^{-1}$ for SbH_2. This is in good agreement with the methyl stabilization energies calculated by Kapp

Table 2.20: C=X double bond systems. Methyl stabilization energies MSE for the pnicto carbenium ions $[H_2C=XH_2]^+$ and the ylide dications $[H_2C-XH_3]^{2+}$ according to the isodesmic reactions (Rxn. 2.6) and (Rxn. 2.7), respectively (X = N, P, As, Sb). [a]

X	(Rxn. 2.6)			(Rxn. 2.7)
	this work	Kapp[b]	exp	
N	97.7	93.9	95.0	−150.7
P	59.7	61.4		−141.0
As	51.7	50.7		−132.7
Sb	47.9	45.2		−121.0

[a] CCSD(T)/VTZP[1] data.

[b] in [Kapp et al. 1996].

et al. [1996]. The reduction of the stabilization energies is rationalized in terms of the cost of planarization energies of trigonal coordinated X centers which increase in the order N $\ll$ P $<$ As $<$ Sb. This argument can be also used to explain why $[H_2C=AsH_2]^+$ and $[H_2C=SbH_2]^+$ tend to adapt the trans-bent structures **As-6a** and **Sb-6a**. However, as shown by Kapp et al. [1996], adding the intrinsic pyramidalization energy to the MSE values, the *inherent* stabilization by π donation is almost the same for all X = N, P, As, Sb.

In contrast, the stabilization energies are strongly negative for the ylide dications $[H_2C-XH_3]^{2+}$ (**X-9a**) and show the inverse trend, i.e. they become less exothermic in going from the ammonium to the stibonium substituted dications. In other words, the dication $[H_2C-SbH_3]^{2+}$ is thermodynamically more stable than its lighter congeners. This is not surprising since protonation of the monocations $[H_2C=XH_2]^+$ destroys the π-system. Thus, charge transfer in the dications to the formally electron deficient carbon center is solely due to σ-donation, which is most effective for the most electropositive substituent.

The energy profile for the dications $[\text{CXH}_5]^{2+}$ is shown in Fig. (2.7) (X = N, P, As, Sb). For all three pairs of the heavier systems with X = P, As, Sb we found the C_s-symmetric structures **X-13a**$^{\text{TS}}$ as transition states for the rearrangement of X-site to C-site protonated isomers via 1,2-hydrogen shift. This is in contrast to the ethyl cation $[\text{C}_2\text{H}_5]^+$, where the C_{2v}-symmetric H-bridged structure corresponds to the global minimum on the energy hypersurface [Raghavachari et al. 1981]. The energy barrier for the $[\text{H}_2\text{C--XH}_3]^{2+} \rightarrow [\text{H}_3\text{C--XH}_2]^{2+}$ hydrogen migration is rather small, increasing from 4.5 kcal mol^{-1} for X = P, to 5.2 kcal mol^{-1} for X = As, and 6.0 kcal mol^{-1} for X = Sb. While the rearrangement of methylene phosphonium $[\text{H}_2\text{C--PH}_3]^{2+}$ to $[\text{H}_3\text{C--PH}_2]^{2+}$ is almost thermoneutral (-0.1 kcal mol^{-1}), it becomes increasingly exthothermic for the heavier homologues with X = As, Sb by -11.0 kcal mol^{-1} and -28.2 kcal mol^{-1}, respectively. Thus, the barrier for the reverse process, i.e. 1,2-hydrogen shift from the more stable C-site protonated species to the X-site protonated species is rather high for X = As (16.2 kcal mol^{-1}) and X = Sb (34.2 kcal mol^{-1}).

$$[\text{H}_2\text{C--XH}_3]^{2+} \longrightarrow \text{CH}_2^{\bullet+} + \text{XH}_3^{\bullet+} \qquad \text{(Rxn. 2.8)}$$

$$[\text{H}_3\text{C--XH}_2]^{2+} \longrightarrow \text{CH}_3^+ + \text{XH}_2^+ \qquad \text{(Rxn. 2.9)}$$
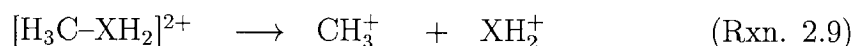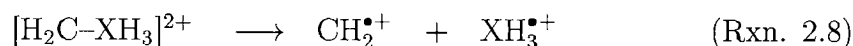
In order to study the decomposition pathways for the dications $[\text{CXH}_5]^{2+}$, we examined the dissociation processes (Rxn. 2.8) and (Rxn. 2.9), respectively. For $[\text{H}_2\text{C--NH}_3]^{2+}$ and $[\text{H}_2\text{C--PH}_3]^{2+}$, Yates et al. [1986] showed that the fragmentation processes are exothermic having substantial activation barriers. Our results presented in Tab. (2.21) are in general agreement with these findings. Direct homolytic C-X bond cleavage of $[\text{H}_2\text{C--XH}_3]^{2+}$ into the radical fragments $\text{CH}_2^{\bullet+}$ and $\text{XH}_3^{\bullet+}$ is exothermic for all X = N, P, As, Sb, ranging from -23.5 kcal mol^{-1} to -25.8 kcal mol^{-1}. For the corresponding transition states, saddle points of first (**X-14a**$^{\text{TS}}$, X = N, P) and second order (X = As, Sb) were located. However, the second negative vibrations are small in magnitude ($< 20i$ cm^{-1}, see Tab. (2.15)),

Table 2.21: C–X dications. Dissociation energies D_0 for the C–X fragmentation reactions (Rxn. 2.8) and (Rxn. 2.9) for the dications **X-9a** and **X-11a** (X = N, P, As, Sb).

X	(Rxn. 2.8)		(Rxn. 2.9)	
	this work[a]	Yates[b]	this work[a]	Yates[b]
N	−23.5 (27.8)	−28.0		
P	−23.7 (−28.9)	−27.2	−65.0 (−71.0)	−65.2
As	−25.8 (−30.0)		−71.4 (−76.8)	
Sb	−24.2 (−29.3)		−65.0 (−70.7)	

[a] ZPE corrected $CCSD(T)/VTZP^2$ values obtained using the $QCISD/VDZP^1$ optimized geometries in kcal mol^{-1} ($VTZP^1$ values in parentheses).

[b] in [Yates et al. 1986].

indicating that the PES in that region is very flat. This is caused by the free internal rotation owing to the long C–X bonds in **X-14a**^{TS}. Therefore, the differences of the total energies of **X-14a**^{TS} and **X-9a** can be taken as a good approximation for the activation barriers of (Rxn. 2.8) for all X = N, P, As, Sb. Within these limits, the values of these barriers are 63.3 kcal mol^{-1} for X = N, 49.7 kcal mol^{-1} for X = P, 45.2 kcal mol^{-1} for X = As, and 41.5 kcal mol^{-1} for X = Sb. We are aware that single-configuration treatment do not describe homolytic bond cleavage of the type (Rxn. 2.8) particularly well and may lead to an overestimation of the barriers by as much as 20 kcal mol^{-1} as pointed out by Yates et al. [1986]. Including this correction does not affect the principal conclusion that there remain substantial residual barriers to homolytic fragmentation.

Decomposition of the C-site protonated dications $[H_3C–XH_2]^{2+}$ into the singlet ground states of the monocationic fragments CH_3^+ and XH_2^+ is exothermic by 65.0 kcal mol^{-1} for X = P, Sb and 71.4 kcal mol^{-1} for X = As. Taking **X-15a**^{TS} as transition states, we found considerably smaller activation barriers for (Rxn. 2.9)
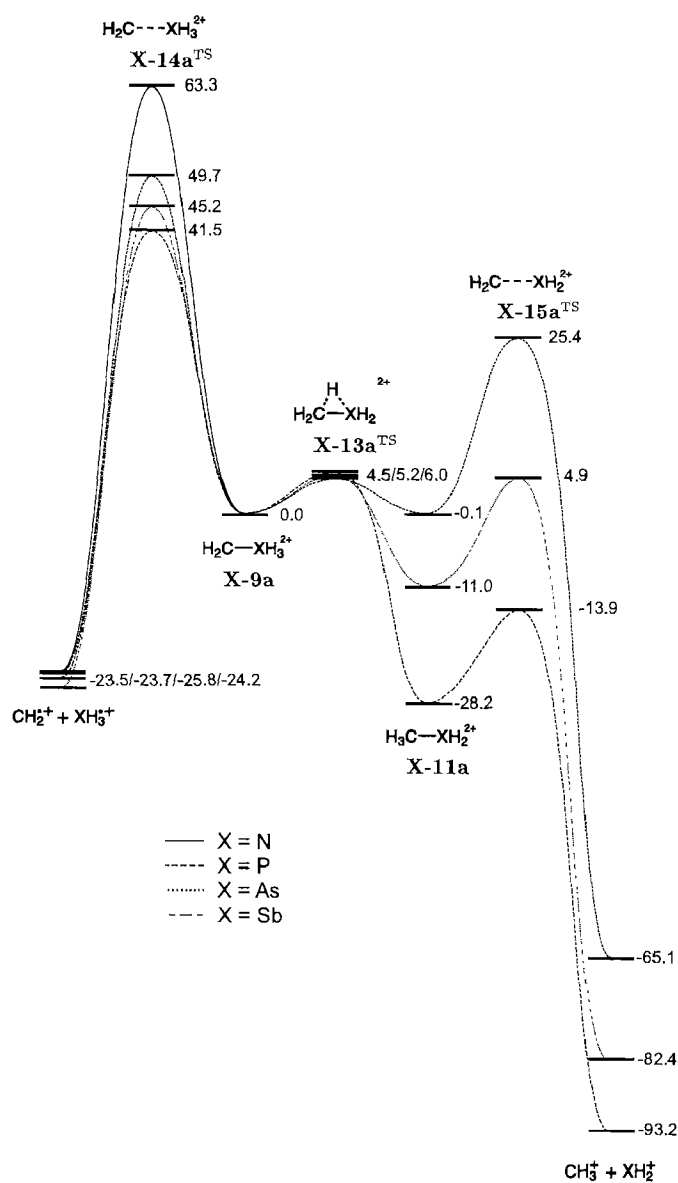
Figure 2.7: Schematic energy profile for the dissociative processes in the dications **X-9a** and **X-11a**.

compared to (Rxn. 2.8), decreasing from $25.5\,\text{kcal}\,\text{mol}^{-1}$, over $15.9\,\text{kcal}\,\text{mol}^{-1}$ to $14.3\,\text{kcal}\,\text{mol}^{-1}$.

These results show that although the stability of the dications increase with P < As < Sb, the phosphorus stabilized dications **P-11a** and **P-9a** are kinetically more persistent against C–X bond fission than their heavier homologues. Are the dications stable enough against Coulomb-explosions, due to repulsive interactions of the pos-

itive charges, to be generated experimentally? The exothermic $(23 - 26 \, \text{kcal mol}^{-1})$ *homolytic* dissoziations into the radicals $CH_2^{\bullet+}$ and $XH_3^{\bullet+}$ are hindered by substantial barriers in the range of $40 - 60 \, \text{kcal mol}^{-1}$. The dissociation of $[H_3C–XH_2]^{2+}$ (**X-11a**, X = P, As, Sb) into CH_3^+ and the singlet carbenoid fragments XH is even more exothermic by about $65 - 70 \, \text{kcal mol}^{-1}$ for all X = P, As, Sb. The associated barriers are smaller for this reaction, ranging between $14 - 26 \, \text{kcal mol}^{-1}$. Here, the thermodynamically most stable C-site protonated dications **As-11a** and **Sb-11a** are kinetically the most labile. It should be possible, however, to generate these dications under suitable conditions, i.e. long life stable ions, and use themselves or their fragmentation products, i.e. XR_2^+ species, as building blocks which possess either a highly electrophilic carbon center or hetero element center.

3. Homonuclear Double Bonding in Group 15: Neutral and Cationic Dipnictenes

Seite Leer /
Blank leaf

Like the famous heavier group 14 analogues of ethylene, the main group 15 dipnictenes have played a central role in the development of the chemistry of multiple bonding in higher row elements. The lightest derivatives are the ubiquitous azo compounds (diazenes) already known for decades. The idea of kinetic stabilization of reactive double bonds by very bulky substituents was the synthetic key to the higher congeners of the diazenes: Yoshifuji et al. [1981] presented the first stable diphosphene, Mes*P=PMes*, a true milestone in inorganic chemistry. Since then, numerous other diphosphenes have been synthesized and structurally characterized (for a up-to-date list of trans- and cis-diphosphenes see Power [1999]). A common synthetic strategy to diphosphenes and related systems is the reductive coupling of dichlorophosphanes $RPCl_2$ by magnesium metal. This approach was also successfully utilized to synthesize the first two diarsenes, $Mes^*As=AsCH(SiMe_3)_2$ and $(SiMe_3)_3CAs=AsC(SiMe_3)_3$ by Cowley et al. [1983, 1985]. The story of As=As double bonds was supplemented only recently by two novel compounds presented in [Twamley et al. 1999], using the very bulky m-terphenyl ligands $-C_6H_3$-2,6-Mes_2 and $-C_6H_3$-2,6-$Trip_2$. This authors also succeeded in the synthesis of the corresponding higher distibenes as well as the dibismutenes. However, the first compounds with such Sb=Sb and Bi=Bi double bonds were synthesized by Tokitoh et al. [1998, 1997]. The synthesis, structures and reactivities of the diphosphenes and their higher congeners have been comprehensively reviewed earlier by Cowley [1984], Cowley and Norman [1986] and Yoshifuji [1990], and more recently by Weber [1992] and Power [1999].

Theoretical works on the diphosphene HP=PH showed that the LUMO is the π^* orbital and that the two HOMOs are the π^* orbital and n_+ lone pair combination. These two orbitals are very close in energy with the lone pair slightly more stable (ca. 0.1 eV) [Ito and Nagase 1986, Nagase et al. 1990]. Consistent with the increasing s character of the lone pair, calculations of the heavier dipnictenes HX=XH (X = P,

As, Sb, Bi) showed that the n_+ molecular orbital becomes increasingly more stable relative to the π HOMO [Nagase et al. 1990].

Accordingly, any attempts to synthesize and isolate protonated or alkylated dipnictenium ions, in analogy to the well known amino phosphenium ions $[R_2N=PR]^+$ [Cowley and Kemp 1985], failed for a long time. Only Lately, the first and so far only species of this type, the phosphanyl phosphenium ion $[Mes^*MeP=PMes^*]^+$, was successfully generated and structurally characterized [Loss et al. 1999]. One major difficulty in the synthesis of such cations is certainly the enhanced nucleophility of the $X=X$ double bond in the dipnictenes of the higher row elements.

3.1 Selected molecular structures of X_2H_2 and their protonated forms $[X_2H_3]^+$ and $[X_2H_4]^{2+}$.

The various dipnictenes investigated are presented in Fig. (3.1), corresponding structural data is given in Tab. (3.2). The flap angle ϕ_X is used as a measure of the deviation from planarity of a pyramidalized atomic center X within a molecule (For a graphical representation see Scheme 2.1 on page 26). Calculated total and relative energies for all species are presented in Tab. (3.1).

We re-examined the neutral *trans* dipnictenes **X-16a** and their corresponding skewed triplet minima **X-17a** for the sake of completeness. Previous theoretical works have shown that the trans form of $HX=XH$ represent the global minima for all $X = N$, P, As, Sb. We refer to Ito and Nagase [1986] and Jensen et al. [1987] for a discussion of the various possible isomers of the N_2H_2 PES and to Nagase et al. [1990] and Schoeller et al. [1997] for corresponding calculations of the heavier congeners $HX=XH$ with $X = P$, As,Sb, Bi.

Table 3.1: X=X double bond systems. Energetics for neutral dipnictenes HX=XH (**X-16a**), their protonated derivatives $[H_2X=XH]^+$ (**X-19a**) and $[H_2X=XH_2]^{2+}$ (**X-23a/X-24a**) and related systems (X = N, P, As, Sb).[a]

| | | CCSD(T)/BS(1,2)//MP2/BS(1)[b] |
		E_{opt}	ZPE	N	E^1_{ref} [c]	E^2_{ref} [d]	ΔE_{opt}	ΔE^1_{ref}	ΔE^2_{ref}
N-16a		−20.882482	18.0	0	−20.937951	−20.993954	0.0	0.0	0.0
N-17a	^{3}B	−20.806384	15.9	0	−20.863948	−20.921832	45.6	44.3	43.1
N-19a		−21.196914	27.1	0	−21.252631	−21.306153	0.0	0.0	0.0
N-20a	^{3}A$''$	−21.120208	24.7	0	−21.172779	−21.225848	45.7	47.7	48.0
N-21a		−21.056224	22.8	1	−21.117647	−21.170407	84.0	80.4	80.9
N-22a		−21.091570	21.9	1	−21.143141	−21.197004	60.9	63.5	63.3
N-23a		−21.230153	34.2	0	−21.282360	−21.334121	0.0	0.0	0.0
N-25a	^{3}A$_2$	−21.122242	30.6	0	−21.179239	−21.228599	64.1	61.1	62.6
N-26a$^{\text{TS}}$		−20.932027	26.5	1	−21.039945	−21.080814	179.4	144.5	151.3
P-16a		−14.124924	11.2	0	−14.191877	−14.272050	0.0	0.0	0.0
P-17a	^{3}B	−14.079914	10.2	0	−14.144635	−14.220864	27.2	28.6	31.1
P-19a		−14.416110	16.8	0	−14.487454	−14.565435	0.0	0.0	0.0
P-20a	^{3}A$''$	−14.377940	16.0	0	−14.445589	−14.518757	23.2	25.5	28.5
P-21a		−14.386564	16.5	0	−14.459749	−14.536665	18.2	17.1	17.7
P-22a		−14.380783	16.2	0	−14.454612	−14.531210	21.6	20.0	20.9
P-23a		−14.462538	21.1	1	−14.537336	−14.612327	0.1	0.6	0.2
P-24a		−14.463341	21.6	0	−14.539028	−14.613356	0.0	0.0	0.0
P-25a	^{3}B	−14.433278	21.5	0	−14.502321	−14.571586	18.8	23.0	26.1
P-26a$^{\text{TS}}$		−14.395433	19.6	1	−14.477414	−14.543768	40.6	36.7	41.7
As-16a		−13.442102	9.9	0	−13.498955	−13.555934	0.0	0.0	0.0
As-17a	^{3}B	−13.405176	9.1	0	−13.458368	−13.513188	22.3	24.6	25.9
As-19a		−13.728167	15.1	0	−13.789642	−13.842669	0.0	0.0	0.0
As-20a	^{3}A$''$	−13.701648	14.5	0	−13.757862	−13.807711	16.1	19.4	21.3
As-21a		−13.717843	15.1	0	−13.780140	−13.833061	6.4	5.9	6.0
As-22a		−13.713062	14.9	0	−13.775990	−13.828794	9.2	8.3	8.5
As-23a		−13.771025	19.4	1	−13.837624	−13.888551	4.8	5.8	5.1
As-24a		−13.779605	20.0	0	−13.847881	−13.897639	0.0	0.0	0.0
As-25a	^{3}B	−13.756672	19.8	0	−13.816988	−13.863767	14.2	19.2	21.1
As-26a$^{\text{TS}}$		−13.748443	18.4	1	−13.817057	−13.862323	18.0	17.8	20.6
Sb-16a		−11.870245	8.4	0	−11.933438	−11.987927	0.0	0.0	0.0
Sb-17a	^{3}B	−11.845133	7.8	0	−11.903348	−11.955807	15.1	18.2	19.5
Sb-19a		−12.158896	12.9	0	−12.229040	−12.280601	0.0	0.0	0.0
Sb-20a	^{3}A$''$	−12.146490	12.5	0	−12.210214	−12.258812	7.4	11.4	13.3
Sb-21a		−12.161917	13.0	0	−12.232713	−12.284791	−1.7	−2.1	−2.5
Sb-22a		−12.158270	12.9	0	−12.229644	−12.281569	0.4	−0.3	−0.6
Sb-23a		−12.216779	16.7	1	−12.297319	−12.347517	11.4	12.4	11.8
Sb-24a		−12.235735	17.2	0	−12.317805	−12.366963	0.0	0.0	0.0
Sb-25a	^{3}B	−12.221254	17.1	0	−12.294510	−12.341414	9.0	14.6	15.9
Sb-26a$^{\text{TS}}$		−12.229912	16.4	1	−12.308033	−12.353211	2.9	5.4	7.9

[a] Total energies E in Hartrees, ZPE and relative energies ΔE (including unscaled ZPE corrections) in kcal mol^{-1}. N: number of imaginary frequencies. For a graphical representation of the structures see Fig. (3.1).

[b] BS(1): VDZP; BS(2): VTZP^2.

[c] Refined energies obtained using BS(1).

[d] Refined energies obtained using BS(2).
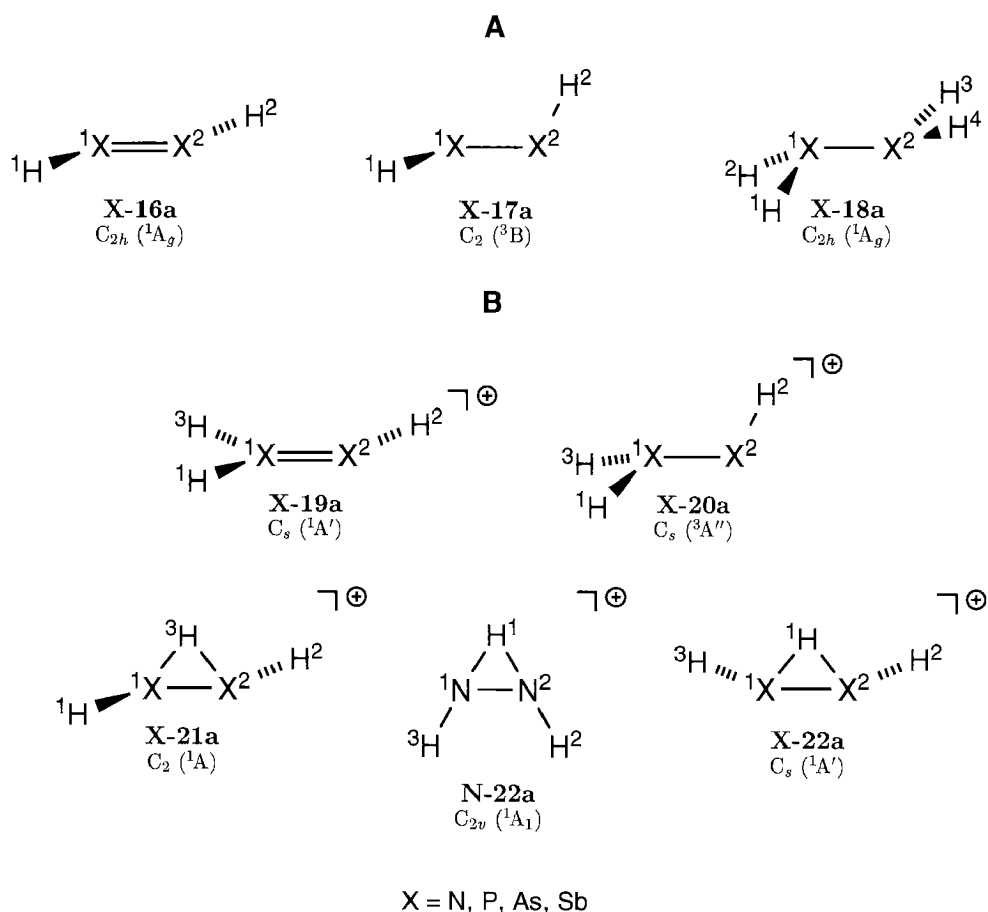
Figure 3.1: Optimized Structures for the neutral dipnictenes X_2H_2 (**A**) and their singly protonated derivatives $[X_2H_3]^+$ (**B**). For bonding parameters see Tab. (3.2).

The bond shortening of the double bond in the dipnictenes **X-16a** ranges from 15% for X = N to 7 − 9% for P > As > Sb, with respect to the equilibrium X–X distances in the trans-bent dipnictanes H_2X–XH_2: 1.482 Å (N–N), 2.271 Å (P–P), 2.470 Å (As–As), 2.862 Å (Sb–Sb). The high margin for the X = N case is attributed to the elongated N–N bond in the diazane H_2N–NH_2, caused by the repulsive 2c-4e π_{nn} interaction of the two adjacent lone pairs at the nitrogens. For the X–X bonds with X = P, As, Sb, the influence of the lone pair repulsion on the bond length of the corresponding dipnictanes is much smaller, decreasing from P to Sb. As we expect from the increasing inability of the heavier group 15 elements to hybridize,

X = N, P, As, Sb
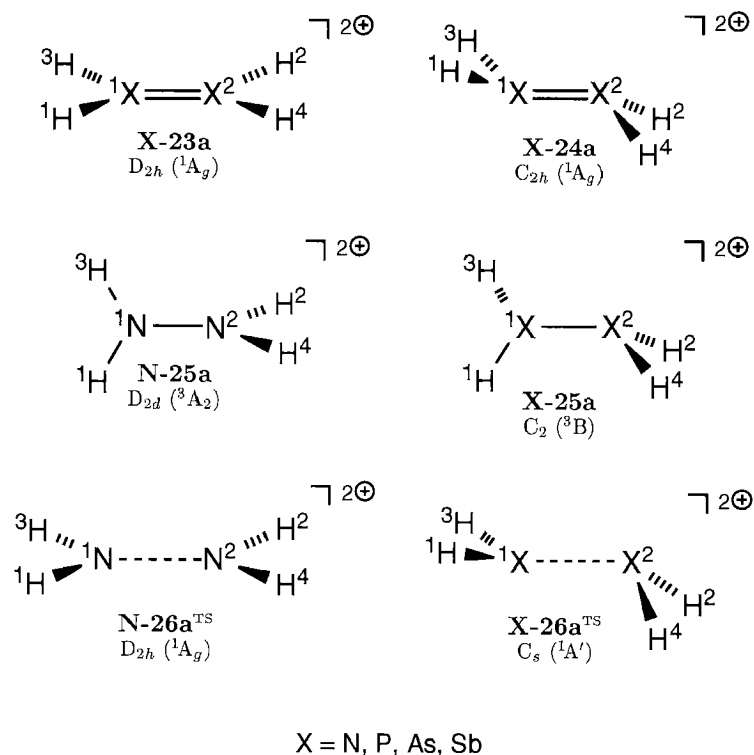
Figure 3.2: Optimized structures for the dications $[X_2H_4]^{2+}$. For bonding parameters see Tab. (3.2).

the $\angle$HXX in the dipnictenes **X-16a** goes toward 90 ° when X goes from nitrogen to antimony. The X=X double bond in the dipnictenes **X-16a** increases in steps of 65% (N=N $\rightarrow$ P=P), 10% (P=P $\rightarrow$ As=As) and 17% (As=As $\rightarrow$ Sb=Sb), ranging from 1.262 Å to 2.676 Å. The significant difference in the bond lengths between the diimine HN=NH and its higher congeners reveal the increasing influence of the *mutual* interatomic Pauli repulsion for the heavier group 15 elements phosphorus, arsenic and antimony. For comparison, the C=X heteronuclear double bond in H_2C=PH is only 30% longer than in the imine H_2C=NH.

The corresponding skewed triplets **X-17a** were optimized in C_2 symmetry. Frequence analyses identified the stationary points as local minima at the T^1 hypersurface. For the heavier systems with X = P, As, Sb our results are in good agreement

Table 3.2: X=X double bond systems. Selected structural data for the neutral dipnictenes HX=XH (**X-16a**), their protonated derivatives $[H_2X=XH]^+$ and $[H_2X=XH_2]^{2+}$ and related systems (X — N, P, As, Sb).[a]

	symmetry/ state	parameters	X			
			N	P	As	Sb
X-16a	C_{2h} ^1A_g	X(1)X(2)	1.262	2.077	2.283	2.676
		H(1)X(1)X(2)	105.0	93.51	91.9	90.6
X-17a	C_2 ^3B	X(1)X(2)	1.255	2.231	2.452	2.858
		H(1)X(1)X(2)	117.9	94.2	92.4	91.3
		H(1)X(1)X(2)H(2)	103.6	90.4	90.0	90.6
X-18a	C_{2h} ^1A_g	X(1)X(2)	1.482	2.271	2.470	2.862
		H(1)X(1)H(3)	102.1	93.5	91.4	91.1
		ϕ_X	69.1	84.9	87.0	88.5
X-19a	C_s $^1A'$	X(1)X(2)	1.235	2.042	2.243	2.637
		H(1)X(1)X(2)	116.7	120.2	121.6	124.0
		H(1)X(1)H(3)	118.2	112.8	111.2	108.9
		X(1)X(2)H(2)	110.0	89.0	86.9	84.4
X-20a	C_s $^3A''$	X(1)X(2)	1.295	2.215	2.444	2.874
		H(1)X(1)H(3)	118.3	104.2	101.8	99.6
		X(1)X(2)H(2)	123.7	95.3	92.7	90.3
		ϕ_X	29.2	53.9	55.6	57.1
X-21a	C_2 ^1A	X(1)X(2)	1.313	2.151	2.365	2.767
		X(1)H(3)	1.274	1.644	1.738	1.941
		H(1)X(1)X(2)	106.1	92.0	89.8	87.8
		X(1)H(3)X(2)	62.0	81.6	85.8	90.9
X-22a [b]	C_s $^1A'$	X(1)X(2)	1.271	2.164	2.379	2.785
		X(1)H(1)	1.247	1.645	1.741	1.943
		H(3)X(1)X(2)	123.5	96.7	94.3	90.9
		X(1)H(1)X(2)	61.3	82.1	86.2	91.6
X-23a	D_{2h} ^1A_g	X(1)X(2)	1.238	2.032	2.214	2.598
		H(1)X(1)H(3)	120.1	124.3	124.8	124.8
X-24a	C_{2h} ^1A_g	X(1)X(2)		2.051	2.277	2.732
		H(1)X(1)H(3)		120.9	114.1	108.4
		ϕ_X		28.7	45.7	52.7
X-25a [c]	C_2 ^3B	X(1)X(2)	1.368	2.261	2.468	2.894
		H(1)X(1)H(3)	122.4	115.4	113.7	112.0
		H(1)X(1)X(2)H(2)	90.0	57.7	65.1	79.8
		ϕ_X	0.0	47.7	51.8	55.7
X-26a[TS] [d]	C_s ^3A	X(1)X(2)	2.273	3.011	3.086	3.271
		H(1)X(1)H(3)	108.3	99.7	99.4	100.5
		H(2)X(2)H(4)	108.3	93.5	92.1	91.4
		ϕ_{X^1}	0.0	12.0	7.4	2.4
		ϕ_{X^2}	0.0	87.6	93.3	102.5

[a] $MP2/VDZP^1$ data. Bond lengths in Å, angles in degrees (°). The XH bond lengths are omitted (NH: 1.01 − 1.05 Å; PH: 1.40 − 1.43 Å; AsH: 1.48 − 1.52 Å, SbH: 1.66 − 1.71 Å). Numbering as in Fig. (3.1).

[b] **N-22a** converges to C_{2v} (^1A_g).

[c] **N-25a** converges to D_{2d} $(^3A_2)$.

[d] **N-26a**[TS] converges to D_{2h} (^1A_g).

with the MCSCF bond parameters presented in [Schoeller et al. 1997]. The X=X bond lengths in the triplets **X-17a** (X = P, As, Sb) are nearly as long as in the corresponding singly bonded dipnictanes H_2X–XH_2. On the other hand, the resulting N–N bond length found for the triplet **N-17a** at the MP2/VDZP[1] level was 1.255 Å, 0.007 Å shorter than in the diazene HN=NH. Optimization at the MP2/6-311G(d,p) level confirmed this surprising result. However, at the QCISD/6-311G(d,p) level, the ordering in the NN bond lengths is reversed, with 1.250 Å for **N-16a** and 1.289 Å for **N-17a** respectively. Conversely, much longer N–N bond lengths of 1.312 Å [Ito and Nagase 1986 , HF/6-31G(d,p)] and 1.436 Å [Schmidt et al. 1987 , MCSCF/3-21G(d)] for **N-17a** are reported in the literature.[1] It seems that the SCF calculations tend to give N–N bond lengths that are too long, while the MP2 calculations obviously result in N–N bond lengths that are too short. Taking the QCISD result into account, most probably the N–N bond in **N-17a** is in fact elongated with respect to the N=N bond in the diazene HN=NH, but to a much smaller extent than reported in the literature so far.

Single protonation of one lone-pair in the dipnictenes HX=XH is leading to the monocationic derivatives $[H_2X=XH]^+$ which all have planar geometries. In the following discussion, the protonated X center is referred to X(1) (see Fig. (3.1)). Compared to the the neutral dipnictenes **X-16a**, the X=X bond lengths in the monocations **X-19a** are slightly shortened by 0.02 − 0.04 Å, ranging from 1.235 to 2.637 Å when X goes down the row from N to Sb. A more detailed discussion of the double bond lengths follows in the next section (Sec. (3.2)).

Little variation is seen in the bond angles at the protonated pnictogen centers, whereas the $\angle X(1)X(2)H(2)$ decreases from 110.0 ° for X = N to < 90.0 ° for X = P, As, Sb. Again, this is *the* geometrical evidence for the increasing s character of the remaining lone-pair at the XH center when X goes down the row from N to Sb.

---

[1]However, the bond lengths for **N-16a** are in good agreement, cf. Tab. (3.4) on page 86

The calculated MP2 frequency (unscaled) of the vibrational mode, corresponding to pyramidalization at the XH_2 center, is 1121 cm^{-1} in **N-19a**, dropping to 388 cm^{-1} in **P-19a**, 286 cm^{-1} in **As-19a** and 187 cm^{-1} in **Sb-19a**. This is reminiscent to the findings for the trans-bending motion in the heteronuclear monocationic double bond systems $[H_2C=XH_2]^+$. Thus, we can describe the homonuclear monocations of the heavier group 15 elements as planar *soft* double bond systems.

In order to obtain suitable π-bond energies for the monocationic ground states of $[H_2X=XH]^+$ (**X-19a**), we also investigated the triplet structures **X-20a** which were optimized as open-shell biradicals in C_s symmetry. Vibrational analyses characterized all skewed triplets **X-20a** as true minima. Accordingly to the triplet skewed isomers **X-2a** of $H_2C=XH$, we only examined the isomers **X-20a** in which the $X(1)H_2$ centers are trans-bent to $X(2)H$. The deviation from planarity in theses centers, indicated by the flap angle $\phi_{X(1)}$, increase in the order $N(1)H_2 \ll P(1)H_2 \approx As(1)H_2 \approx Sb(1)H_2$, going from 29.2 ° to 57.1 °. The reason for the pyramidalization in **X-20a** is different for X = N than for the heavier homologues with X = P, As, Sb. In the diazenium ion triplet **N-20a**, pyramidalization of the $N(1)H_2$ unit results in a increased stabilization due to the enhanced 2c-3e interaction between the singly occupied orbital on $N(1)$ and the lone-pair at $N(2)$, similar than for the analogous twisted triplet **N-2a** (cf. Scheme 2.3 on page 48). On the other hand, pyramidalization at the $X(1)H_2$ centers in the heavier congeners **X-20a**, mainly occurs due to the increasing inversion barriers for P < As < Sb $\ll$ N. As a result, the N–N bond in **N-20a** is only 0.06 Å longer than in the corresponding planar diazenium **N-19a**, whereas bond lengthening by as much as $0.17 - 0.24$ Å is observed in the heavier homologues **X-20a** with respect to **X-19a** (X = P, As, Sb).

We continue our discussion with the hydrogen bridged singlet monocations **X-21a** and **X-22a** which were optimized in C_2 and C_s symmetry. For the X = N case, however, **N-22a** is a planar C_{2v} symmetric structure and both **N-21a** and **N-22a** are transition states of the degenerate $H_2N=NH \rightarrow HN=NH_2$ isomeriza-

tion. The C_{2v} symmetric cation **N-22a** was calculated to be 17.6 kcal mol^{-1} more stable than **N-21a**, 63.3 kcal mol^{-1} above **N-19a** and in perfect agreement with the findings of Øiestad and Uggerud [1997]. Going from the nitrogen systems to the heavier element systems, these isomers become true minima at the respective PES, now with **X-21a** more stable than **X-22a** by 3.2 kcal mol^{-1} (X = P), 2.5 kcal mol^{-1} (X = As), and 1.9 kcal mol^{-1} (X = Sb). For **X-21a**, the relative stability with respect to the planar double bond systems **X-19a** rapidly decreases in the order ΔE_{ref}^2 (**P-21a**) $> \Delta E_{ref}^2$ (**As-21a**) $> 0 > \Delta E_{ref}^2$ (**Sb-21a**), ranging from 17.7 kcal mol^{-1} to -2.5 kcal mol^{-1} (see Tab. (3.1)). In other words, **Sb-21a** even becomes the global minimum on the electronic hypersurface of $[Sb_2H_3]^+$!

Further protonation of the remaining lone-pair at X(2) yields the dications $[H_2X=XH_2]^{2+}$. Formally, the core functional, i.e the double bond, is still preserved in these systems. Optimization of the dicationic hydrazine $[H_2N=NH_2]^{2+}$ results in the planar D_{2h} symmetric structure **N-23a**. For the heavier homologues $[H_2X=XH_2]^{2+}$ on the other hand, the planar structures **X-23a** were all identified as transition states. Here, the corresponding trans-bent minima **X-24a** are more stable in the order P < As < Sb with respect to the transition states **X-23a**. The gain in stability caused by the trans bending motion only amounts to 0.2 kcal mol^{-1} for the dication $[H_2P=PH_2]^{2+}$, but increases to 5.1 kcal mol^{-1} and 11.8 kcal mol^{-1} for $[H_2As=AsH_2]^{2+}$ and $[H_2Sb=SbH_2]^{2+}$ respectively. Although the energy is very small to convert the trans-bent structure for $[H_2P=PH_2]^{2+}$ to the planar form, the deviation from planarity in **P-24a** is significant, given by $\phi_P = 28.7°$. The flap angle ϕ_X further increases with increasing atomic number of X to $\phi_{As} = 45.7°$ and $\phi_{Sb} = 52.7°$ in the corresponding dications **As-24a** and **Sb-24a** respectively.

In analogy to the previous neutral and monocationic double bond systems, the corresponding twisted triplet dications were considered in order to obtain a lower-limit for the π-bond contribution in the X=X bonds of the dications $[H_2X=XH_2]^{2+}$. These energies are discussed in Sec. (3.2.2) together with the corresponding π-bond

energies of the dipnictenes and dipnictenium ions HX=XH and $[H_2X=XH]^+$. Again, geometrical differences between the nitrogen containing triplet **N-25a** and its higher congeners are apparent. While the former isomer converges to D_{2d} symmetry ($^3A_2$) having planar NH_2 centers on one hand, the latter isomers prefer the C_2 (^3B) symmetric triplets **X-25a** with pyramidalized XH_2 centers ($\phi_P = 47.7\,°$, $\phi_{As} = 51.8\,°$, $\phi_{Sb} = 55.7\,°$) on the other hand. The two XH_2 centers are twisted in such a way that the empty lone pair at one X is axial to one X–H bond of the other X. The X–X bonds in all triplets **X-25a** are considerably longer than the X=X bond lengths in the singlet ground state minima $[H_2X=XH_2]^{2+}$: 0.10 Å for X = N and $0.20 - 0.30$ Å for X = P < As < Sb.

3.2 Properties of HX=XH and their protonated derivatives $[H_2X=XH]^+$ and $[H_2X=XH_2]^{2+}$.

In this section, we discuss in detail the properties of the X=X double bonds in the three sets of neutral and cationic homonuclear group 15 compounds $[X_2H_{2+n}]^{n+}$ with n = 0, 1, 2. According to the reactions (Rxn. 3.1) and (Rxn. 3.2), stepwise protonation of the planar dipnictenes **X-16a** is leading to the mono- and dicationic derivatives $[H_2X=XH]^+$ and $[H_2X=XH_2]^{2+}$. As already discussed in the previous section, the former cations all prefer the planar structures **X-19a**, whereas the latter cations prefer either a planar structure for X = N (**N-23a**) or trans-bent structures for X = P, As, Sb (**X-23a**).

$$HX=XH \quad + \quad H^+ \quad \longrightarrow \quad [H_2X=XH]^+ \qquad \text{(Rxn. 3.1)}$$

$$[H_2X=XH]^+ \quad + \quad H^+ \quad \longrightarrow \quad [H_2X=XH_2]^{2+} \qquad \text{(Rxn. 3.2)}$$
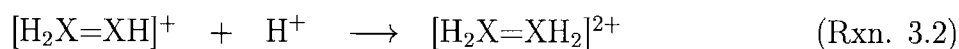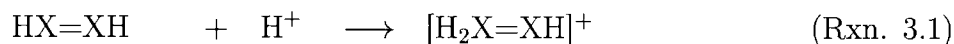
The corresponding PA values for the neutral and monocationic minimum ground states HX=XH and $[H_2X=XH]^+$ (X = N, P, As, Sb) are presented in Tab. (3.3). For

Table 3.3: X=X double bond systems. Proton affinities (PAs) for the neutral dipnictenes HX=XH and their protonated derivatives $[H_2X=XH]^+$ according to the protonation reactions (Rxn. 3.1) and (Rxn. 3.2) (X = N, P, As, Sb).[a]

X	(Rxn. 3.1)		(Rxn. 3.2)
N	188.3	214.1[b]	11.9
P	179.7	183.0[b],185.5[c]	26.5
As	175.9		30.9
Sb	180.2		51.0

[a] CCSD(T)/VTZP^2 data.

[b] in [Ito and Nagase 1986](HF).

[c] in [Cruz et al. 1997](G2).

all dipnictenes **X-16a**, first protonation is highly exothermic resulting in positive PA values between $180.0 - 190.0$ kcal mol^{-1} in the order N > Sb > P > As. Comparison with other calculations is possible for the diazene **N-16a** and diphosphene **P-16a**. Despite some disagreements possibly induced by the different computational methods, the qualitative result remains the same. Second protonation of the monocationic $[H_2X=XH]^+$ is still exothermic for all X = N, P, As, Sb but to a much smaller extent. Here, the PA values increase from 11.9 kcal mol^{-1} to 51.0 kcal mol^{-1} in the order N < P < As < Sb. The reason for this trend can be understood in the accompanying pyramidalization when the X(2)H group is protonated, which becomes increasingly favorable when X goes down the row from N to Sb.

In Tab. (3.4), we compare our calculated X=X bond lengths of the neutral and cationic dipnictenes HX=XH, $[H_2X=XH]^+$ and $[H_2X=XH_2]^{2+}$ at various levels of theory (this work) with a representative selection of other recent *ab initio* calculations (others) and experimental data (exp), where possible. It should be mentioned that we only list a representative selection of data available.

Table 3.4: X=X double bond systems. Comparison of calculated and experimental equilibrium X=X bond lengths R_e and flap angles ϕ_X for the neutral dipnictenes HX=XH (**X-16a**) and their protonated derivatives $[H_2X=XH]^+$ (**X-19a**) and $[H_2X=XH_2]^{2+}$ (**X-23a/X-24a**) (X = N, P, As, Sb).[a]

| | \multicolumn{6}{c}{this work} | others | exp |
| | \multicolumn{2}{c}{6-31G(d,p)} | \multicolumn{2}{c}{6-311G(d,p)} | \multicolumn{2}{c}{VDZP} | | |
	R_e	ϕ_X	R_e	ϕ_X	R_e	ϕ_X	R_e	$d_{X=X}$
N-16a	1.267	0.0			1.262	0.0	1.216[b],1.269[c]	1.252[i]
N-19a	1.240	0.0			1.235	0.0	1.240[d]	
N-23a	1.242	0.0			1.238	0.0		
P-16a	2.045	0.0			2.078	0.0	2.005[e],2.099[f]	1.985 − 2.034[j]
P-19a	2.014	0.0			2.042	0.0	2.005[g]	2.024[k]
P-23a	2.010	0.0			2.032	0.0		
P-24a	2.027	28.1			2.051	28.7	1.968[h]	
As-16a			2.282	0.0	2.283	0.0	2.227[e],2.326[f]	2.224 − 2.285[j]
As-19a			2.244	0.0	2.243	0.0		
As-23a			2.220	0.0	2.214	0.0		
As-24a			2.271	44.6	2.277	45.7		
Sb-16a					2.676	0.0	2.608[e],2.731[f]	2.642 − 2.668[j]
Sb-19a					2.637	0.0		
Sb-23a					2.598	0.0		
Sb-24a					2.732	52.9		

[a] Bond lengths in Å, flap angles in degree (°).

[b] in [Ito and Nagase 1986] (HF).

[c] in [Schmidt et al. 1987] (MCSCF).

[d] in [Øiestad and Uggerud 1997] (HF).

[e] in [Nagase et al. 1990] (HF).

[f] in [Schoeller et al. 1997] (MCSCF).

[g] in [Cruz et al. 1997] (MP2).

[h] in [Niemann et al. 1991] (SCF).

[i] in [Harmony et al. 1979] (HN=NH).

[j] in [Power 1999] (ranges of the X=X bond lengths in organodipnictenes with X = P, As, Sb).

[k] in [Loss et al. 1999] ([Mes*MeP=PMes*]+).

For the neutral dipnictenes **X-16a** comparison with previous theoretical works is possible for all X = N, P, As, Sb. Among other isomers of the X_2H_2 PES, Ito and Nagase [1986] investigated HN=NH at the HF/6-31G(d,p) level. Nagase et al. [1990] calculated the diphosphene HP=PH and all remaining higher congeners up to HBi=BiH at the same level of theory with ECPs at P, As, Sb and Bi. In their evaluation of the π-bond strengths, Schoeller et al. [1997] re-examined the same set of dipnictenes at the MCSCF level using comparable basis sets. Our calculated MP2/VDZP[1] bond lengths are in good agreement with all these results, lying in between the HF and MCSCF values. Comparison with experimental structures shows that our MP2 values are in the upper field of X=X bond lengths of the heavier organodipnictenes. The situation is different for the protonated species: the monocationic dipnictenium ions $[H_2X=XH]^+$ have been investigated only for **N-19a** and **P-19a** so far. While numerous stable diphosphenes are known, only one phosphanyl phosphenium ion was recently synthesized and structurally characterized by Loss et al. [1999]. For the dications $[H_2X=XH_2]^{2+}$, theoretical data are available for $[H_2P=PH_2]^{2+}$ [Niemann et al. 1991]. Experimentally, only derivatives of the dicationic hydrazine (**N-23a**) have been detected by cyclic voltammetry [Dietrich et al. 1986].

For the nitrogen containing systems, the first protonation step (**N-16a** $\xrightarrow{H^+}$ **N-19a**) leads to a bond shortening by 0.027 Å, whereas the second protonation step (**N-19a** $\xrightarrow{H^+}$ **N-23a**) causes a minimal bond lengthening by 0.003 Å. Considering only planar structures for the heavier analogues, a somewhat different picture arises: bond shortening is observed for both protonation steps from HX=XH over $[H_2X=XH]^+$ to $[H_2X=XH_2]^{2+}$ in ranges of 0.036 − 0.039 Å and 0.010 − 0.039 Å, respectively (X = P, As, Sb). However, relaxation of the planar structures **X-23a** to the ground states **X-24a** results in a increasing X=X bond lengthening by as much as 0.019 Å for X = P, 0.063 Å for X = As, and 0.134 Å for X = Sb! This is a direct consequence of the fact that trans-bending of the

fragments in a double bond system with elements of the higher rows stabilizes the system to a greater degree than bond lengthening destabilizes it. In other words, the hypersurface around the equilibrium X=X bond length R_e is much steeper for the flap angle ϕ_X than for the bond distance R. The trans-bending of the stibonium dication $[H_2Sb{=}SbH_2]^{2+}$ from **Sb-23a** to **Sb-23a** illustrates this fact very well, where the X=X bond length significantly increases by ≈ 0.13 Å, while the system is stabilized by $\approx 12\,\mathrm{kcal\,mol^{-1}}$.

Atom and group charges for the X=X double bond systems are listed in Tab. (3.7). Due to the homonuclearity, σ charge transfer only occurs between the pnictogen centers and the hydrogens, which is determined by the ordering of the electronegativities $\mathcal{X}_X$ relative to $\mathcal{X}_H$. As a result, considerable negative charge is accumulated at the nitrogen centers in the neutral diazene **N-16a**, since $\mathcal{X}_X < \mathcal{X}_H$, whereas in the heavier congeners **X-16a** an increasing amount of positive charge is located at X, according to $\mathcal{X}_{Sb} < \mathcal{X}_{As} < \mathcal{X}_P < \mathcal{X}_H$. Obviously, the XH group charges in these compounds are all equal to zero. The σ charge transfer from H to N on one hand and from X to H, on the other hand, is reflected in the increasing σ population at the hydrogen atoms p_σ^H, ranging from $0.67\,e$ in **N-16a** to $1.04 - 1.18\,e$ in **X-16a** (X = P, As, Sb) (Tab. (3.6)).

X = N, P, As, Sb
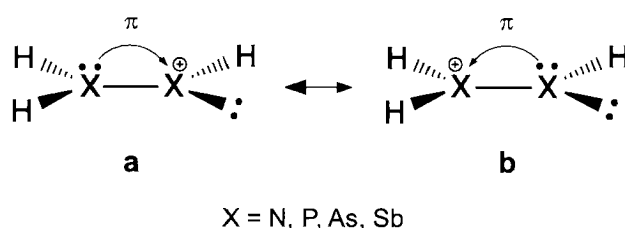
Scheme 3.1

Formally, the π bonding in the C_s symmetric monocations $[H_2X(1){=}X(2)H]^+$ is governed by the resonance structures **a** and **b**, shown in Scheme 3.1. Analyses of the π populations, presented in Tab. (3.6), give ratios of $p_\pi^{X(1)} : p_\pi^{X(2)}$ in between

Table 3.5: X=X double bond systems. Atomic and group charges for the dipnictenes HX=XH (**X-16a**) and their protonated derivatives $[H_2X=XH_2]^{2+}$ (**X-19a**) and $[H_2X=XH_2]^{2+}$ (**X-23a/X-24a**) (X = N, P, As, Sb).[a]

atoms/	X			
groups	N	P	As	Sb
X-16a X	−0.326	0.046	0.094	0.189
H	0.326	−0.046	−0.094	−0.189
X-19a X(1)	−0.261	0.378	0.422	0.626
X(2)	−0.084	0.412	0.498	0.626
H(1)	0.479	0.095	0.059	−0.053
H(2)	0.409	0.017	−0.041	−0.152
H(3)	0.457	0.098	0.063	−0.047
XH_2	0.675	0.571	0.543	0.525
XH	0.325	0.429	0.457	0.475
X-23a X	−0.112	0.593	0.657	0.887
H	0.556	0.203	0.172	0.056
X-24a X		0.616	0.742	1.032
H		0.192	0.129	−0.016

[a] $MP2/VDZP^1$ data. Numbering as in Fig. (3.1).

1.5 : 1 (**N-19a**) and 1.2 : 1 (**Sb-19a**) which reveals X(2) → X(1) π charge transfer in all monocations **X-19a** with X = N, P, As, Sb. Additionally, σ charge transfer between X and H is apparent. Again, the direction of this shifts, from X to H or vice versa, are following the ordering in the ENs $\mathcal{X}_X$ vs. $\mathcal{X}_H$. As a result of all these factors, the N atoms in the diazenium ion $[H_2N=NH]^+$ are negatively charged by $-0.26\,e$ for N(1) $< -0.08\,e$ for N(2). In the heavier homologues **X-19a** the charge distribution is reversed with increasing positive charges $q^+[X(1)] < q^+[X(2)]$ located at X = P < As < Sb. On the other hand, little variation is observed in the group charges, where the $+1\,e$ charge is approximately distributed between $X(1)H_2$ and X(2)H in the ratios ≈ 2:1 for X = N and ≈ 1:1 for X = P, As, Sb.

Table 3.6: X=X double bond systems. σ and π populations for the neutral dipnictenes HX=XH (**X-16a**) and their protonated derivatives $[H_2X=XH]^+$ (**X-19a**) and $[H_2X=XH_2]^{2+}$ (**X-23a**) (X = N, P, As, Sb).[a]

atoms		X							
		N		P		As		Sb	
		p_σ	p_π	p_σ	p_π	p_σ	p_π	p_σ	p_π
X-16a	X(1)	4.26	0.99	3.87	0.98	3.84	0.99	3.76	0.99
	H(1)	0.67		1.04		1.09		1.18	
X-19a	X(1)	4.02	1.19	3.38	1.14	3.38	1.12	3.21	1.10
	X(2)	4.22	0.80	3.68	0.82	3.58	0.85	3.44	0.87
	H(1)	0.52		0.90		0.94		1.05	
	H(2)	0.54		0.90		0.93		1.04	
	H(3)	0.59		0.98		1.03		1.15	
X-23a	X(1)	4.07	0.99	3.34	0.98	3.29	0.98	3.07	0.98
	H(1)	0.44		0.79		0.82		0.94	

[a] MP2/VDZP[1] data derived from NBO analyses. Numbering as in Fig. (3.1).

Due to the central D_{2d} (C_{2h}) symmetry in the dications $[H_2X=XH_2]^{2+}$, σ and π electron transfer between the $+1\,e$ charged XH_2 units are equally distributed. Within the XH_2 groups σ charge transfer takes place between X and H, again simply according $\mathcal{X}_X$ vs. $\mathcal{X}_H$. Firstly, only the planar dications are considered. Within these structures **X-23a** the charges at the X centers are more positive with increasing atomic number of X, ranging from $-0.11\,e$ (X = N) to $0.89\,e$ (X = Sb). Accordingly, the σ and π populations for X and H atoms in the planar dications **X-23a** are all shifted to smaller values, compared to the corresponding populations for the dipnictenes HX=XH. Allowing the higher dications $[H_2X=XH_2]^{2+}$ to relax into their ground state minimum structures **X-24a**, further increases the positive charge at X in the order $q^+(P) < q^+(As) \ll q^+(Sb)$. The high resulting positive charges located at the neighboring atoms X in the heavier dications $[H_2X=XH_2]^{2+}$ (X = P, As, Sb) parallels the increasing bond lengthening observed in the trans-bending **X-23a** → **X-23a** .

Table 3.7: X=X double bond systems. Stretching frequencies $\nu_{X=X}^{calc}$ for the neutral dipnictenes HX=XH (**X-16a**) and their protonated derivatives HX=XH (**X-19a**) and $[H_2X=XH]^+$ (**X-23a/X-24a**) (X = N, P, As, Sb).[a]

	this work[b]	others	$\nu_{X=X}^{exp}$
N-16a	1525 (1526)	1882[c]	1529[e]
N-19a	1634 (1630)		
N-23a	1569 (1564)		
P-16a	587 (614)	701[d]	610[f]
P-19a	612 (636)		
P-23a	630 (650)		
P-24a	624 (646)		
As-16a	338	392[d]	
As-19a	353		
As-23a	374		
As-24a	322		
Sb-16a	220	254[d]	
Sb-19a	227		
Sb-23a	241		
Sb-24a	176		

[a] Frequencies in cm^{-1}.

[b] MP2/VDZP^1 (MP2/6-31G(d,p)) data, unscaled.

[c] in [Schmidt et al. 1987] (SCF unscaled).

[d] in [Nagase et al. 1990] (HF unscaled).

[e] in [Bondybey and Nibler 1973] (HN=NH).

[f] in [Yoshifuji et al. 1981] (Mes*P=PMes*).

The X=X stretching frequencies $\nu_{X=X}^{calc}$, calculated at the MP2/VDZP^1 level, are listed in Tab. (3.7). Comparison with the few theoretical and experimental data is possible for the neutral dipnictenes, showing good overall agreement. For all three series of X=X double bonds systems HX=XH, $[H_2X=XH]^+$ and $[H_2X=XH_2]^{2+}$, $\nu_{X=X}^{calc}$ rapidly decreases in the order N=N $\gg$ P=P > As=As > Sb=Sb. However, the drop of the stretching frequencies does not have to imply a similar decrease in the double bond strengths. It rather indicates the increasing flatness of the PES around

the equilibrium structure, due to the increasing influence of the interatomic Pauli repulsion, when X goes down the row from N to Sb.

The first protonation of the diazene HN=NH results in an increase of $\nu_{N=N}^{calc}$ by 109 cm^{-1} while the second protonation reduces the N=N stretching frequency by 65 cm^{-1}. Note that the trend in the N=N stretching frequencies agree with the ordering found for the corresponding N=N bond lengths of HN=NH > $[H_2N=NH_2]^{2+}$ > $[H_2N=NH]^+$ (cf. Tab. (3.4)). Considering first the planar structures for the heavier dipnictenes, stepwise protonation according to the reactions (Rxn. 3.1) and (Rxn. 3.2) is leading to an overall increase of $\nu_{X=X}^{calc}$ by 43 cm^{-1} for X = P, 36 cm^{-1} for X = As, and 21 cm^{-1} for X = Sb. It is the trans-bending from **X-23a** to **X-24a** which further lowers $\nu_{X=X}^{calc}$, especially for the heavier dications $[H_2As=AsH_2]^{2+}$ and $[H_2Sb=SbH_2]^{2+}$. In analogy to the nitrogen systems, the trends observed in the X=X stretching frequencies for the higher congeners also correlate well with the trends in the respective bond lengths (cf. Tab. (3.4)).

3.2.1 Derivatives of the phosphanyl phosphenium ion $[H_2P=PH]^+$

The first phosphanyl phosphenium ion, $[Mes^*MeP=PMes^*]^+$ (**P-19e**), was synthesized in our research group [Loss et al. 1999]. Its crystal structure is depicted in Fig. (3.3). In this section we present calculations for corresponding derivatives **P-19(a-d)**, presented in Fig. (3.4). These series of monocations can be regarded as a stepwise approach to the complexity of the real molecule **P-19e**. Comparison of the theoretical results for **P-19(a-d)** provides insights into differences between protonation and methylation (**P-19a** vs. **P-19b**) as well as the differing influence of hydrogen, alkyl and allyl substituents (**P-19b** vs. **P-19c** vs. **P-19d**).

The selected P=P bonding parameters for the derivatives **P-19(a-e)** are given in Tab. (3.8). The results show little variation in the bond lengths with a slight
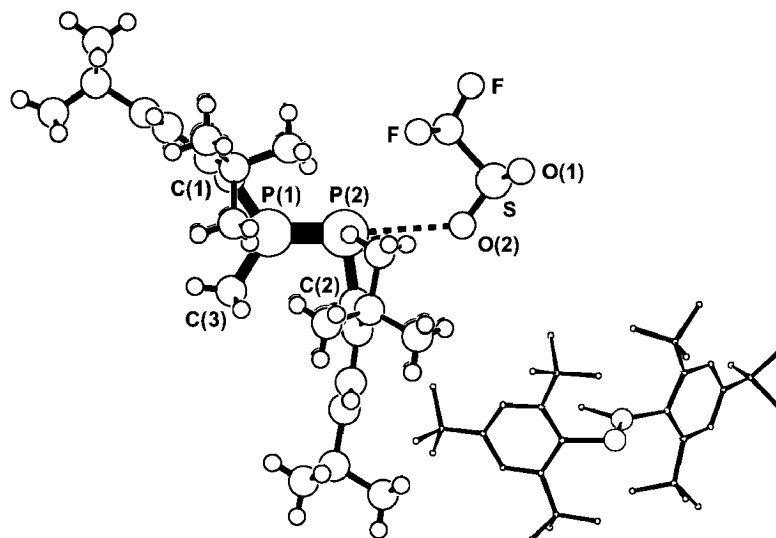
Figure 3.3: Two different views of the molecular structure of **P-19e**. The mirror plane running through S, O(2), P(2), P(1), C(2), C(3), C(1) coincides with the paper plane. For selected bonding parameters see Tab. (3.8).

increase of the equilibrium P=P bond lengths for $R^{1,2}$ = Ph, Mes* by $\approx$ 0.01 Å. In contrast, the angle $\angle P^1 P^2 Y^2$ (Y = H^2, C^2) significantly changes, ranging from $\approx$ 90 ° (**P-19(a,b)**) to 102.7 ° (**P-19c**) and 98.7 ° (**P-19d**). The reason for the wide angle $\angle P^1 P^2 C^2$ in **P-19c** can be found in the repulsive interaction of the hydrogens bonded at C(2) and C(3) which both are in the P=P double bond plane (cf. Fig. (3.5)). It arises that the changes in the bonding parameters, i.e. increase of the P=P bond length and widening of the angle $\angle P^1 P^2 Y^2$ in **P-19(c,d)**, particularly stem from the steric interaction between R^2 and R^3. Thus, it is not surprising that structural parameters of the derivative **P-19d** are closest to the experimental values derived from the X-ray analyses for the phosphanyl phosphenium ion $[\text{Mes}^*\text{MeP}=\text{PMes}^*]^+$ (**P-19e**). Note that for the very bulky supermesityl Mes* steric interactions also occur between the ^{t}Bu groups above and below the P=P double bond plane (cf. Fig. (3.3)).
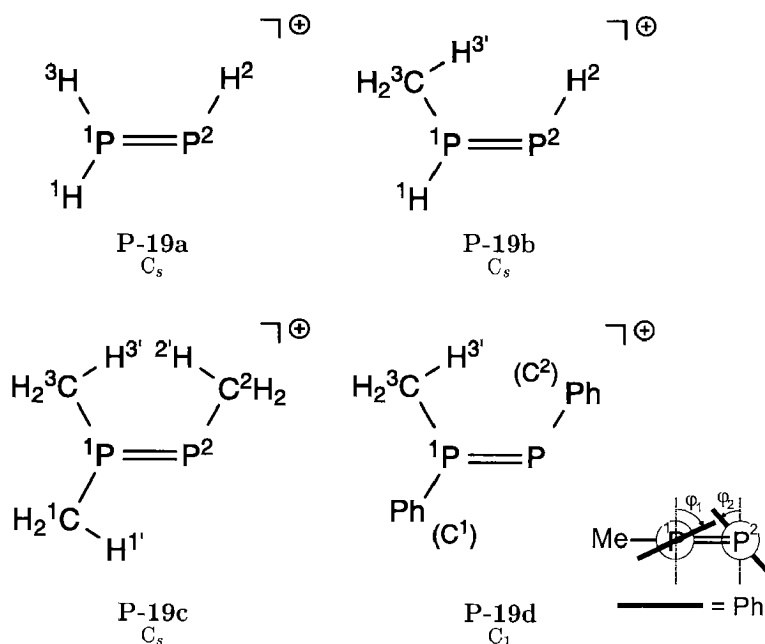
Figure 3.4:   Calculated derivatives **P-19(a-d)**. The former three monocations are C_s symmentric, whereas the latter has C_1 symmetry. The conformations of **P-19(b-d)** are indicated by the hydrogen atoms $H^{i\prime}$ lying within the P=P double bond plane. The tilt of the phenyl rings in **P-19d** is given by $\varphi_{1,2}$. For bonding parameters see Tab. (3.8).

Next, the results from the NBO analyses (Tab. (3.9)) for the derivatives **P-19(a-d)** are discussed. The atomic charges of the phosphorus atoms increase remarkably for P(1) from $0.39\,e$ in **P-19a** to $\approx 0.9\,e$ in **P-19(c,d)**. Concomitantly, the positive charge at P(2) decreases from $0.40\,e$ to $0.35\,e$ when going from **P-19a** to **P-19b** and increase again to $\approx 0.50\,e$ for **P-19(c,d)**. In order to understand these trends in the atomic charges it is useful to inspect the corresponding σ and π populations for P(1) and P(2), also collected in Tab. (3.9). The decreasing σ populations clearly reveal P $\rightarrow$ C σ charge transfer, according to the ordering of the electronegativities $\mathcal{X}_C \gg \mathcal{X}_H > \mathcal{X}_P$. On the other hand, the π populations of P(1) and (P2) remains almost constant for all monocations **P-19(a-d)**. Notwith-

Table 3.8: P=P double bond systems. Selected structural data for the monocationic derivatives $R^1R^3P^1{=}P^2R^2$ **P-19(a-d)** (calc) and **P-19e** (exp).[a]

P-19	$R^{1,2}$	R^3	P^1P^2	$Y^1P^1P^2$	$P^1P^2Y^2$	$Y^3P^1P^2$
a	H	H	2.014	120.1	89.5	126.7
b	H	Me	2.014	115.4	90.1	131.1
c	Me	Me	2.019	117.7	102.7	130.0
d[b]	Ph	Me	2.023	118.4	98.7	127.0
			(2.044)	(118.0)	(103.5)	(127.4)
e	Mes*	Me	2.024	123.1	99.4	125.2

[a] MP2/6-31G(d,p) data. B3LYP/6-31G(d,p) data for **P-19d** in parentheses. Bond lengths in Å, angles in degree (°). Y denotes the hydrogen or carbon atoms bonded to P(1) and P(2), respectively. Numbering as in Fig. (3.4).

[b] the values for $\varphi_{1,2}$ are 60.2 ° (64.7 °) and 33.8 ° (42.2 °).

standing, the slight decrease of the charge at P(2) can be attributed to a higher π charge transfer from P(1) to P(2) in **P-19b**!

Table 3.9: P=P double bond systems. Atomic charges together with the σ and π populations for the phosphorus atoms P(1,2) in the phosphanyl phosphenium ions **P-19(a-d)**.[a]

P-19	P(1)			P(2)		
	q	p_σ	p_π	q	p_σ	p_π
a	0.39	3.38	1.14	0.40	3.70	0.83
b	0.67	3.14	1.11	0.35	3.68	0.88
c	0.91	2.88	1.12	0.53	3.50	0.89
d	0.89	2.90	1.15	0.50	3.53	0.86

[a] MP2/6-31G(d,p) (B3LYP/6-31G(d,p)) data for **P-19(a-c)** (**P-19d**), derived from NBO analyses.

Finally, we discuss the P=P double bond stretching frequencies $\nu_{P=P}^{calc}$ for the series of derivatives **P-19(a-d)**. The frequencies of the associated normal modes, displayed in Fig. (3.5), are presented in Tab. (3.10). For the most simple phosphenium ion $[H_2P=PH]^+$, the frequency for the P=P stretch is undoubtly 636 cm^{-1} (Fig. (3.5), **A**). This corresponds to an increase in $\nu_{P=P}^{calc}$ by 22 cm^{-1} with respect to the P=P stretching frequency for HP=PH, as presented in Tab. (3.7). Guided by these results, we firstly assigned an intensive absorption band at 638 cm^{-1} in the IR spectra of **P-19e** as the normal mode of the P=P double bond stretch, as reported in Loss et al. [1999].

Table 3.10: P=P double bond systems. Frequencies of selected normal modes for the phosphanyl phosphenium ions **P-19(a-d)** (ν^{calc}) and **P-19e** (ν^{exp}).[a]

P-19	ν^{calc}			ν^{exp}		
a	636					
b	580	784				
c	532	762				
d	568	719	767			
e				551	—	—

[a] MP2/6-31G(d,p) (B3LYP/6-31G(d,p)) data for **P-19(a-c)** (**P-19d**). For a graphical representation of the corresponding normal modes see Fig. (3.5).

However, a more extensive analysis of the normal modes of the higher derivatives **P-19(b-d)** revealed that this assignment is not correct. The essential reason for this is already present in the methylated diphosphene **P-19b**: the P=P stretching mode now is coupled with the C–P stretching mode which yields two asymmetric stretching modes at 580 cm^{-1} and 784 cm^{-1}, as shown by the two selected normal modes in Fig. (3.5) (**B**). Comparison with **P-19a** shows that the lower normal mode in **P-19b** at 580 cm^{-1} is closer to the P=P stretch, whereas the higher normal mode at 784 cm^{-1} is more related to the C–P stretch. Similar findings are observed
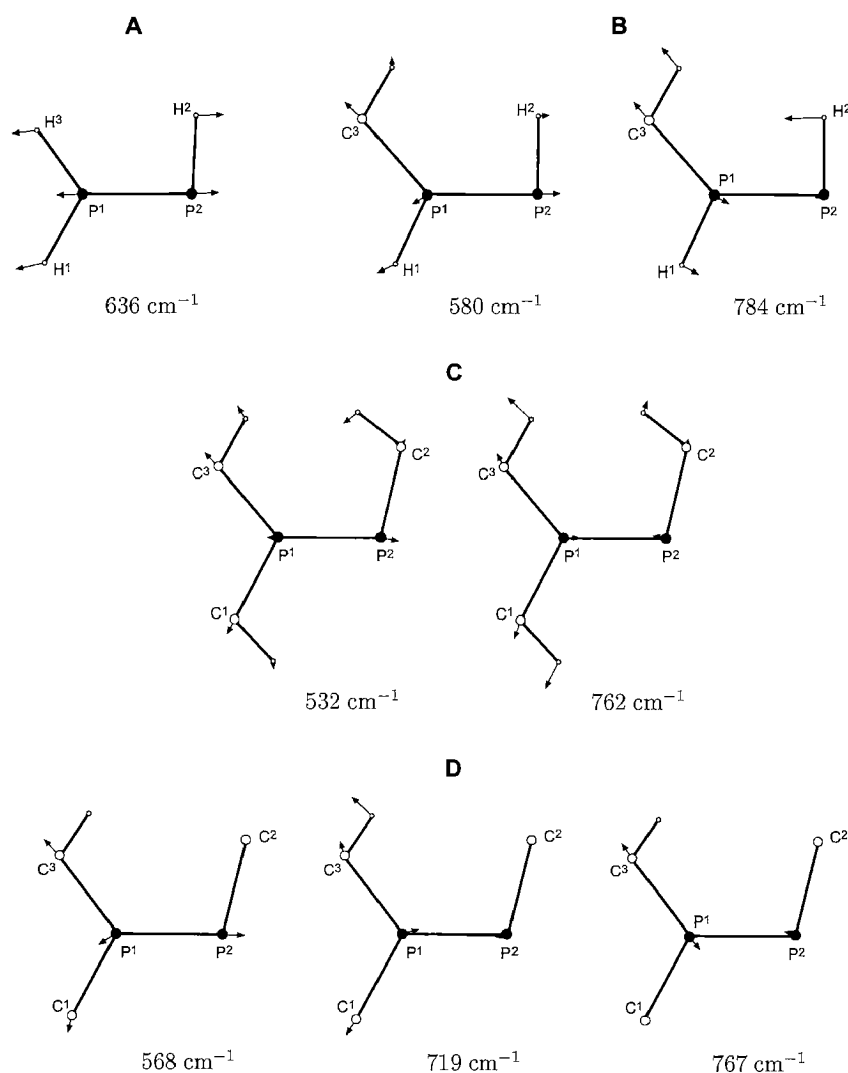
Figure 3.5: Selected normal modes for the parent phosphenium ion **P-19a** (**A**) and its derivatives **P-19b** (**B**), **P-19c** (**C**) and **P-19d** (**D**). The corresponding frequencies are taken from Tab. (3.10). Only atoms within the P=P double bond plane are depicted. Numbering as in Fig. (3.4). Black (grey) bullets refer to phosphorus (carbon) atoms. Small white circles refer to hydrogens.

for **P-19c** (Fig. (3.5), **C**) and **P-19d** (Fig. (3.5), **D**). In the methyl substituted monocation **P-19c** the P=P stretching frequency of 532 cm^{-1} is even lower than in **P-19b** due to the coupling with two C–P stretching modes. For the phenyl substituted derivative **P-19d** the coupling of the different stretching modes for the

P=P double bond with the C^3-P(1) (alkyl) and C^1-P(1) (allyl) single bonds results in three normal modes at 568 cm^{-1}, 719 cm^{-1} and 767 cm^{-1}. Again, the predominant contribution to the distortion pattern in the lowest normal mode is the P=P double bond stretch. Based on these results, we assign now a rather intense absorbtion band at 551 cm^{-1} in the Raman spectra of **P-19e** to the P=P stretching mode.

3.2.2   Bonding energies

In this section we present an analysis of the double bond energetics for the systems HX=XH and their protonated derivatives $[H_2X=XH]^+$ and $[H_2X=XH_2]^{2+}$. Dissociation energies D_0 are obtained from the reaction enthalpies of the bond fissions reactions (Rxn. 3.3) – (Rxn. 3.5). The results are presented in Tab. (3.12). The π-bond strengths presented in Tab. (3.14) are obtained by the energy gaps between the singlet ground state double bond systems and the corresponding twisted triplet minima.

$$HX=XH \qquad \longrightarrow \quad XH \quad + \quad XH \qquad \qquad \text{(Rxn. 3.3)}$$

$$[H_2X=XH]^+ \qquad \longrightarrow \quad XH_2^+ \quad + \quad XH \qquad \qquad \text{(Rxn. 3.4)}$$

$$[H_2X=XH_2]^{2+} \qquad \longrightarrow \quad XH_2^+ \quad + \quad XH_2^+ \qquad \qquad \text{(Rxn. 3.5)}$$
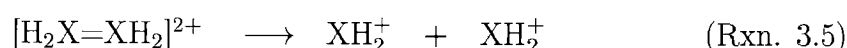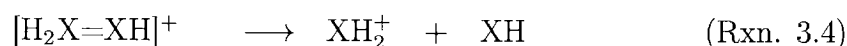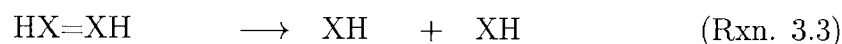
The energies of the singlet and triplet ground states of the group 15 monohydrides XH have been already discussed in Sec. (2.2.1). The corresponding energetics, derived from geometries optimized at the MP2/VDZP[1] level, are listed in Tab. (3.11) for completeness. The singlet-triplet energy gaps significantly differ at the MP2/VDZP[1] level compared to the QCISD/VDZP[1] values presented in Tab. (2.8) on page 42. However, at the CCSD(T) levels, the $\Delta E_{s \to T}$ values perfectly coincide.

The total energies obtained for the hydrides were used in conjunction with the total energies of the double bond systems HX=XH, $[H_2X=XH]^+$ and $[H_2X=XH_2]^{2+}$,

Table 3.11: X=X bonding energies. Energetics of the group 15 hydrides XH and XH_2^+ including singlet-triplet excitation energies $\Delta E_{S\to T}$ (X = N, P, As, Sb).[a]

	state	CCSD(T)/BS(2,3)//MP2/BS(1)[b]				$\Delta E_{S\to T}$		
		E_{opt}	ZPE	E^1_{ref} [c]	E^2_{ref} [d]	ΔE_{opt}	ΔE^1_{ref}	ΔE^2_{ref}
NH	$^1\Delta$	-10.250256	4.9	-10.299473	-10.327183			
	$^3\Sigma^-$	-10.345372	4.8	-10.375320	-10.399671	-59.7	-47.6	-45.5
NH_2^+	$^1A_1$	-10.535940	11.7	-10.578065	-10.601240			
	$^3B_1$	-10.601391	11.2	-10.628799	-10.649062	-41.1	-31.8	-30.0
PH	$^1\Delta$	-6.945202	3.4	-6.9917074	-7.028314			
	$^3\Sigma^-$	-7.010397	3.4	-7.0418669	-7.073746	-40.9	-31.5	-28.5
PH_2^+	$^1A_1$	-7.262796	8.8	-7.3054435	-7.337991			
	$^3B_1$	-7.247675	8.6	-7.2817989	-7.310949	9.5	14.8	17.0
AsH	$^1\Delta$	-6.615601	3.2	-6.655907	-6.682486			
	$^3\Sigma^-$	-6.678539	3.2	-6.703848	-6.726022	-39.5	-30.1	-27.3
AsH_2^+	$^1A_1$	-6.939132	8.2	-6.975076	-6.995803			
	$^3B_1$	-6.908849	8.0	-6.938968	-6.958097	19.0	22.7	23.7
SbH	$^1\Delta$	-5.846145	2.9	-5.887757	-5.913015			
	$^3\Sigma^-$	-5.903770	2.8	-5.930846	-5.952100	-36.2	-27.0	-24.5
SbH_2^+	$^1A_1$	-6.176083	7.2	-6.216348	-6.236688			
	$^3B_1$	-6.139462	7.0	-6.175483	-6.194421	23.0	25.6	26.5

[a] Total energies E in Hartrees, ZPE and relative energies ΔE (without ZPE corrections) in kcal mol^{-1}. XH are optimized in $C_{\infty v}$ symmetry. XH_2^+ are optimized in C_{2v} symmetry. A negative $\Delta E_{S\to T}$ indicates the triplet to be the more stable multiplicity.

[b] BS(1): VDZP^1; BS(2): VTZP^1; BS(3): VTZP^2.

[c] Refined energies obtained using BS(2).

[d] Refined energies obtained using BS(3).

in order to calculate the dissociation energies D_0, according to reactions (Rxn. 3.3) – (Rxn. 3.5). As shown in Tab. (2.10), the D_e values are improved significantly by 6 – 11 kcal mol^{-1} when going from VTZP^1 to VTZP^2. Notwithstanding, the corresponding ZPE corrected dissociation energies D_0 are still systematically lower by 6 – 9 kcal mol^{-1}, compared with the G2 values obtained for all doubly bonded structures with X = N, P, As. This is very similar in range compared to the differences observed for the D_0 values of the C=X bonded systems (cf. Tab. (2.10) on page 44).

We first look at the dissociation energies of the neutral dipnictenes HX=XH ($\mathbf{X}$-$\mathbf{16a}$) and its singly protonated derivatives $[\mathrm{H_2X{=}XH}]^+$ ($\mathbf{X}$-$\mathbf{19a}$). For the former systems, the dissociation energies D_0 decrease in steps ΔD_0 of $40.0\ \mathrm{kcal\,mol^{-1}}$ (N $\rightarrow$ P), $12.2\ \mathrm{kcal\,mol^{-1}}$ (P $\rightarrow$ As) and $11.9\ \mathrm{kcal\,mol^{-1}}$ (As $\rightarrow$ Sb), ranging from $113.8\ \mathrm{kcal\,mol^{-1}}$ for $\mathbf{N}$-$\mathbf{16a}$ to $49.7\ \mathrm{kcal\,mol^{-1}}$ for $\mathbf{Sb}$-$\mathbf{16a}$. For the latter systems the same trend in D_0 is observed, dropping from $150.5\ \mathrm{kcal\,mol^{-1}}$ ($\mathbf{N}$-$\mathbf{19a}$) to $54.8\ \mathrm{kcal\,mol^{-1}}$ ($\mathbf{Sb}$-$\mathbf{19a}$) in steps ΔD_0 of $58.7\ \mathrm{kcal\,mol^{-1}}$ (N $\rightarrow$ P), $19.7\ \mathrm{kcal\,mol^{-1}}$ (P $\rightarrow$ As) and $17.3\ \mathrm{kcal\,mol^{-1}}$ (As $\rightarrow$ Sb). If we take the corresponding dissociation energies D_0 as a measure of the double bond strength $\Delta E^0_{\mathrm{TBE}}$, we see that the X=X bond in the monocations $\mathbf{X}$-$\mathbf{19a}$ becomes stronger upon protonation for *all* X = N, P, As, Sb. However, the increase in the double bond strengths declines from $36.7\ \mathrm{kcal\,mol^{-1}}$ for X = N over $18.0\ \mathrm{kcal\,mol^{-1}}$ for X = P and $10.5\ \mathrm{kcal\,mol^{-1}}$ for X = As to $5.1\ \mathrm{kcal\,mol^{-1}}$ for X = Sb. This decrease in the bond strength can be attributed to the planarization of the $\mathrm{X(1)H_2}$ substituents, which requires significantly more energy for P < As < Sb ($35 - 50\ \mathrm{kcal\,mol^{-1}}$) than for N ($< 10\ \mathrm{kcal\,mol^{-1}}$) (NOH effect as discussed in Ch. (2) on page 45). Consequently, this energy is gained upon dissociation. But why does protonation of the dipnictenes leads to stronger X=X bonds? Protonation results in a higher degree of hybridization at the planar $\mathrm{X(1)H_2}$ centers which particularly strengthens the σ increment of the X=X double bond owing to better valence orbital overlap [Kutzelnigg 1978 , p. 239 ff.]. The strengthening of the X=X double bond upon protonation is even more remarkable, since we know from the group charges of $\mathbf{X}$-$\mathbf{19a}$ that the $\mathrm{X(1)H_2}$ and $\mathrm{X(2)H}$ fragments are positively charged. Thus, the corresponding dissociation energies D_0 for these monocations are additionally lowered by the contributions of the coulombic repulsion between the $\mathrm{XH_2}$ and XH fragments to the steric repulsion term ΔE^0 (cf. Eq. (1.6) on page 9).

Next, we discuss the dissociation energies for the doubly protonated species $[\mathrm{H_2X{=}XH_2}]^{2+}$, which are completely different than those obtained for the for-

Table 3.12: X=X double bond systems. Dissociation energies D_0 for the neutral dipnictenes HX=XH (**X-16a**) and their protonated derivatives $[H_2X=XH]^+$ (**X-19a**) and $[H_2X=XH_2]^{2+}$ (**X-24a**) (X = N, P, As, Sb).[a]

| | D_e [b] | corrections | | D_0 | | | |
		ΔZPE [c]	ΔBS [d]	this work[e]		others	exp
N-16a	117.5	−8.3	4.6	113.8	(122.8)	120.7[f]	121.8[g]
N-19a	155.9	−11.0	5.6	150.5	(158.2)		
N-23a	15.5	−11.7	7.1	10.9	(20.0)		
P-16a	67.9	−4.4	10.3	73.8	(83.7)		
P-19a	87.9	−4.7	8.5	91.8	(97.9)		
P-24a	−45.1	−4.1	5.8	−43.4	(−44.5)		
As-16a	57.3	−3.6	7.9	61.6	(67.9)		
As-19a	69.5	−3.8	6.4	72.1	(76.9)		
As-24a	−64.2	−3.6	5.2	−62.6	(−57.9)		
Sb-16a	45.0	−2.8	7.5	49.7			
Sb-19a	51.4	−2.9	6.3	54.8			
Sb-24a	−72.1	−2.8	5.3	−69.6			

[a] Results in kcal mol^{-1} calculated from total and zero-point energies presented in Tab. (3.1) ("X=X") and Tab. (3.11) (XH, and XH$_2^+$).

[b] CCSD(T)/VDZP^1 data on MP2/VDZP^1 optimized geometries.

[c] Difference for ZPE (unscaled) between doubly bonded species and their constituting ground state fragments.

[d] Difference between the D_e values in the VTZP^1 and VTZP^2 basis sets.

[e] ZPE corrected CCSD(T)/VTZP^2 data: $D_e + \Delta$ZPE $+ \Delta$BS. (G2 values in parentheses).

[f] in [Langhoff and W. Bauschlicher 1991] (MRCI).

[g] in [Willis et al. 1976].

mer neutral and monocationic dipnictenes HX=XH and $[H_2X=XH]^+$. For the planar dicationic hydrazine **X-23a**, dissociation into two triplet NH$_2^+$ groups is slightly endothermic by 10.9 kcal mol^{-1}, whereas for the heavier congeners **X-24a** with X = P, As, Sb, the resulting D_0 values are highly negative, decreasing from -43.4 kcal mol^{-1} to -69.6 kcal mol^{-1}. The key to understand this result is found in the enhanced coulomb repulsion between the two $+1\,e$ charged XH$_2$ units of the dications $[H_2X=XH_2]^{2+}$. In the dicationic hydrazine $[H_2N=NH_2]^{2+}$ the destabiliza-

tion of the N=N bonding as a result of the coulombic repulsion is smaller than the stabilizing "$\sigma + \pi$" bond energy $E_{\sigma+\pi}$. In contrast, in the heavier homologues, the high coulombic repulsion between the XH_2^+ units becomes predominant, resulting in highly negative reaction enthalpies for the dissociation reaction (Rxn. 3.5). As a consequence, the D_0 values for the dications $[H_2X=XH_2]^{2+}$ are not a valid source to determine the total bond strength ΔE_{TBE}^0 anymore. This is the same reason that the dissociation energies for the dications $[H_2C–XH_3]^{2+}$ and $[H_3C–XH_2]^{2+}$ do not reflect correctly the corresponding C–X single bond strengths (cf. Sec. (2.3)).

If the heavier dicationic dipnictenes $[H_2X=XH_2]^{2+}$ are not persistent thermo-dynamically against coulomb explosion, are they stable kinetically? In order to answer this question, we calculated the transition states $\mathbf{X\text{-}26a}^{TS}$ for the dissociation reactions according to (Rxn. 3.5) for X = N, P, As, Sb. The structures of the transition states are shown graphically in Fig. (3.1) on page 78. The corresponding bonding parameters are given in Tab. (3.2). For the X = N case, $\mathbf{N\text{-}26a}^{TS}$ has D_{2h} symmetry with planar NH_2 groups. On the other hand, the symmetry in the heavier homologues $\mathbf{X\text{-}26a}^{TS}$ is reduced to C_s, with one XH_2 center slightly (ϕ_{X^1} = 12.0 → 2.4 °) and the other strongly pyramidalized (ϕ_{X^2} = 87.6 → 102.5 °). The bending in these transition states can be explained by the interaction of two car-benic fragments XH_2^+ in their singlet states, according to Trinquier and Malrieu [1987]. Formally, the doubly occupied n_σ orbital at X(1) still forms a dative bond with with the empty p_π orbital at X(2), whereas the other electron pair is located in the perpendicular n_σ orbital on X(2). The slight pyramidalization at the X(1) center reveals some weak π_{np} backdonation from X(2) to X(1). The barriers for the bond fission reactions (Rxn. 3.5) strongly decrease in the order N ≫ P > As > Sb, ranging from 151.3 kcal mol^{-1} to 7.9 kcal mol^{-1}. However, the barriers for the dications $[H_2P=PH_2]^{2+}$ and $[H_2As=AsH_2]^{2+}$ are still considerable 41.7 kcal mol^{-1} and 20.6 kcal mol^{-1}, respectively. Notwithstanding, only derivatives of the dication $[H_2N=NH_2]^{2+}$ have been detected by cyclic voltammetry so far Dietrich et al. [1986].

The reaction profiles for the dissociation reaction (Rxn. 3.5) are shown schematically in Fig. (3.6).
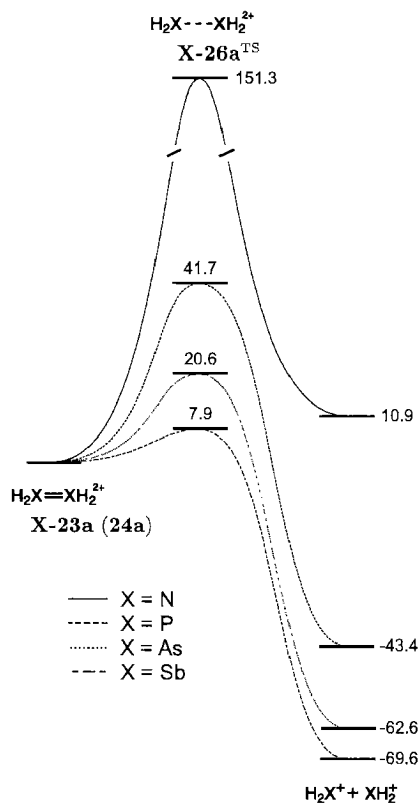
Figure 3.6: Schematic energy profile for the dissociative processes in the dications **N-23a** and **X-24a** (X = P, As, Sb).

What does the CGMT model predict for the neutral and cationic group 15 double bond system? Obviously, all neutral dipnictenes HX=XH with X = N, P, As, Sb prefer classical planar structures since all XH fragments are triplets. Another reason for their classical behavior is that they are able to form a "$\sigma + \pi$" double bond systems through p orbital overlap, while the lone pairs retain more s character with increasing atomic number of X. For the more controversial protonated derivatives [H$_2$X=XH]$^+$, the values for $\Sigma\Delta E_{s\to T}$ and $1/2E_{\sigma+\pi}$, listed in Tab. (3.13), show that, according to inequality Eq. (1.2) (see on page 7), all monocations should prefer the planar structures **X-19a**. This is in accordance with the relative stabilities found for the various [X$_2$H$_3$]$^+$ isomers with X = N, P, As (cf. Tab. (3.1)). However, the

CGMT-model fails to predict that the hydrogen bridged isomer **Sb-21a** is the global minimum on the $[Sb_2H_3]^+$ hypersurface.

Table 3.13: X=X bonding energies. Application of the CGMT model to the dipnictenium ions $[H_2X=XH]^+$ (X = N, P, As, Sb) according to the inequalities (1.2)–(1.4) (cf. Sec. (1.1.1) on page 4).[a]

system	$\Sigma\Delta E_{S\rightarrow T}$	$\frac{1}{2}\Delta E^0_{TBE}$	$\frac{1}{2}E_{\sigma+\pi}$	structure
$[H_2N=NH]^+$	-75.5	75.3	80.8	p
$[H_2P=PH]^+$	-11.5	45.9	56.7	p
$[H_2As=AsH]^+$	-3.6	36.1	49.8	p
$[H_2Sb=SbH]^+$	2.0	27.4	42.1	p

[a] All energies in $kcal\,mol^{-1}$. $\Sigma\Delta E_{S\rightarrow T}$ refers to the sum of the singlet-triplet splitting energies, taken from Tab. (3.11). ΔE^0_{TBE} refers to D_0, taken from Tab. (3.12). $E_{\sigma+\pi}$ refers to the ZPE uncorrected reaction enthalpy for the dissociation of the planar double bond systems into their triplet fragments. p = planar , tb = trans-bent.

It would be interesting to apply the CGMT condition for the higher trans-bent homologues of the dication $[H_2N=NH_2]^{2+}$. Unfortunately, it is difficult to approximate values for $E_{\sigma+\pi}$, since the corresponding dissociation energies of the dications are no longer reliable indicators for the double bond strengths. For the dicationic hydrazine $[H_2N=NH_2]^{2+}$, it is simple to predict a planar geometry, since $\Sigma\Delta E_{S\rightarrow T}$ remains negative ($-60.0\ kcal\,mol^{-1}$), i.e the unbound NH_2^+ fragment has a triplet ground state. In contrast, for the higher congeners $[H_2X=XH_2]^{2+}$, $\Sigma\Delta E_{S\rightarrow T}$ becomes considerable positive, increasing from $34.0\ kcal\,mol^{-1}$ (X = P) over $47.4\ kcal\,mol^{-1}$ (X = As) to $53.0\ kcal\,mol^{-1}$ (X = Sb). Assuming that the intrinsic double bond strengths for mono- and dications are similar, trans-bent structures would be predicted within the framework of the CGMT model for $[H_2As=AsH_2]^{2+}$ and $[H_2Sb=SbH_2]^{2+}$. In the case of the dicationic phosphazine $[H_2P=PH_2]^{2+}$, $\Sigma\Delta E_{S\rightarrow T}$ is presumably of the same magnitude than $\frac{1}{2}E_{\sigma+\pi}$ and therefore both planar and trans-bent structures are possible. This is in accordance with the finding

that the energy required to convert **P-24a** into the planar form **P-23a** is very small $(< 1.0 \, \text{kcal} \, \text{mol}^{-1})$.

Let us now turn to the discussion of the π-bond strengths for all three series of doubly bonded species HX=XH, $[\text{H}_2\text{X}=\text{XH}]^+$ and $[\text{H}_2\text{X}=\text{XH}_2]^{2+}$. The π-bond energies are collated in Tab. (3.14). Comparison with data reported in the literature shows significant differences only in the π increment of the diazene HN=NH. For the dipnictenes, containing elements from the higher rows, the values are in good overall accordance. For the cationic systems, no other data is available so far. The result for the diazene needs some explanation. Firstly, rotation around

Table 3.14: X=X bonding energies. π-bond energies for the neutral dipnictenes HX=XH (**X-16a**) and their protonated derivatives $[\text{H}_2\text{X}=\text{XH}]^+$ (**X-19a**) and $[\text{H}_2\text{X}=\text{XH}_2]^{2+}$ (**X-23a/X-24a**) (X = N, P, As, Sb).

	this work[a]	Kutzelnigg[b]	Schmidt[c]	Schoeller[d]	others
N-16a	43.1 (87.1)	94.0	60.0		
N-19a	48.0 (82.6)				
N-23a	62.6				
P-16a	31.1	34.0	34.0	32.5	
P-19a	28.5				
P-24a	26.1				
As-16a	25.9	29.0		25.4	
As-19a	21.3				
As-24a	21.1				
Sb-16a	19.5			18.0	20.0[e]
Sb-19a	13.3				
Sb-24a	15.9				

[a] CCSD(T)/VTZP[2] data. ZPE correted values in $\text{kcal} \, \text{mol}^{-1}$ taken from Tab. (3.1) on page 77. the π-bond strengths in parentheses for **N-16a** and **N-19a** are derived using the method descibed in [Schleyer and Kost 1988].

[b] in [Kutzelnigg 1984].

[c] in [Schmidt et al. 1987] (SOCI).

[d] in [Schoeller et al. 1997] (MRCI).

[e] in [Power 1998].

the N–N axis in the planar diazene **N-16a**, diminishes the repulsive interaction be-
tween the neighboring lone pairs. This effect counterbalances the increase in the
bond length as a result of the π-bond cleavage. Secondly, each singly occupied
p orbital at each nitrogen undergoes a 2c-3e interaction with the lone-pair of the
other nitrogen. As a result, both nitrogen centers are pyramidalized which is indi-
cated by a dihedral $\angle$HNNH $>$ 100.0 $^\circ$ (MP2/VDZP[1]: 103.6 $^\circ$; MP2/6-311G(d,p):
103.7 $^\circ$; QCISD/6-311G(d,p):100.7 $^\circ$). This is in contrast to the heavier triplets
X-17a, where $\angle$HXXH $\approx$ 90 $^\circ$ for all X = P, As, Sb. Conversely, Schmidt et al.
[1987] reported an dihedral $\angle$HNNH = 90.1 $^\circ$ for **X-17a** together with a much
longer N–N bond length of 1.436 Å, as discussed in the previous section Sec. (3.1)
on page 81. This would indicate "perfect" cleavage of the π-bond in **N-17a** with
negligible residual π interactions. In contrast to these findings, our result indicates
that considerable π bondings still exists. As a result, we can state that the method
of rotational barrier fails to give a valuable π-bond strength for the diazene HN=NH.
Accordingly, Kutzelnigg [1984] obtained a much higher value for the π-bond incre-
ment of 94.0 kcal mol^{-1}, derived from diatomic data. Moreover, the resulting π-bond
strengths derived from the method proposed by Schleyer and Kost [1988] is of sim-
ilar magnitude (vide supra). It is interesting that for the heavier dipnictenes, the
D_π values are similar, regardless from which method derived, ranging in between
32.0 kcal mol^{-1} and 19.0 kcal mol^{-1} for X = P $>$ As $>$ Sb.

Also for the diazenium ion [H$_2$N=NH]$^+$, the rotational barrier D_π seems to
be a bad approximate for the real π-bond strength. The reason is again found in
the 2c-3e interaction which results in a considerable pyramidalization of the NH$_2$
center in the twisted triplet ground state **X-19a**. This type of argument has already
been employed in Sec. (2.2) to account for the lowering of D_π for H$_2$C=NH (cf. on
page 48). This becomes even more evident by the higher D_π value of 62.6 kcal mol^{-1}
obtained for the double protonated hydrazine dication [H$_2$X=XH$_2$]$^{2+}$! Obviously,
there is no reason for an increase in the π-bond strength in going from the diazene

N-16a to the dicationic derivative **N-23a**. Rather, it emphasizes that the D_π values for both, HN=NH and $[H_2N=NH]^+$, are not a valuable measure for the π-bond strengths existing in these species. We therefore additionally calculated the π-bond strength of these species with the method proposed by Schleyer and Kost [1988] at the G2 level. The values obtained with this method are approximately double the size than those obtained by rotational barriers. For the diazene E_π is slightly lower $(89.7\,\mathrm{kcal\,mol}^{-1})$ than the π increment given by Kutzelnigg [1984].

As discussed in Sec. (3.1), the XH_2 groups in the heavier twisted triplets **X-20a** with P, As, Sb, are bent away considerably from planarity by $\phi_X \approx 55.0\,°$. In contrast to the nitrogen system, this is not effected by the np_π interaction, but rather a consequence of the tendency of the higher row elements to pyramidalize. Again, the resulting D_π values are therefore lower limits for the actual π-bond strengths in the heavier monocations **X-19a**, and ranging from $28.5\,\mathrm{kcal\,mol}^{-1}$ to $13.3\,\mathrm{kcal\,mol}^{-1}$ for X = P > As > Sb. Remarkably, the π-bond increments obtained for the dications $[H_2X=XH_2]^{2+}$ are similar, decreasing from $26.1\,\mathrm{kcal\,mol}^{-1}$ for **P-24a**, over $21.1\,\mathrm{kcal\,mol}^{-1}$ for **As-24a** to $15.9\,\mathrm{kcal\,mol}^{-1}$ for **Sb-24a**. Why is it possible to obtain considerable π-bond strengths for the dications when the dissociation energies are even negative? Remember that the D_π values are derived from the energy gap between the singlet ground state double bond systems (planar or trans-bent) and the corresponding twisted biradical ground states on the triplet hypersurfaces. For each pair of molecules, the high coulombic repulsion remains almost the same. On the other hand, dissociation of the dications results in a significant stabilization of the fragments XH_2^+ obtained after bond cleavage which do not suffer anymore from the destabilizing electrostatic interaction.

The bond energies can be now resolved in σ and π increments. Since the total bond energies of the heavier monocations $[H_2X=XH]^+$ with X = P, As, Sb also include contributions from the promotion energy $\Delta E_{s \to T}$ of the XH_2^+ fragments, it is better to take $E_{\sigma+\pi}$ for all species considered. Remember that the energy term

Table 3.15: X=X double bond systems. σ and π increments of the double bond energy $E_{\sigma+\pi}$ for the neutral dipnictenes HX=XH and their protonated derivatives $[H_2X=XH]^+$ (X = N, P, As, Sb).[a]

X	HX=XH		$[H_2X=XH]^+$	
	$E_{\sigma+\pi}$	σ/π	$E_{\sigma+\pi}$	σ/π
N	122	$49/87^b(38/94)^c$	162	$79/83^b$
P	78	$47/31\ (48/34)^c$	113	84/29
As	65	$39/26\ (35/28)^c$	100	79/21
Sb	53	$33/20\ (31/20)^d$	84	71/13

[a] CCSD(T)/VTZP^2 data. $E_{\sigma+\pi}$ refers to the ZPE uncorrected reaction enthalpy for the dissociation of the planar double bond systems into their triplet fragments. The π-bond increments are taken from Tab. (3.14) except for X = N. The σ-bond increments are readily obtained from $E_\sigma = E_{\sigma+\pi} - E_\pi$.

[b] The π-bond values are calculated according to Schleyer and Kost [1988] at the G2 level.

[c] in [Kutzelnigg 1984].

[d] in [Power 1998].

$E_{\sigma+\pi}$ refers to the double bond energy of a classical planar system. The values for $E_{\sigma+\pi}$ and its σ/π contributions are presented in Tab. (3.15). Note that for the π-bond strengths of HN=NH and $[H_2N=NH]^+$, the G2 values obtained according to Schleyer and Kost [1988] are taken. The results for the neutral dipnictenes show excellent agreement with the values presented in [Kutzelnigg 1984] for X = N, P, As and [Power 1998] for X = Sb. This values are abstracted from experimental dissociation energies of diatomic group 15 molecules from [Huber and Herzberg 1979] and corresponding single bond strengths. The relevant difference between the diazene and its higher congeners is the reversing of the $\sigma{:}\pi$ ratio from 1:2 for HN=NH to 1.5:1 for HX=XH with X = P, As, Sb. Kutzelnigg [1984] pointed out that the increments for diazene reflect the instability of single N–N bonds, and

that normally N prefers to exhibit multiple bonds. On the other hand, group 15 homonuclear single bonded species from the higher row elements have been known long before the unsaturated dipnictenes.

In going from the neutral double bond systems to the monocations $[H_2X=XH]^+$, it becomes evident that the relative increase in the bond energies upon protonation can be attributed mainly to the remarkable increase of the σ-bond increments by a factor of 1.5–2! In contrast, the π-bond contributions to the overall double bond energy $E_{\sigma+\pi}$ even slightly decreases when comparing each pair of species **X-16a** vs. **X-19a**. As a result the σ:π ratio for $[H_2N=NH]^+$ is 1:1, whereas for the higher congeners the ratios decrease from 3:1 for $[H_2P=PH]^+$, over 4:1 for $[H_2As=AsH]^+$ to 5:1 for $[H_2Sb=SbH]^+$.

3.2.3   Bader Analysis

The properties of the electron density at the (3,-1) bond critical points for the dipnictenes HX=XH (**X-16a**), as well as for their singly and doubly protonated derivatives $[H_2X=XH]^+$ (**X-16a**) and $[H_2X=XH]^+$, are listed in Tab. (3.16). For the heavier systems of the dications $[H_2X=XH]^+$ with X = As, Sb, we present results for both, the planar (**X-23a**) and the trans-bent (**X-24a**) structures. Corresponding two-dimensional plots of the *negative* Laplacian, $-\nabla^2\rho(\mathbf{r})$ are displayed in Fig. (3.7)–(3.9), including the contour lines of the interatomic surfaces which define the space taken by atoms within molecules.

In the neutral dipnictenes HX=XH, the BCPs, which are given as the ratios between the distances $\mathbf{X}_\alpha$-$\mathbf{r}_b/R_e$, are located at the midpoint of the X–X bond path for all X = N, P, As, Sb, according to the central symmetry in these molecules. The ρ_b value is indicative of the charge concentration along the X–X bond path, and is highest for the N–N bond, decreasing in the order N=N $\ll$ P=P < As=As < Sb=Sb from 3.1 e Å^{-3} to 0.5 e Å^{-3}. Note that the charge density at the BCP (ρ_b) for the

Table 3.16: X=X topographical analysis. Bond critical point data for the X=X double bonds of the neutral dipnictenes HX=XH (**X-16a**) and their protonated derivatives [H$_2$X=XH]$^+$ (**X-19a**) and [H$_2$X=XH$_2$]$^{2+}$ (**X-23a**/**X-24a**) (X = N, P, As, Sb).[a]

	bond	R_b (Å)	$X_\alpha-r_b$ (Å)	r_b	ρ_b (e Å^{-3})	$\nabla^2\rho_b$ (e Å^{-5})	$H(r)$ (Hartree Å^{-3})	ϵ_b
X-16a	N=N	1.262	0.631	0.500	3.059	−24.752	−3.743	0.172
	P=P	2.077	1.038	0.500	0.945	−5.411	−0.637	0.282
	As=As	2.282	1.141	0.500	0.689	−1.555	−0.352	0.331
	Sb=Sb	2.675	1.338	0.500	0.471	−0.072	−0.179	0.322
X-19a	N=N	1.235	0.649	0.526	3.203	−27.648	−4.120	0.163
	P=P	2.043	1.284	0.629	0.930	−3.651	−0.856	0.359
	As=As	2.242	1.215	0.542	0.684	0.259	−0.331	0.427
	Sb=Sb	2.637	1.398	0.530	0.465	0.594	−0.176	0.436
X-23a	N=N	1.237	0.619	0.500	3.211	−27.986	−4.017	0.274
	P=P	2.031	1.016	0.500	1.023	−7.008	−0.736	0.609
	As=As	2.213	1.106	0.500	0.761	−2.115	−0.411	0.757
	Sb=Sb	2.597	1.299	0.500	0.523	−0.327	−0.218	0.725
X-24a	P=P	2.050	1.025	0.500	1.001	−6.764	−0.702	0.460
	As=As	2.276	1.138	0.500	0.710	−2.232	−0.367	0.344
	Sb=Sb	2.732	1.366	0.500	0.448	−0.419	−0.163	0.244

[a] Derived from MP2/6-31G(d,p) (X = N, P) and MP2/DZP(AE) (X = As, Sb) wavefunctions of the MP2/VDZP[1] geometries. For a graphical presentation of the negative laplace distribution $-\nabla^2\rho(r)$, see Fig. (3.7) (HX=XH), Fig. (3.8) ([H$_2$X=XH]$^+$) and Fig. (3.9) ([H$_2$X=XH$_2$]$^{2+}$).

diazene HN=NH is considerable higher by 0.5 e Å^{-3} than those found in the imine H$_2$C=NH. On the other hand, for the heavier dipnictenes, the reverse ordering is found: ρ_b values for HX=XH are increasingly smaller than those found for the species H$_2$C=XH by as much as 0.2 e Å^{-3} for X = P and 0.4 e Å^{-3} for X = As, Sb. Notwithstanding, the double bonds formed between carbon and group 15 elements in the systems H$_2$C=XH are significantly stronger than the respective X=X double bonds in the dipnictenes HX=XH (cf. Tab. (2.10) on page 44 and Tab. (3.12)).[2] The

---

[2]In order to determine the relative bond strengths of different types of A–B bonds, the respective charge densities *integrated* over the interatomic surface S_{AB} have to be compared, as described in

Laplacian $\nabla^2 \rho_b$ and the energy density H_b are further valuable sources to characterize the nature of a bond. Both quantities are negative for all systems HX=XH which reveals the nonpolar covalent character of the double bonding between the X nuclei for all n = 0, 1, 2. However, the trend in $\nabla^2 \rho_b$ and H_b towards negative values close to zero in the dipnictenes **X-16a** with increasing atomic number of X, indicates the decrease in the covalent strengths of the X=X double bonds in the order X = N $\gg$ P > As > Sb. The decrease in the charge concentration in the interatomic regions within the dipnictenes HX=XH is shown graphically by the two-dimensional plots of their Laplace distributions in Fig. (3.7). Charge concentration is indicated by solid lines and charge depletion by broken lines. The Laplacians close to zero and non-observable lone pairs at the As and Sb centers are the effects of the large atomic basins of arsenic and antimony in which the valence electrons are poorly localized.

The ellipticity ϵ_b, defining the anisotropy of ρ at the BCP, is largest for the arsenic arsenic bond (0.33) and decreases in the order As=As $\approx$ Sb=Sb > P=P > N=N. In order to understand this ordering it is helpful to compare the magnitudes of the curvatures λ_1 and λ_2. Consider the small value of ϵ_b of 0.17 for the diazene HN=NH compared with the considerable larger ellipticity of 0.28 for the diphosphene HP=PH. The magnitudes of λ_1 and λ_2 for **N-16a** are 1.10 and 0.94 au, whereas for **P-16a**, magnitudes of 0.16 and 0.13 au are obtained, respectively. If we compare the relative changes in λ_1 and λ_2, it is evident that the decrease in the magnitude of $\lambda_2(\textbf{N-16a})$: $\lambda_2(\textbf{P-16a})$ $\approx$ 8 : 1 is more pronounced, than the concomitant decrease in $\lambda_1(\textbf{N-16a})$: $\lambda_1(\textbf{P-16a})$ $\approx$ 7 : 1. The same trend is observed for the heavier homologues **As-16a** and **Sb-16a**. As a result, the increasing ellipticity is in fact due to the relative increase of charge density in the "π space" above and below the molecular plane which possibly occurs because the valence p orbitals of the higher row elements are more extended in space. Furthermore, in the case of

---

[Cremer and Kraka 1984]. However, these authors also demonstrated, that comparison of ρ_b values within one class of bond, e.g CC bonds, is suitable to measure their relative strength.

N-16a

P-16a

As-16a

Sb-16a
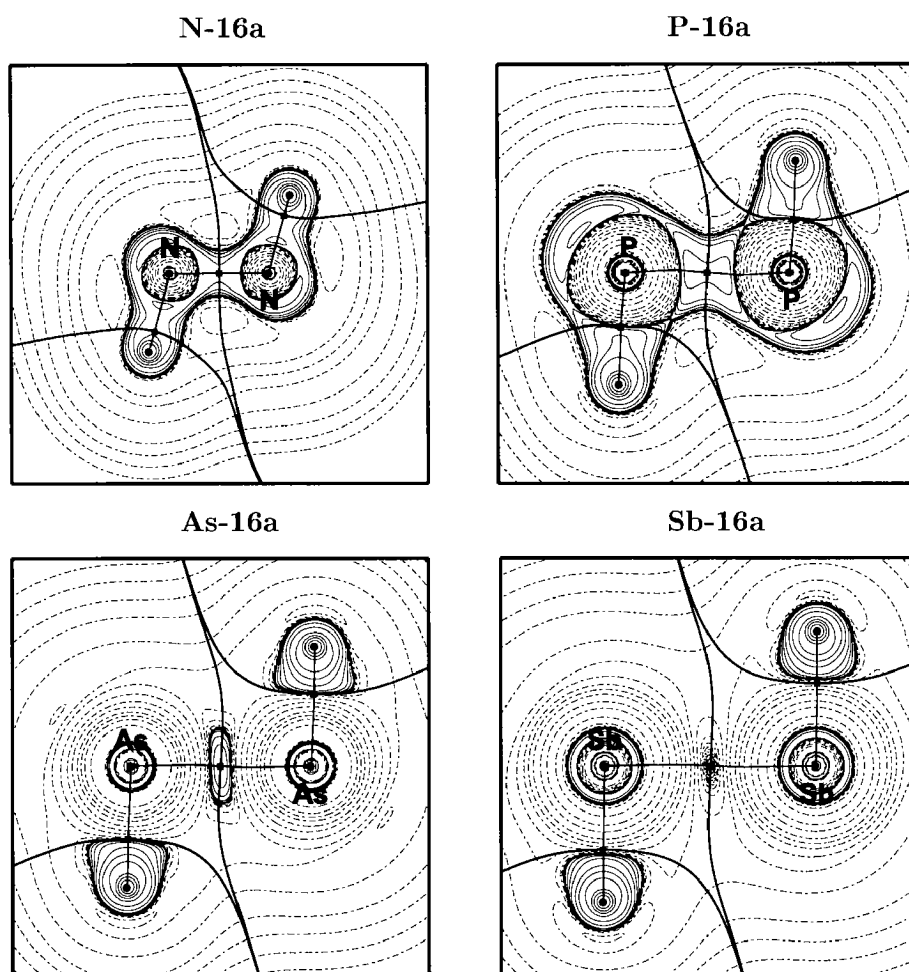
Figure 3.7: Two-dimensional contour plots of the negative Laplacians $-\nabla^2\rho(\mathbf{r})$ for the neutral dipnictenes HX=XH (**X-16a**), within the molecular plane. Solid contour lines indicate regions of charge concentration $(-\nabla^2\rho(\mathbf{r}) > 0)$, dashed contour lines indicate regions of charge depletion $(-\nabla^2\rho(\mathbf{r}) < 0)$. Contour lines of the interatomic zero-flux surfaces (—) and bond paths (—) are shown as solid bold lines. Bond critical points are indicated by black squares (■). For the corresponding BCP data of the X=X double bonds see Tab. (3.16).

the diazene, these electrons located in a purely π_{pp} type orbital are not repelled by core electrons in p-type orbitals (Pauli repulsion) at the nitrogen centers. Since the heavier congeners P–Sb do have populated innershell p orbitals, the valence electrons in the X=X bond suffer from these 3e-2c repulsions.

In the protonated species $[H_2X^1\!=\!X^2H]^+$, the BCPs are shifted towards X(2), given by r_b values ranging between ≈ 0.53 (X = N, As, Sb) and 0.63 (X = P), indicating that electron density is more accumulated in the X(1) basin, rather than in the X(2) basin for all X = N, P, As, Sb. While the Laplacian of the N=N double bond in $[H_2N\!=\!NH]^+$ becomes more negative upon protonation, the reverse effect is observed for the higher homologues HX=XH, and $\nabla^2\rho_b$ increase, ranging from a negative value of $-3.7\,e\,\text{Å}^{-5}$ for X =P to *positive* values of 0.2 and 0.6 $e\,\text{Å}^{-5}$ for X = As, Sb respectively. However, the local energy density H_b remains negative for all monocations $[H_2X\!=\!XH]^+$, ranging from -3.7 to -0.2 Hartree Å^{-3}. Thus, the bond critical point data for the X=X bonds in the monocations **X-19a** emphasize the increasing ionic character of the X=X bond with increasing atomic number of X. This is in accordance with the increasing positive atomic charges found for the neighboring X atoms in the monocations **X-19a** of the higher row elements (cf. Tab. (3.5)). The π character of the X=X bonds in the monocations $[H_2X\!=\!XH]^+$, given by ϵ_b, with respect to the neutral dipnictenes, decreases slightly for X = N, whereas ϵ_b increases considerably for the the heavier homologues with X = P, As, Sb. In Fig. (3.8), the Laplacian $\nabla^2\rho(\mathbf{r})$ is shown graphically for the monocations **X-19a**. The shift of the X=X bond critical point is demonstrated as well as the *Umpolung* of the XH bonds, when going from **N-19a** ($\mathcal{X}_H \ll \mathcal{X}_N$) to the higher congeners ($\mathcal{X}_H > \mathcal{X}_X$) with X = P, As, Sb.

For the dications $[H_2X\!=\!XH_2]^{2+}$, we firstly consider only the planar structures **X-23a** for all X = N, P, As, Sb. For the nitrogen containing system, little variation is seen in the bond critical point data when going from the mono- to the dicationic species **N-19a** and **N-23a**, respectively. Surprisingly, the second protonation is

N-19a   **P-19a**

As-19a   **Sb-19a**
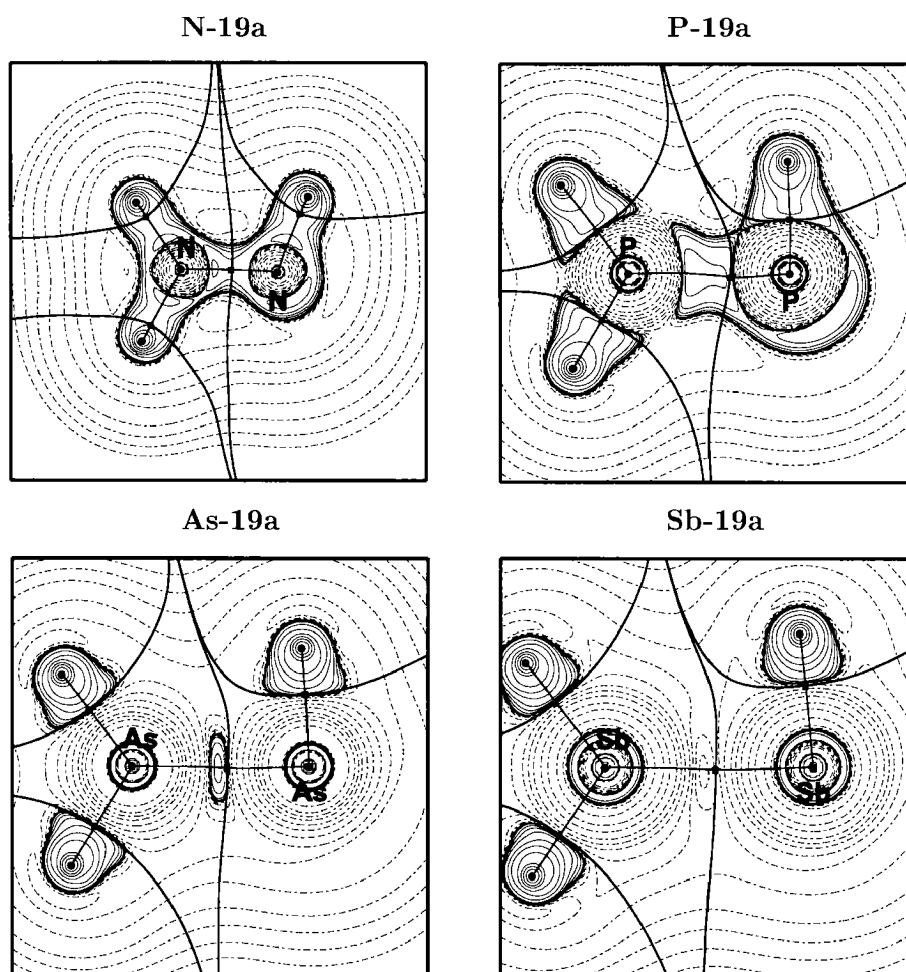
Figure 3.8: Two-dimensional contour plots of the negative Laplacians $-\nabla^2\rho(\mathbf{r})$ of the monocations $[\mathrm{H_2X{=}XH}]^+$ (**X-19a**), within the molecular plane. Solid contour lines indicate regions of charge concentration $(-\nabla^2\rho(\mathbf{r}) > 0)$, dashed contour lines indicate regions of charge depletion $(-\nabla^2\rho(\mathbf{r}) < 0)$. Contour lines of the interatomic zero-flux surfaces (—) and bond paths (—) are shown as solid bold lines. Bond critical points are indicated by black squares (■). For the corresponding BCP data of the X=X double bonds see Tab. (3.16).

N-23a   P-24a

As-24a   Sb-24a
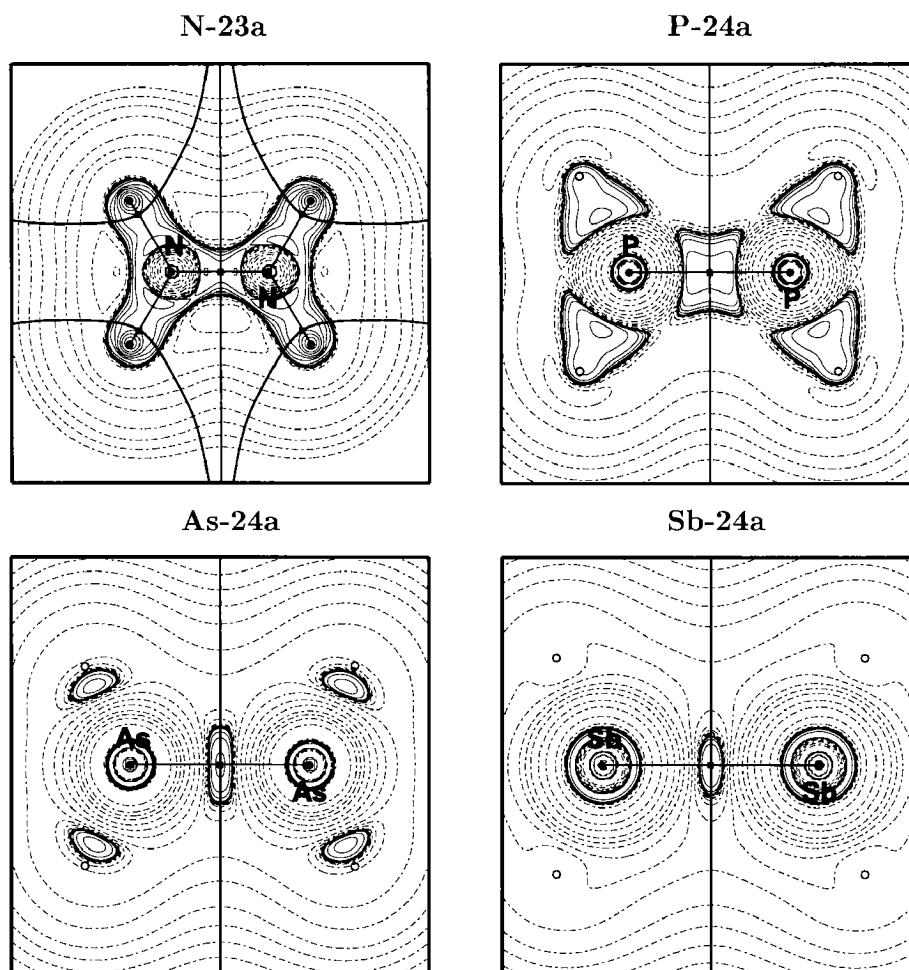
Figure 3.9: Two-dimensional contour plots of the negative Lapla-
cians $-\nabla^2\rho(\mathbf{r})$ of the planar (**N-23a**) and trans-bent (**X-24a**, X =
P, As, Sb) dications $[\mathrm{H_2X{=}XH_2}]^{2+}$, along the X–X bond path. Solid
contour lines indicate regions of charge concentration ($-\nabla^2\rho(\mathbf{r})$
> 0), dashed contour lines indicate regions of charge depletion
($-\nabla^2\rho(\mathbf{r}) < 0$). Contour lines of the interatomic zero-flux surfaces
(—) and bond paths (—) are shown as solid bold lines. Bond crit-
ical points are indicated by black squares (■). Small black circles
indicate hydrogen atoms above (solid) and below (dashed) the plot
plane. For the corresponding BCP data of the X=X double bonds
see Tab. (3.16).

leading to a remarkable increase of ρ_b in the dications of the higher row elements. Furthermore, the corresponding values of $\nabla^2 \rho_b$ decrease to even more negative values than found for the respective dipnictenes HX=XH, increasing in the order P (-7.0 Hartree Å^{-3}) < As (-2.1 Hartree Å^{-3}) < Sb (-0.3 Hartree Å^{-3}). Additionally, the local energy density H_b remains negative for all dications $[H_2X=XH_2]^{2+}$ with magnitudes even larger than in the dipnictenes HX=XH for all X = N, P, As, Sb. Furthermore, the ellipticities of the X=X bonds are much higher, increasing from 0.24 to 0.76 in the order N=N $\ll$ P=P < Sb=Sb $\approx$ As=As. The key to understand the results is that the increase in ellipticity of the X=X bond for the planar dications is primarily a result of the increased contraction of the density towards the bond path, as seen from the increasing magnitudes of λ_1 upon protonation, whereas the changes in λ_2 are marginal.[3] As a result, the large ϵ_b values do not account for an increase in the π character of the doubly protonated X=X bonds, but rather show the high charge concentration in the X=X bonding region: valence charge is "trapped" between the two neighboring pnictogen centers and contracted towards the X–X bond path due to the enhanced forces evoked by the positively charged fragments. Trans-bending in the heavier dications $[H_2X=XH_2]^{2+}$ (X = P, As, Sb) significantly lowers the values for ϵ_b, which now decreasing from 0.46 to 0.24 with increasing atomic number of X. The reason for this is, that a portion of equally distributed "π density" above and below the molecular plane in the planar systems is shifted towards the X centers in the trans-bent structures. Consequently, since ϵ_b measures the ellipticity expressed by the two curvatures λ_1 and λ_2 of the plane (almost) perpendicular to the X–X bond path including the BCP, the remaining electron distribution becomes here more cylindrically shaped. This is emphasized by the observation that the values for ρ_b, which measures the charge concentration

---

[3]For example, for the arsenic monocation $[H_2As=AsH]^+$, protonation increases the magnitude of λ_1 from 0.09 to 0.11 au in the planar dication **As-23a**. Concomitantly, the magnitude of the curvature λ_2 (0.06 au) along the principal axis, perpendicular to the molecular plane, remains constant.

along the X–X bond path, decreases upon trans-bent distortion for all X = P, As, Sb.

3.2.4 ELF

In Fig. (2.4) two-dimensional plots of the ELF distribution for the neutral dipnictenes HX=XH are shown graphically. Surprisingly, the expected bond attractor pattern, i.e. two ELF maxima M^1 and M^2 above and below the X–X axis, for a double bond system is only found for the diarsene HAs=AsH and the distibene HSb=SbH. In the ELF distribution of the lighter homologues, the diazene HN=NH as well as the diphosphene HP=PH, show only a single ELF maxima, positioned at the inversion center of each molecule. This is reminiscent to the findings for the triple bond attractor of acetylene which is a ring, whereas it corresponds to a single point in dinitrogen, as shown in [Silvi and Savin 1994]. In order to understand this results, we calculated ELF distributions derived from different basis sets and methods. A small selection of these calculations for the diazene HN=NH is presented in Fig. (3.11). First we compare the results obtained from wavefunction derived at the HF level. In the ELF distribution derived from the minimal basis set STO-3G, two ELF maxima M^1 and M^2 appear in the bonding region! These maxima degenerate to give one single attractor in any ELF distributions using basis sets of better quality, e.g. 6-31G(d,p). Using the same basis sets at the MP2 level give qualitatively similar findings, i.e. minimal basis sets give rise to two separated maxima, while those of higher quality give only one. This is evident, since ELF is formulated within the context of the Hartree-Fock density matrix. Hence, contributions from the correlation effects of electrons with *opposite* spin are not considered in the ELF distribution. From this it is clear that the degeneration of the double bond attractors to a single one is only basis set dependent. A possible explanation for this phenomenon is that the difference in the ELF values of the maxima $M^{1,2}$ and the related minima on the X–X bond path might be smaller than the uncer-

tainty in the localization of the bond attractors. ELF accounts for the *probability* to find a pair of electrons with opposite spin in a given space. Thus, for double bond attractors which are hardly separated in space and to not much differ from the ELF values on the bond path in between, degeneration of the attractor pattern to one single point becomes possible. This is certainly the case for systems containing second row elements, where the valence electron are strongly contracted to the cores. It is well known that the minimal basis sets such as STO-3G are inadequate to describe aspherical charge distributions, as it is true for double bond systems Hehre et al. [1986]. Notwithstanding, this lack of flexibility in the radial parts of the valence functions in the STO-3G basis sets is useful to detect degenerated ELF bond attractors! On the other hand, a true single bond attractor remains one single point somewhere along the X–X bond path, regardless from which basis set the ELF distribution is calculated. Furthermore, the collapse of the ELF maxima $M^{1,2}$ has been only observed for systems of the second and third rows, i.e. the dipnictenes **N-16a** and **P-16a** for the double bond character of the N=N and P=P bond is not in question.

For the heavier dipnictenes **As-16a** and **Sb-16a**, the ELF maxima $M^{1,2}$ are equidistantly localized above and below the midpoint of X–X bond path (cf. Fig. (3.7)). The region within both maxima M^1 and M^2 in these dipnictenes are found, is given by the ELF contour lines of 0.88 for the former and 0.80 for the latter. The lowering of this boundaries indicates that the double bond attractors are increasingly separated from each other when going from the arsenic to the antimony system. However, the ELF value on the bond X–X vector in the middle of the connection line between M^1 and M^2 is still considerable high (> 0.8). Thus, the ELF attractor pattern found for the heavier dipnictenes HAs=AsH and HSb=SbH readily identifies them to fall within the category of classical double bonds.

As shown in Fig. (3.12), again for the diazenium ion, only one single maximum on the X–X bond vector was encountered when using the electron density derived
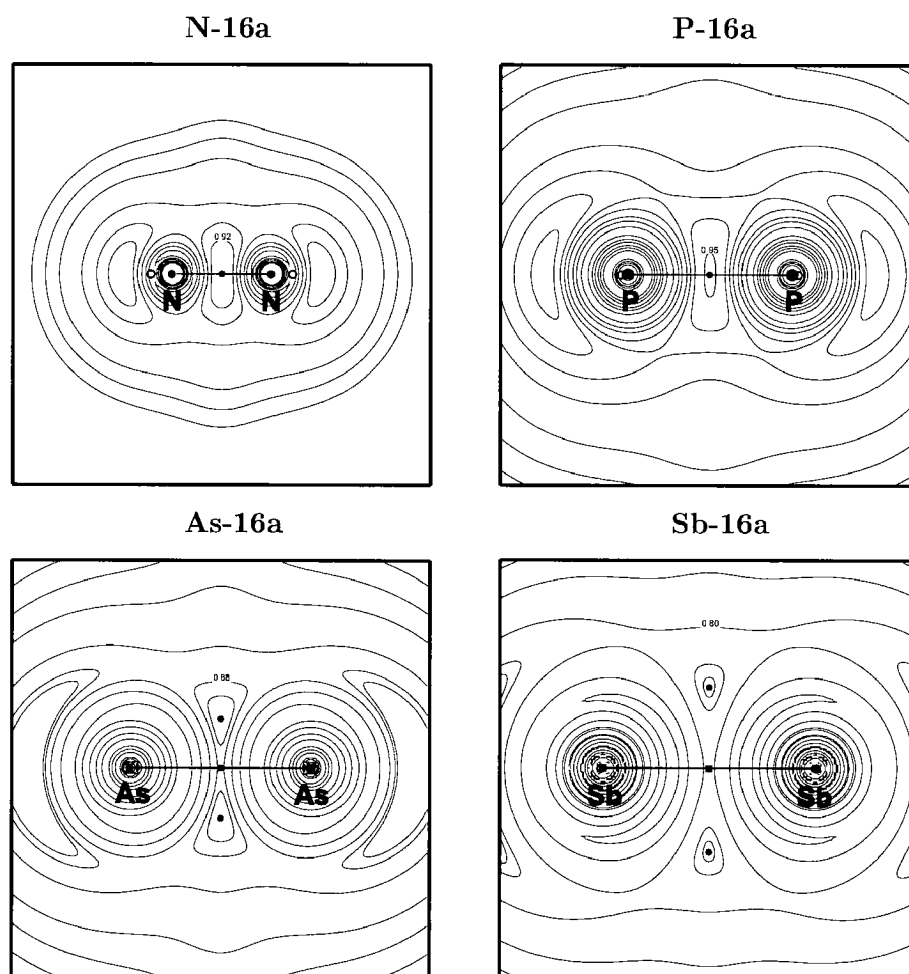
N-16a   **P-16a**

As-16a   **Sb-16a**

Figure 3.10: Two-dimensional contour plots (perpendicular to the molecular plane) of the ELF distribution in the dipnictenes HX=XH, overlayed with the BPs (—) and the BCPs (■) from the Bader Analyses of the X=X double bonds. The inner contour lines (—) correspond to ELF values of 0.8, 0.88, 0.92 for X = N, P and 0.8, 0.88, 0.90 for X = As, Sb. Local ELF maxima > 0.92, i.e. the bond attractors above (M^1) and below (M^2) the X–X bond paths, are indicated by black dots (●). The grey colored regions represent domains within both maxima, M^1 and M^2, are found (N: ELF > 0.92; P: ELF > 0.95; As: ELF > 0.88; Sb: ELF > 0.80). Nuclei above and below the plot plane are indicated by black circles (○).
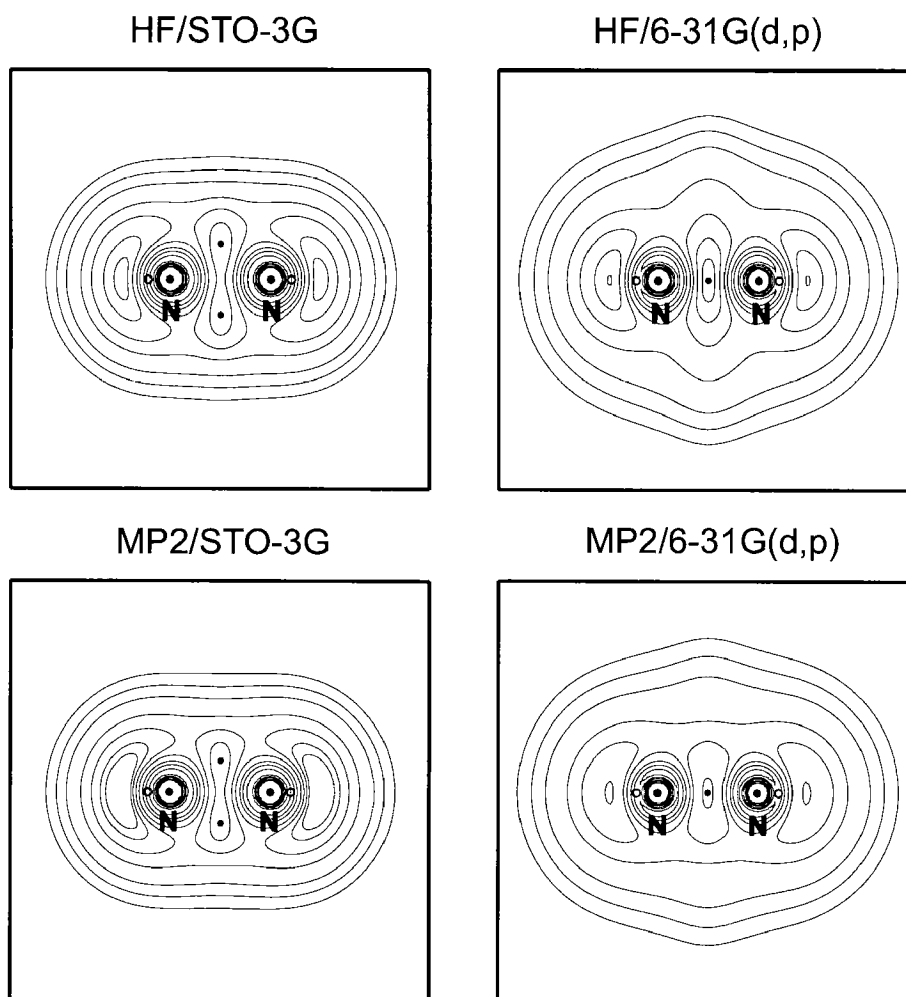
Figure 3.11: Two-dimesional contour plots (perpendicular to the molecular plane) of the ELF distribution in the diazene HN=NH, derived from electron densities, calculated with the STO-3G and 6-31G(d,p) basis sets at the HF and MP2 levels, resprectively. The bond attractors above (M^1) and below (M^2) the X–X bond path, are indicated by black dots (•). The grey colored regions represent the ELF region within both maxima, M^1 and M^2, are found. Nuclei above and below the plot plane are indicated by black circles (○).
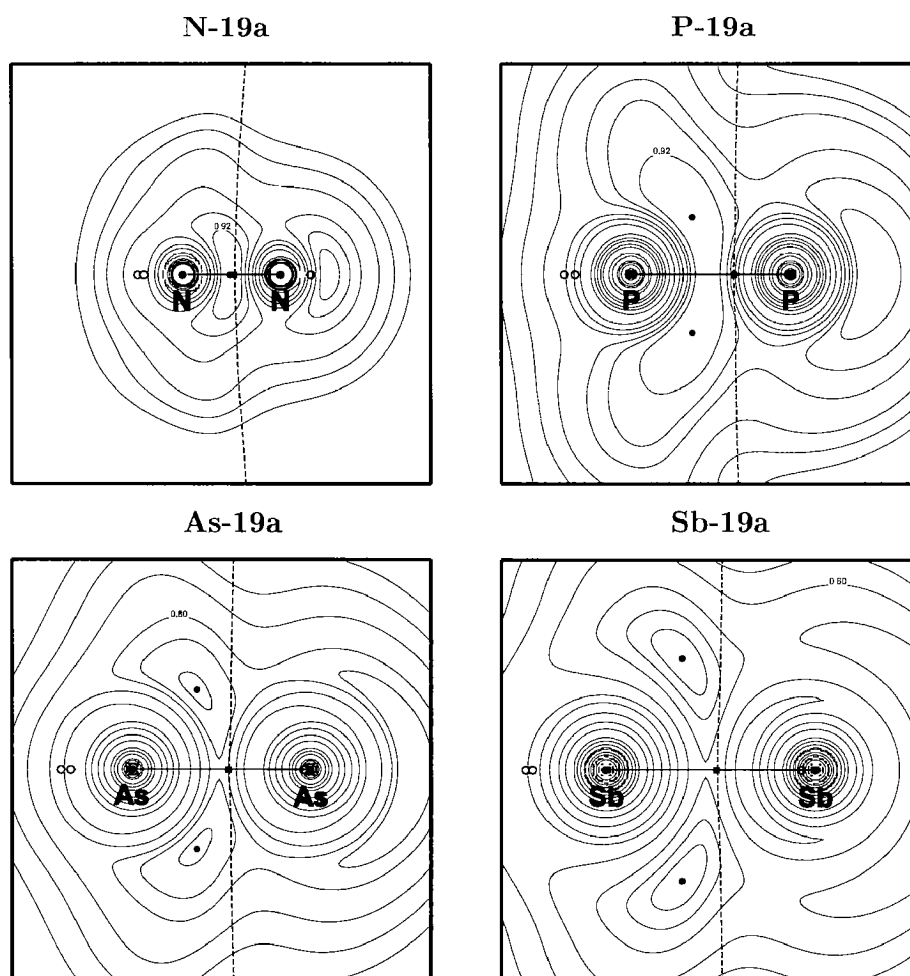
Figure 3.12: Two-dimesional contour plots (perpendicular to the molecular plane) of the ELF distribution in the monocations $[H_2X=XH]^+$, overlayed with the BPs (—), BCPs (■) and the IASs (- -) from the Bader Analyses of the X=X double bonds. The inner contour lines (—) correspond to ELF values of 0.8, 0.88, 0.92 for X = N, P, Sb and 0.8, 0.88, 0.94 for X = As. Local ELF maxima > 0.94, i.e. the bond attractors above (M^1) and below (M^2) the X–X bond path, are indicated by black dots (●). The grey colored regions represent domains within both maxima, M^1 and M^2, are found (N, P: ELF > 0.92; As: ELF > 0.80; Sb: ELF > 0.60). Small black circles indicate hydrogen atoms above (solid) and below (dashed) the plot plane.

from the 6-31G(d,p) wavefunction. Calculations with the STO-3G basis set revealed that this single point is the degenerate form of a typical double bond attractor pattern, i.e. the two weakly separated ELF maxima $M^{1,2}$ above and below a local ELF minimum on the X–X bond vector. In the ELF distributions of the higher congeners **X-19a**, two ELF maxima appear in the bonding region, regardless of the basis set used (see Fig. (3.12)). For all systems, the X=X double bond domains (ELF > 0.80) can be described as a dumb-bell shaped region bended around the XH_2 pnictogen centers. With increasing atomic number of X, the two bonding attractors are equally shifted away from the X–X bond paths according to the fact that the valence electrons for the higher row elements (principal quantum number $n \geqslant 3$) are more expanded in space and interatomic Pauli repulsion increase. As seen from the decreasing boundary values of the ELF regions in which both M^1 and M^2 are located, the two double bond attractors become more separated from each other. Notwithstanding, all monocations still feature a typical attractor pattern of classical double bond systems.

Finally, we have a look at the ELF distributions for the doubly protonated derivatives $[H_2X=XH_2]^{2+}$. In the planar dicationic hydrazine **X-23a**, the ELF bonding domain can be described as a dumb-bell shaped region (ELF > 0.88) with two weakly separated maxima close above and below the N–N bond midpoint. For the higher trans-bent analogues, **X-24a**, the ELF double bond domains (ELF > 0.80) show the typical S-shape for slipped double bond systems with considerable ELF density localized over the X = P, As, Sb centers. Again, the two maxima found are increasingly separated from each other when X goes down the row from P to Sb. They are, however, still localized in a common region of high ELF values with the corresponding local ELF minima positioned at the molecular inversion center.

N-23a   **P-24a**

As-24a   **Sb-24a**
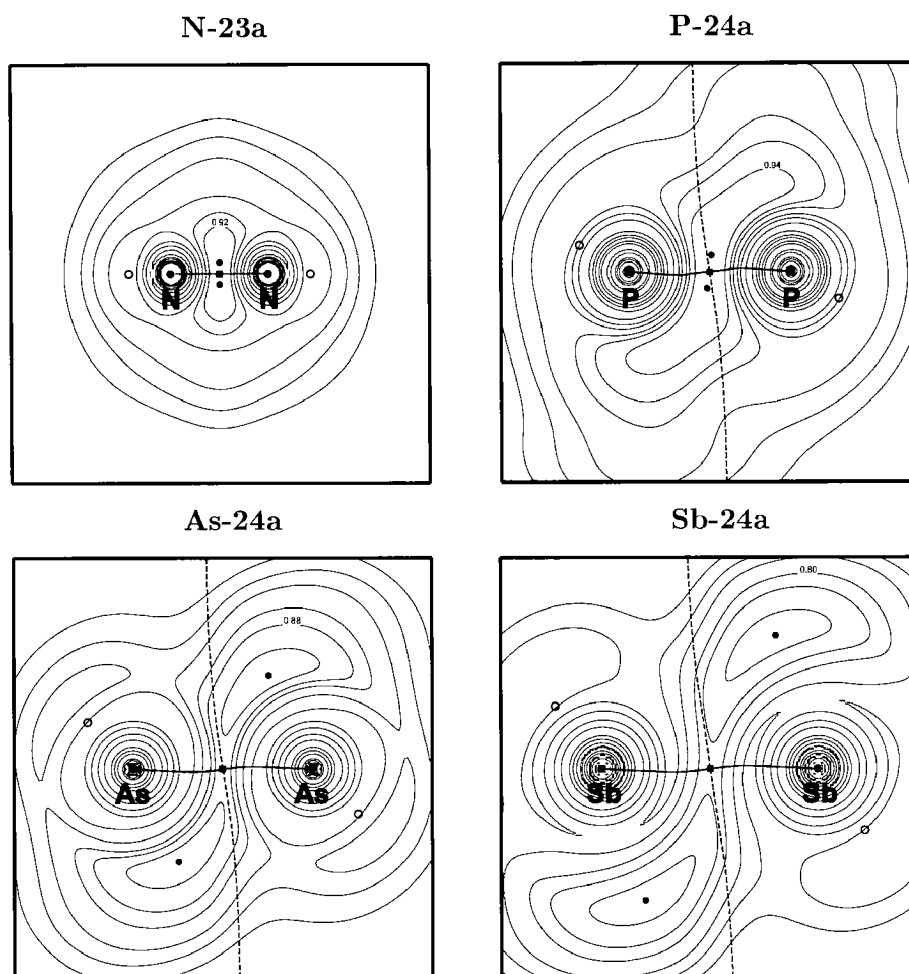
Figure 3.13: Two-dimesional contour plots (within the σ_v symmetry plane) of the ELF distribution in the dications $[H_2X\!=\!XH_2]^{2+}$, overlayed with the BPs (—), the BCPs (■) and the IASs (- -) from the Bader Analysis of the X=X double bonds. The inner contour lines (—) correspond to ELF values of 0.8, 0.88, 0.92 for X = N and 0.8, 0.88, 0.94 for X = P, As, Sb. Local ELF maxima > 0.94, i.e. the bond attractors above (M^1) and below (M^2) the X–X bond path, are indicated by black dots (●). The grey colored regions represent domains within both maxima, M^1 and M^2, are found (N: ELF > 0.92; P: ELF > 0.94; As: ELF > 0.88; Sb: ELF > 0.80). Nuclei above and below the plot plane are indicated by black circles (○).

Seite Leer /
Blank leaf

Bibliography

R. Appel. *Multiple Bonds and Low Coordination in Phosphorus Chemistry*. Georg Thieme Verlag, Stuttgart, 1990. Section D, Chapter 4.

R. F. W. Bader. *Atoms in Molecules – A Quantum Theory*. Oxford University Press, New York, 1990.

R. F. W. Bader and H. Essen. *J. Chem. Phys.*, 80:1943, 1984.

R. F. W. Bader, P. J. MacDoughall, and C. D. H. Lau. *J. Am. Chem. Soc.*, 106: 1594, 1984.

R. J. Bartlett, J. D. Watts, S. A. Kucharski, and J. Noga. *Chem. Phys. Lett.*, 165: 513, 1990.

A. D. Becke and K. E. Edgecombe. *J. Chem. Phys.*, 92:5397, 1990.

G. Z. Becker. *Anorg. Allg. Chem.*, 423:242, 1976.

G. Z. Becker and G. Gutekunst. *Angew. Chem. Int. Ed. Engl.*, 16:463, 1977.

A. Bergner, M. Dolg, W. Küchle, H. Stoll, and H. Preuss. *Mol. Phys.*, 80:1431, 1993.

J. Berkowitz. *J. Chem. Phys.*, 89:7065, 1988.

J. Berkowitz and H. Cho. *J. Chem. Phys.*, 90:1, 1989.

F. Bernardi, A. Bottoni, and A. Venturini. *J. Am. Chem. Soc.*, 108:5395, 1986.

F. Bernardi, I. G. Czimadia, H. B. Schlegel, and S. Wolfe. *Can. J. Chem.*, 53:1144, 1975.

D. Bond. *J. Am. Chem. Soc.*, 113:385, 1991.

V. E. Bondybey and J. W. Nibler. *J. Chem. Phys.*, 58:2125, 1973.

R. D. Brown, P. D. Godfrey, and D. McNaughton. *Aust. J. Chem.*, 34:465, 1981.

P. E. Cade. *Can. J. Phys.*, 46:1989, 1968.

E. A. Carter and W. A. Goddard III. *J. Phys. Chem.*, 90:998, 1986.

A. H. Cowley. *Polyhedron*, 3:389, 1984.

A. H. Cowley and R. A. Kemp. *Chem. Rev.*, 85:367, 1985.

A. H. Cowley, J. G. Lasch, N. C. Norman, and M. Pakulski. *J. Am. Chem. Soc.*, 105:5506, 1983.

A. H. Cowley and N. C. Norman. *Proc. Inorg. Chem*, 34:1, 1986.

A. H. Cowley, N. C. Norman, and M. Pakulski. *J. Chem. Soc. Dalton Trans.*, :383, 1985.

C. J. Cramer, F. J. Dulles, J. W. Storer, and S. E. Worthington. *Chem. Phys. Lett.*, 218:387, 1994.

D. Cremer and E. Kraka. *Croatia Chem. Acta*, 57:1259, 1984.

E. M Cruz, X. L. Lopez, M. A. Ayerbe, and J. M. Ugalde. *J. Phys. Chem. A*, 101: 2166, 1997.

L. A. Curtiss, M. P. McGrath, J-P. Blandeau, N. E. Davis, Jr. R. C. Binning, and L. Radom. *J. Chem. Phys.*, 103:6104, 1995.

L. A. Curtiss, K. Raghavachari, G. W. Trucks, and J. A. Pople. *J. Chem. Phys.*, 94:7221, 1991.

P. J. Davidson, D. H. Harris, and M.F. Lappert. *J. Chem. Soc. Dalton Trans.*, : 2268, 1976.

A. Decken, C. Carmalt, J. A. Clyburne, and A. H. Cowley. *Inorg. Chem.*, 36:3741, 1997.

D. J. DeFrees and A. D. McLean. *J. Comp. Chem.*, 3:321, 1986.

M. Dietrich, J. Heinze, H. Fischer, and F. A. Neugebauer. *Angew. Chem. Int. Ed. Engl.*, 25:1021, 1986.

K. B. Dillon, F. Mathey, and J. F. Nixon. *Phosphorus: The Carbon Copy*. Wiley, Chichester, 1998.

K. D. Dobbs, J. E. Boggs, and A. H. Cowley. *Chem. Phys. Lett.*, 141:372, 1987.

M. Driess and H. Grützmacher. *Angew. Chem. Int. Ed. Engl.*, 35:828, 1996.

K. Findeisen, H. Heitzer, and K. Dehnicke. *Synthesis*, :702, 1981.

M. M. Francl, W. J. Petro, W. J. Hehre, J. S. Binkley, M. S. Gordon, D. J. DeFrees, and J. A. Pople. *J. Chem. Phys.*, 77:3654, 1983.

M. J. Frisch, G. W. Trucks, H. B. Schlegel, P. M. W. Gill, B. G. Johnson, M.A. Robb, J. R. Cheeseman, T. Keith, G. A. Petersson, J. A. Montgomery, K. Raghavachari, M. A. Al-Alaham, V. G. Zakrzewski, J. V. Ortitz, J. B. Foresman, J. Cioslowski, B. B. Stefanov, A. Nanayakkara, M. Challacombe, C. Y. Peng, P. Y. Ayala, W. Chen, M. W. Wong, J. L. Andres, E. S. Replogle, R. Gomperts, R. L. Martin, D. J. Fox, J. S. Binkley, D. J. Defrees, J. Baker, J. J. P. Stewart, M. Head-Gordon, C. Gonzalez, and J. A. Pople. *Gaussian94, Revision C3*. Gaussian Inc., Pittsburgh PA, 1995.

M. J. Frisch, J.A. Pople, and J.S. Binkley. *J. Chem. Phys.*, 80:3265, 1984.

S. T. Gibson, J. P. Greene, and J. Berkowitz. *J. Phys. Chem.*, 83:4319, 1985.

D. G. Gilheany. *Chem. Rev.*, 4:1339, 1994.

R. J. Gillespie. *Molecular Geometry*. Van Nostrand Reinhold, London, 1972.

H. Grützmacher and T. Fässler. *Angew. Chem. Int. Ed. Engl.*, in press, 2000.

H. Grützmacher and C. M. Marchand. *Coord. Chem. Rev.*, 163:287, 1997.

H. Grützmacher and H. Pritzkow. *Angew. Chem. Int. Ed. Engl.*, 30:709, 1991.

H. Grützmacher and H. Pritzkow. *Angew. Chem. Int. Ed. Engl.*, 31:99, 1992.

Y. Hamada, K. Hashiguchi, M. Tsuboi, Y. Koga, and S. Kondo. *J. Mol. Spectrosc.*, 105:70, 1984.

M. D. Harmony, V. W. Laurie, R. L. Kuczkowksi, R. H. Schwendemann, D. A. Ramsay, F. J. Lovas, W. J. Lafferty, and A. G. Maki. *J. Phys. Chem. Rev. Data*, 8:619, 1979.

W. J. Hehre, L. Radom, P. von Ragué Schleyer, and J. A. Pople. *Ab initio Molecular Orbital Theory*. Wiley-Interscience, New York, 1986. Chapter 4, p. 71.

U. Heim, H. Pritzkow, H. Schönberg, and H. Grützmacher. *J. Chem. Soc., Chem. Commun.*, :673, 1993.

P. B. Hitchcock, C. Jones, and J. F. Nixon. *Angew. Chem. Int. Ed. Engl.*, 34:492, 1995.

R. F. Hout, B. A. Levi, and W. J. Hehre. *J. Comp. Chem.*, 3:234, 1982.

K. P. Huber and G. Herzberg. *Constants of Diatomic Molecules*. Nostrand-Reinhold, New York, 1979.

S. Huzinaga. *Gaussian Basis Set for Molecular Calculations*. Elsevier Science Puplishers, Amsterdam, 1984.

A. Igau, A. Baceireido, H. Grützmacher, H. Pritzkow, and G. Bertrand. *J. Am. Chem. Soc.*, 111:6853, 1989.

K. Ito and S. Nagase. *J. Phys. Lett.*, 126:531, 1986.

H. Jacobsen and T. Ziegler. *J. Am. Chem. Soc.*, 116:3667, 1994.

H. J. Jensen, P. Jørgensen, and T. Helgaker. *J. Am. Chem. Soc.*, 109:2895, 1987.

C. Jones, J. W. Steed, and R. C. Thomas. *J. Chem. Soc. Dalton Trans.*, :1541, 1999.

J. Kapp, C. Schade, A. M. El-Nahasa, and P. von Ragué Schleyer. *Angew. Chem. Int. Ed. Engl.*, 35:2236, 1996.

H. Kollmar and V. Staemmler. *Theor. Chim. Acta*, 48:223, 1978.

R. Krishnan, J.S. Binkley, R. Seeger, and J.A. Pople. *J. Chem. Phys.*, 72:650, 1980.

W. Kutzelnigg. *Einführung in die Theoretische Chemie, Bd. 2: Die chemische Bindung*. Verlag Chemie, Weinheim, 1978.

W. Kutzelnigg. *Angew. Chem. Int. Ed. Engl.*, 23:272, 1984.

S. R. Langhoff and Jr. W. Bauschlicher. *Chem. Phys. Lett.*, 180:88, 1991.

L. L. Lohr, H. B. Schlegel, and K. Morokuma. *J. Phys. Chem.*, 88:1981, 1984.

S. Loss, C. Widauer, and H. Grützmacher. *Angew. Chem. Int. Ed. Engl.*, 38:3329, 1999.

L. Mahé and J.-C. Barthelat. *J. Phys. Chem.*, 99:6819, 1995.

C. Møller and M. S. Plesset. *Phys. Rev.*, 46:618, 1934.

S. Nagase, S. Suzuki, and T. Kurakake. *J. Chem. Soc., Chem. Commun.*, :1724, 1990.

J. Niemann, W. W. Schoeller, V. von der Gönna, and E. Niecke. *Chem. Ber.*, 124:828, 1991.

F. Ogliaro, D.L. Cooper, and P.B. Karadakov. *Int. J. Quant. Chem.*, 74:233, 1999.

G. A. Ohla and P. von Ragué Schleyer. *Carbonium Ions*. Wiley, New York, 1976. vols. I-V.

A. M. L. Øiestad and E. Uggerud. *Int. J. Mass Spectrom. Ion Proc.*, 167/168:117, 1997.

D. C. Pestana and P.P. Power. *Inorg. Chem.*, 30:528, 1991.

P. L. A. Popelier. *MORPHY98*. EU, Manchester, England, 1998. with a contribution from R. G. A Bone, UMIST.

J. A. Pople, M. Head-Gordon, and K. Raghavachari. *Chem. Phys. Lett.*, 89:7382, 1987.

P. P. Power. *Angew. Chem. Int. Ed. Engl.*, 30:449, 1990.

P. P. Power. *J. Chem. Soc. Dalton*, 18:2939, 1998.

P. P. Power. *Chem. Rev.*, 99:2363, 1999.

K. Raghavachari, R. A. Whiteside, J. A. Pople, and P. von Ragué Schleyer. *J. Am. Chem. Soc.*, 103:5649, 1981.

A. E. Reed, L. A. Curtis, and F. Weinhold. *Chem. Rev.*, 3:321, 1988.

H. F. Schaefer III. *Synthesis*, 231:1100, 1986.

P. von Ragué Schleyer and D. Kost. *J. Am. Chem. Soc.*, 110:2105, 1988.

M. W. Schmidt, P. N. Truong, and M. S. Gordon. *J. Am. Chem. Soc.*, 109:5217, 1987.

W . W. Schoeller. *Multiple Bonds and Low Coordination in Phosphorus Chemistry.* Georg Thieme Verlag, Stuttgart, 1990. Section D, Chapter 1.

W. W. Schoeller, C. B. Bergmann, U. Tubbesing, and J. Strutwolf. *J. Chem. Soc., Faraday Trans.*, 93:2957, 1997.

P. A. Schultz and R.P. Messmer. *J. Am. Chem. Soc.*, 113:433, 1991.

P. A. Schultz and R.P. Messmer. *J. Am. Chem. Soc.*, 115:10925, 1993a.

P. A. Schultz and R.P. Messmer. *J. Am. Chem. Soc.*, 115:10938, 1993b.

P. A. Schultz and R.P. Messmer. *J. Am. Chem. Soc.*, 115:10945, 1993c.

A. Sierraalta and F. Ruete. *J. Comp. Chem.*, 15:313, 1994.

B. Silvi and A. Savin. *NATURE*, 371:683, 1994.

N. Tokitoh, Y. Arai, Okazaki, and S. Nagase. *Science*, 277:78, 1997.

N. Tokitoh, Y. Arai, T. Sasamori, R. Okazaki, S. Nagase, H. Uekusa, and Y. Ohashi. *J. Am. Chem. Soc.*, 120:433, 1998.

G. Trinquier. *J. Am. Chem. Soc.*, 112:2130, 1990.

G. Trinquier. *J. Am. Chem. Soc.*, 113:144, 1991.

G. Trinquier and J.-P. Malrieu. *J. Am. Chem. Soc.*, 109:5303, 1987.

B. Twamley, C. D. Sofield, M. M. Olmstead, and P. P. Power. *J. Am. Chem. Soc.*, 121:3357, 1999.

R. A. Volkmann. *Comprehensive Organic Synthesis, vol. 1.* Pergamon Press, Oxford, 1991. p. 355.

A. F. Voter, M. M. Goodgame, and W. A. Goddard. *Chem. Phys.*, 98:7, 1985.

S. F. Vyboishchikov, A. Sierraalta, and G. Frenking. *J. Comp. Chem.*, 18:416, 1996.

Y. Wang and R. A. Poirier. *J. Phys. Chem. A*, 101:907, 1997.

L. Weber. *Chem. Rev.*, 92:1839, 1992.

L. Weber. *Chem. Ber.*, 129:367, 1996.

J. C. White, R. J. Cave, and E. R. Davidson. *J. Am. Chem. Soc.*, 110:6308, 1988.

C. Willis, F. P. Lossing, and R. A Back. *Can. J. Phys.*, 54:1, 1976.

B. F. Yates, W. J. Bouma, and L. Radom. *J. Am. Chem. Soc.*, 108:6545, 1986.

M. Yoshifuji. *Multiple Bonds and Low Coordination in Phosphorus Chemistry.* Georg Thieme Verlag, Stuttgart, 1990. Section D, Chapter 9.

M. Yoshifuji, I. Shima, and N. Inamoto. *J. Am. Chem. Soc.*, 103:4587, 1981.

Curriculum Vitae

Name:	Christoph Widauer
Date of birth:	December 4, 1967
Place of birth:	Basel (Switzerland)
Nationality:	Swiss
Parents:	Olaf Widauer and Marie-Louise Widauer (b. Monsch)

Education

Apr. 1975 – Mar. 1980	attended elementary school at Allschwil (Switzerland).
Apr. 1980 – Mar. 1985	attended the Pro-Gymnasium at Allschwil (Switzerland).
Apr. 1985 – Mar. 1989	attended the Mathematische Naturwissenschaftliche Gymnasium Basel (Switzerland). Matura in March 1989.

Studies

Oct. 1989 – Oct. 1994	studied Chemistry at the ETH Zürich. graduated as Diplom-Chemiker (ETH). diploma thesis in the group of Prof. R. Nesper about Alkali-metal intercalation compounds with C_{60}.
Mar. 1995 – Oct. 1996	postgraduate studies in the group of Prof. A. Vasella at the organic chemistry laboratory of the ETH.
Apr. 1997 – Apr. 2000	postgraduate studies in the group of Prof. H. Grützmacher at the inorganic chemistry laboratory of the ETH.
Aug. 1998 – Nov. 1998	research visit in the group of Prof. T. Ziegler at the chemistry department of the University of Calgary in Alberta, Canada.